NASA TECHNICAL NOTE

NASA TN D-4407

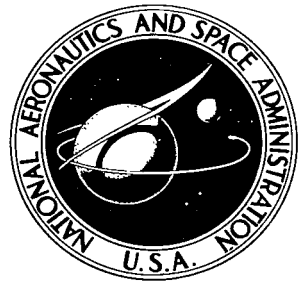

NASA TN D-4407

EFFECTS OF 22 MeV PROTON AND 2.4 MeV ELECTRON RADIATION ON BORON- AND ALUMINUM-DOPED SILICON SOLAR CELLS

by Gilbert A. Haynes and Walter E. Ellis

Langley Research Center
Langley Station, Hampton, Va.

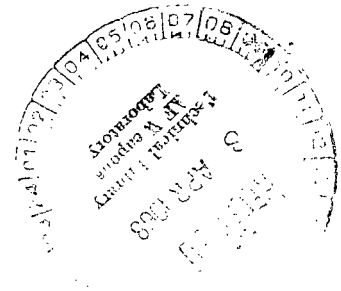

NATIONAL AERONAUTICS AND SPACE ADMINISTRATION • WASHINGTON, D. C. • APRIL 1968

EFFECTS OF 22 MeV PROTON AND 2.4 MeV ELECTRON RADIATION ON BORON- AND ALUMINUM-DOPED SILICON SOLAR CELLS

By Gilbert A. Haynes and Walter E. Ellis

Langley Research Center
Langley Station, Hampton, Va.

NATIONAL AERONAUTICS AND SPACE ADMINISTRATION

For sale by the Clearinghouse for Federal Scientific and Technical Information
Springfield, Virginia 22151 – CFSTI price $3.00

EFFECTS OF 22 MeV PROTON AND 2.4 MeV ELECTRON RADIATION ON BORON- AND ALUMINUM-DOPED SILICON SOLAR CELLS

By Gilbert A. Haynes and Walter E. Ellis
Langley Research Center

SUMMARY

A comparative analysis is presented of the effects of proton and electron irradiation on the electrical properties of boron-doped and aluminum-doped, N on P, silicon solar cells having base resistivities of 1 ohm-cm and 10 ohm-cm. Electrical measurements were made before and after irradiation at various flux levels up to 2.1×10^{12} protons per square centimeter at 22 MeV, and 1.0×10^{16} electrons per square centimeter at 2.4 MeV.

Measurements of short-circuit current and maximum power under illumination with a tungsten light source and a solar simulator indicate that 1 ohm-cm aluminum-doped cells are slightly more resistant to damage by 2.4 MeV electrons than 1 ohm-cm boron-doped cells; however, 10 ohm-cm boron-doped cells were found to be more resistant to electron damage than 10 ohm-cm aluminum-doped cells. Under proton irradiation no significant difference was observed in the radiation resistance of boron-doped and aluminum-doped cells with the same base resistivity.

Spectral response measurements made before and after irradiation indicated no significant difference due to the type of doping element employed. From these spectral response curves, conversion factors were computed for use in predicting the output of solar cells in space sunlight from direct measurements under tungsten light or the solar simulator.

Within the range from 32° C to 71° C, the temperature coefficients of the various parameters changed with irradiation. However, no significant difference in temperature coefficients was noted between the boron-doped and aluminum-doped cells having the same base resistivity.

INTRODUCTION

Considerable effort has been expended during the past few years to enhance the performance of silicon solar cells for use as energy-conversion devices in power systems for space applications. These efforts have resulted in a number of improvements over

the original P on N solar cell – for example, higher conversion efficiencies and extended useful lifetime in the space environment. The more recently developed N on P cells have greatly improved resistance to damage from high-energy particulate radiation (refs. 1, 2, and 3). This resistance was further enhanced by increasing the resistivity of the base material. It has been established that the optimum resistivity of the base material without appreciable sacrifice in efficiency is 10 to 20 ohm-cm (ref. 4). These high-resistivity cells were found to be superior in power output to the 1 ohm-cm cell after irradiation at temperatures up to 100° C (ref. 4).

In reference 5, data have been presented which suggest that a relationship exists between the doping element used as an acceptor or donor in the base region of silicon solar cells and the changes in diffusion length observed after irradiation. Aluminum-doped cells were reported to have a longer diffusion length than boron-doped cells after irradiation with 1.0 MeV electrons, and therefore would be expected to have higher power output.

A sample quantity of aluminum-doped cells with base resistivities of 1 ohm-cm and 10 ohm-cm were obtained, and experiments were conducted to study the effects of proton and electron irradiation on the electrical parameters of primary interest to designers of spacecraft power systems. These parameters are short-circuit current, maximum power, open-circuit voltage, and load current at specific voltages. To provide a reference for comparison, boron-doped cells with the same base resistivities were irradiated and tested simultaneously with the aluminum-doped cells.

The criterion of most importance to the designer of solar-cell power systems for use in space is the amount of power that can be delivered into a specific combination of loads under the radiation and temperature conditions encountered during a defined mission. It has been established (ref. 6) that the power degradation of the cells due to radiation cannot be determined with any reasonable degree of accuracy by the use of any single parameter such as diffusion length or short-circuit current. Ideally, the highest efficiency of a power system can be achieved by operating at the point of maximum power. Unfortunately, the point of maximum power changes with radiation and temperature, and when the load is changed from optimum, the cell no longer operates at maximum power. Numerous methods of loading solar cells are actually employed, depending on the mission requirements and on the power conditioning techniques used. Hence, in studying the effects of radiation on solar cells, it is necessary to obtain output data at a variety of cell loads and temperatures.

SYMBOLS

C	temperature coefficient
e	number of electrons
$f_{su/sim}$	ratio of the cell output from space sunlight to the cell output from the solar-simulator illumination
$f_{su/W}$	ratio of the cell output from space sunlight to the cell output from tungsten illumination
I_L	load current
I_{sc}	short-circuit current
P_{max}	maximum power
p	number of protons
V_{oc}	open-circuit voltage
ϕ_c	critical flux, defined as the flux required to cause 25-percent degradation of the parameter under investigation

EXPERIMENTAL EQUIPMENT AND PROCEDURE

Description of Cells

The aluminum-doped and boron-doped cells used in these experiments were obtained from the same manufacturer and were made by the same basic fabrication techniques. The boron-doped cells were representative of the cells currently being used in spacecraft power systems. All of the cells were N on P type, 1 cm by 2 cm, with nominal efficiencies of 10 percent for zero-air-mass sun illumination. The contacts were of the evaporated, or sintered, type with five grids on the top surface. Only a few cells of each type were acquired, and no attempt was made to match cells in each group. However, the variation in output of the cells in each group was small, being less than ±2 percent at short-circuit current. The four types of cells and the number employed in each experiment are shown in table I. The resistivity listed for each group is that of the base material. The solar cells were cemented to 1/8-inch-thick (0.318-cm) anodized

aluminum strips with silicone rubber adhesive to simulate the mounting techniques employed on spacecraft solar-cell arrays (fig. 1). These aluminum strips served as heat sinks to assure good temperature stability during irradiation and illumination tests and to enable handling without danger of contamination or breakage of the solar cells.

TABLE I

TYPE AND NUMBER OF SOLAR CELLS IRRADIATED IN EACH EXPERIMENT

Solar-cell type	Resistivity, ohm-cm	Number of cells irradiated with 22 MeV protons	Number of cells irradiated with 2.4 MeV electrons
1 ohm-cm boron	1.5 to 3.0	8	4
1 ohm-cm aluminum	1.5 to 3.0	8	4
10 ohm-cm boron	8 to 10	8	4
10 ohm-cm aluminum	8 to 10	8	4

Solar-Cell Characteristic Measurements

The electrical output characteristics of the cells under illumination with both a tungsten light source and a commercial solar simulator were measured before and after irradiation. A simplified sketch of the test setup is shown in figure 2. The tungsten light source was an unfiltered photoflood lamp, operated at a black-body temperature of $2800^{\circ} \pm 20^{\circ}$ K. A two-color optical pyrometer was used periodically to ascertain the lamp voltage necessary to produce this black-body temperature. This voltage was regulated within ±0.4 percent. The commercial solar simulator was basically a xenon short-arc lamp with a well-regulated input current. The light emitted by the lamp was filtered so that the resulting spectral irradiance approximated that of space sunlight over the spectral response range of silicon solar cells.

The light intensity at the test plane under each light source was adjusted so that the short-circuit current output of two calibrated unirradiated silicon solar cells would be the same as that in space sunlight at 1 AU (1 astronomical unit is defined as the mean distance from the earth to the sun, 149 599 000 km). The current output in space sunlight of one of the cells had been determined by tests on Table Mountain in California, and the other had been similarly calibrated by aircraft flight tests at the NASA Lewis Research Center (ref. 7). A third reference cell, mounted on an anodized strip in the same manner as the cells that were irradiated, was included in all tests to monitor the intensity of each light source and to check the repeatability of the instruments used to measure electrical characteristics. The repeatability, including stability of the light intensity, was found to be better than 1 percent.

To obtain the preirradiation and postirradiation electrical output characteristics, current-voltage (I-V) curves were plotted automatically on an x-y recorder while a resistive load across the cell terminals was varied from short-circuit to open-circuit conditions. In addition, the short-circuit current, the open-circuit voltage, and the load current at 0.4 volt were measured on a milliammeter and a digital voltmeter. The additional measurements provided redundancy for the recorded data, the disparity between the short-circuit current data resulting from the two methods of measurement being less than 1 percent. The accuracy of open-circuit voltage, maximum power, and load current at specific voltages was somewhat less than that of short-circuit current since these parameters are more responsive to small temperature variations.

The I-V characteristics were also obtained on one or two cells from each group at incremental temperatures from 32° C to 71° C. The sample strips were mounted on a flat thermal element, and the voltage input to the thermal element was controlled with a rheostat. At each temperature the solar cell was allowed to stabilize to assure a temperature accuracy of ±2° C. A thermocouple was embedded in the center of the aluminum support strip directly under the center of each solar cell, and the temperature was monitored on a potentiometric pyrometer. The temperature gradient between the active portion of the solar cell and the point of measurement was determined through laboratory tests to be less than 1.0° C.

The apparatus used for spectral response measurements consisted of a 1000-watt tungsten projection lamp, a set of 17 narrow band-pass interference filters (100 Å nominal half-width), a reference solar cell, and a low-current readout system. The test procedure was to expose simultaneously the reference cell and a test cell to a beam of monochromatic light and compare the short-circuit current outputs of the two cells. The spectral response of the test cell was determined from this comparison. The repeatability of the system was better than 3 percent. The intensity of the monochromatic light was of the order of 200 microwatts/cm^2. The reference cell was one of known spectral response, having been spectrally calibrated against a thermopile in both the filter system and a monochromator system.

Proton Experiment

The samples were irradiated with 22 MeV protons at the Oak Ridge 86-inch cyclotron. The test setup at the cyclotron (ref. 8) was such that the proton beam from the cyclotron passed through an ionization chamber and exited through the 0.004-inch (0.010-cm) aluminum window of the chamber. This calibrated chamber was used to establish the integrated flux doses to an estimated accuracy of 5 percent. The beam then passed through 5 inches (12.7 cm) of air, resulting in a scattered beam area of about 9 cm^2 at the target. The uniformity of the proton beam over the target area was approximately ±5 percent as determined from an activation-distribution study. This technique

consisted of placing a number of tantalum foil disks, 1/4 inch (0.635 cm) in diameter, on 1-cm centers in the 0° position of the proton beam. The foil was then irradiated, and the isotope production for each disk was subsequently determined by gamma-ray spectrum analyses.

The small size of the test area necessitated the irradiation of one cell at a time. The cells were mounted on two remotely controlled aluminum wheels, which allowed accurate positioning of each cell in the beam. Two of the 20 positions of the wheel contained pieces of polyvinyl chloride film for monitoring the position, size, and shape of the beam. Test samples were mounted on the wheel as shown in figure 3. The eight cells (table I) of each of the four groups were irradiated to the integrated fluxes listed in table II. With the beam controls provided, the values of total integrated flux could not be precisely repeated. The flux rate was approximately 5×10^8 p/cm^2-sec. The temperature of the solar cells during irradiation was maintained between 29° C and 32° C by forced-air cooling.

TABLE II

INTEGRATED FLUX RECEIVED BY SOLAR CELLS

IRRADIATED WITH 22 MeV PROTONS

Cell no.	Integrated flux, p/cm^2	Cell no.	Integrated flux, p/cm^2	Cell no.	Integrated flux, p/cm^2	Cell no.	Integrated flux, p/cm^2
1-B-7	1.23×10^{10}	1-A-4	1.23×10^{10}	10-B-7	1.27×10^{10}	10-A-3	1.20×10^{10}
1-B-3	1.31×10^{10}	1-A-2	1.24×10^{10}	10-B-5	1.29×10^{10}	10-A-2	1.21×10^{10}
1-B-6	1.75×10^{11}	1-A-5	1.56×10^{11}	10-B-4	1.69×10^{11}	10-A-8	1.8×10^{11}
1-B-8	1.82×10^{11}	1-A-7	1.69×10^{11}	10-B-1	1.75×10^{11}	10-A-6	1.99×10^{11}
[a]1-B-1	1.51×10^{12}	1-A-8	1.75×10^{12}	10-B-8	1.87×10^{12}	10-A-5	1.47×10^{12}
1-B-5	1.59×10^{12}	1-A-6	1.86×10^{12}	10-B-3	1.91×10^{12}	10-A-7	1.47×10^{12}
1-B-4	1.65×10^{12}	[a]1-A-1	1.87×10^{12}	[a]10-B-2	1.93×10^{12}	[a]10-A-1	1.52×10^{12}
[a]1-B-2	1.79×10^{12}	1-A-3	1.92×10^{12}	10-B-6	2.08×10^{12}	10-A-4	1.54×10^{12}

[a]Solar cells used in temperature tests.

At the cyclotron site, I-V characteristics were measured at 32° C under tungsten illumination for all cells in each group prior to bombardment and after each of the three exposures. The time interval between termination of irradiation at each integrated flux and the start of measurements under the light source varied from 15 to 30 minutes for the first exposure to a maximum of approximately 8 hours for the final exposure. Two

cells of each group were withheld after each intermediate exposure, and four cells of each group were exposed to the final integrated flux of over 10^{12} p/cm^2. The pre-irradiation and postirradiation tests at the Langley Research Center included measurements of I-V characteristics at 32° C under illumination by tungsten light and the solar simulator, measurements of I-V characteristics at incremental temperatures from 32° C to 71° C under illumination by the solar simulator, and measurements of spectral response. The I-V characteristic measurements made at 32° C under tungsten illumination at the Langley Research Center 3 days after the final exposure agreed with post-irradiation measurements from the same cells taken at the cyclotron site to within ±1.0 percent at all points along the I-V curves.

Electron Experiment

The electron irradiation experiment was conducted with the 3 MeV electron accelerator at Langley Research Center, at an energy of 2.4 MeV. The experimental setup was identical to that in reference 9. The test samples were mounted on a 1/4-inch (0.635-cm) plate as shown in figure 4. The electron beam passed between scan magnets and through a 0.002-inch (0.005-cm) titanium window of the scan horn. The sample plate was mounted in air in close proximity to the titanium window. The electron beam scanned the solar cells at about 10 cycles per second, thus irradiating all 16 cells. The scanned area extended well beyond the end cells to avoid any excess radiation from the "dwell" area caused by reversal of the scan cycle. The uniformity of the elctron beam over the target area was approximately ±5 percent as determined by the use of cobalt-glass slides.

The beam current was monitored by integrating electronically the charge collected on an insulated 1- by 2-cm aluminum detector located in the center of the sample plate as shown in figure 4. The flux rate was maintained at 0.03 microampere/cm^2 for the first and second tests, with integrated fluxes of 1×10^{13} e/cm^2 and 1×10^{14} e/cm^2, respectively. For the third and fourth tests, with integrated fluxes of 1×10^{15} e/cm^2 and 1×10^{16} e/cm^2, respectively, the beam current was increased to a maximum of 0.1 microampere/cm^2 and the in-beam time required was thus decreased. During irradiation, cell temperatures varied between 30° C and 35° C.

Prior to irradiation, and after each exposure, I-V characteristic measurements were obtained at 32° C for all cells in each group under illumination from tungsten light and the solar simulator. The time interval between termination of irradiation at each integrated flux and the start of measurements under the light sources varied from approximately 15 minutes to several hours. The spectral response of all cells was determined prior to irradiation and after each intermediate integrated flux. To determine temperature coefficients, I-V characteristics were obtained using solar-simulator illumination of two cells from each group at incremental temperatures from 32° C to 71° C before

irradiation and after each intermediate exposure. To avoid the effects of any possible annealing on the coefficients, the cells were purposely held at each temperature for no more than 15 minutes.

RESULTS AND DISCUSSION

Proton Irradiation Tests

The effects of 22 MeV protons on the I-V characteristics of a typical cell from each of the four groups of cells (table I) are presented in figures 5 to 8. These curves represent data taken from the tungsten-light measurements made at the cyclotron site. Note that the I-V curves for the aluminum-doped cells were almost identical in shape to those for the boron-doped cells having the same nominal base resistivity. The relatively flat shape of the curves at low voltages before irradiation and a fairly sharp break near the point of maximum power are characteristic of the high quality of the cells used in these tests.

In plots of various parameters as functions of integrated proton flux (figs. 9 to 14), the values presented are the average for the cells for each exposure. Specifically, the average of all eight cells in each group established the preirradiation reference points, the average of two cells was used at each of the two intermediate exposures, and the average of four cells at the maximum integrated flux of about 2×10^{12} p/cm^2 (table II).

The effects of proton irradiation on the average short-circuit current for each group of cells are shown in figures 9 and 10. Each curve represents the percentage of initial short-circuit current remaining after irradiation as a function of integrated flux. Measurements made under both the tungsten light and the solar simulator are shown. Except for the 1 ohm-cm cells under tungsten light, there is no significant difference in the radiation resistance of the aluminum- and boron-doped cells having the same nominal base resistivity. The 10 ohm-cm aluminum-doped cells are more radiation resistant than the 1 ohm-cm aluminum-doped cells, and the 10 ohm-cm boron-doped cells are more radiation resistant than the 1 ohm-cm boron-doped cells by approximately the same factor. In each instance the damage measured under the tungsten light was considerably greater than that under the solar simulator. This is due to the difference in the spectral irradiance of the two lights, which will be discussed later. The critical flux (the flux required to cause 25-percent degradation of the parameter under investigation) and the degradation rate (the slope of the curve between 10^{11} and 10^{12} p/cm^2) are given in table III.

The effects of proton irradiation on the average maximum power P_{max} of each group of cells are shown in figures 11 and 12. The trends are similar to those for I_{sc},

except that the changes in P_{max} are greater. The critical fluxes and degradation rates for P_{max} are also given in table III.

Figures 13 and 14 represent the effects of 22 MeV protons on the open-circuit voltage V_{oc} of each group of cells, as measured under the tungsten light. The results obtained under the solar simulator were the same and are not shown. The curves indicate that for a given flux the percentage decrease in V_{oc} is approximately one-half that in I_{sc}.

TABLE III

CRITICAL FLUX ϕ_c AND DEGRADATION RATE FOR I_{sc} AND P_{max} OF SOLAR CELLS IRRADIATED WITH 22 MeV PROTONS

Solar-cell type	Short-circuit current, I_{sc}				Maximum power, P_{max}			
	ϕ_c, p/cm^2		Rate, %/decade		ϕ_c, p/cm^2		Rate, %/decade	
	Tungsten	Simulator	Tungsten	Simulator	Tungsten	Simulator	Tungsten	Simulator
1 ohm-cm boron	1.7×10^{11}	1.3×10^{12}	24.2	14.5	1.0×10^{11}	5.2×10^{11}	26.0	22.0
1 ohm-cm aluminum	2.6×10^{11}	1.5×10^{12}	24.0	15.0	1.69×10^{11}	5.0×10^{11}	25.5	21.5
10 ohm-cm boron	2.6×10^{11}	3.1×10^{12}	20.0	14.5	1.37×10^{11}	9.0×10^{11}	26.5	18.0
10 ohm-cm aluminum	3.1×10^{11}	2.5×10^{12}	21.0	16.5	2.0×10^{11}	7.4×10^{11}	28.5	17.5

Electron Irradiation Tests

The I-V characteristics of one cell from each group irradiated with 2.4 MeV electrons are shown in figures 15 to 18. These curves are typical of the raw data from all the cells irradiated and were obtained under illumination with a tungsten light source before irradiation and immediately after each intermediate integrated flux.

Figures 19 to 22 show the I-V characteristics of all cells tested in each group as measured under illumination by the solar simulator. The shaded areas represent the limits of current variation observed in each group of cells. As previously stated, no selective matching was attempted because of the small number of cells acquired. Nevertheless, the variation between the cells in each group, before and after irradiation, is small. The aluminum-doped cells exhibited slightly less variation than the boron-doped cells. Such small variations after irradiation have not been found in all solar-cell irradiation tests, even when close matching of one or more electrical parameters was achieved initially. As noted in reference 5, the variations observed in most tests might be attributed to slight differences in impurity concentration and the dislocation density of the parent crystal as well as variations in fabrication techniques.

Figures 23 to 26 show the normalized short-circuit current and maximum power as a function of integrated flux from data taken during illumination with both tungsten light

and the solar simulator. These data are the averages for all cells tested in each group. It can be observed that the 1 ohm-cm aluminum-doped cells are slightly less sensitive to 2.4 MeV electron irradiation than the 1 ohm-cm boron-doped cells, exhibiting from 3 percent to 5 percent less degradation for a given integrated flux. The 10 ohm-cm cells show a reversal of this relationship in that the boron-doped cells appear to be slightly more resistant to electron irradiation at this energy. This may suggest that the optimum base resistivity for aluminum-doped cells is different from that for boron-doped cells. Table IV gives the average integrated flux required for 25-percent degradation, ϕ_c, and the average degradation of the slope between 10^{14} e/cm^2 and 10^{15} e/cm^2 for short-circuit current and maximum power for all cells tested.

TABLE IV

CRITICAL FLUX ϕ_c AND DEGRADATION RATE FOR I_{sc} AND P_{max} OF SOLAR CELLS IRRADIATED WITH 2.4 MeV ELECTRONS

Solar-cell type	Short-circuit current, I_{sc}				Maximum power, P_{max}			
	ϕ_c, e/cm^2		Rate, %/decade		ϕ_c, e/cm^2		Rate, %/decade	
	Tungsten	Simulator	Tungsten	Simulator	Tungsten	Simulator	Tungsten	Simulator
1 ohm-cm boron	6.8×10^{13}	4×10^{14}	22	16	5.4×10^{13}	1.6×10^{14}	24	20
1 ohm-cm aluminum	1.2×10^{14}	6×10^{14}	23	16	8×10^{13}	2.5×10^{14}	27	18
10 ohm-cm boron	2.5×10^{14}	1.4×10^{15}	22	14	1.2×10^{14}	4×10^{14}	24	17
10 ohm-cm aluminum	1.8×10^{14}	1×10^{15}	20	14	1×10^{14}	2.5×10^{14}	24	20

The degradation of open-circuit voltage as a function of integrated flux is shown in figures 27 and 28. These data are the average output of all cells in each group and were obtained under tungsten illumination. The open-circuit voltage is not significantly affected by the difference in spectra of the two light sources. Consequently, data taken under solar-simulator illumination are not included in these figures. No significant difference was observed in the degradation of open-circuit voltage of aluminum-doped and boron-doped cells.

Effects of Radiation on Temperature Coefficients

Figures 29 to 34 illustrate the effect of temperature on short-circuit current, maximum power, and open-circuit voltage before irradiation and after the final integrated flux. Measurements of I-V characteristics were made on two cells from each group in the electron experiment and on one or two cells in each group in the proton experiment. As shown in table II, there was some variation in the final integrated flux received by each cell. These variations must be considered in a comparative analysis of the four

groups in the proton experiment. The I-V characteristic measurements were made under solar-simulator illumination at incremental temperatures from 32° C to 71° C. The outputs of the cells tested from each group were averaged, and the ratio of each parameter to its value at 32° C was plotted as a function of temperature.

Short-circuit current increased linearly with increasing temperature over the range from 32° C to 71° C. The increase in short-circuit current of 1 ohm-cm boron-doped cells was slightly higher before and after irradiation than that of 1 ohm-cm aluminum-doped cells. The increase in short-circuit current of 10 ohm-cm boron-doped cells used in the proton tests was slightly less before and after irradiation than that of 10 ohm-cm aluminum-doped cells. However, for the 10 ohm-cm cells used in the electron tests, no significant difference was observed in the temperature effect on short-circuit current of boron- and aluminum-doped cells before and after irradiation.

Open-circuit voltage and maximum power decreased approximately linearly with increasing temperature for unirradiated and irradiated cells, the amount of change in open-circuit voltage being slightly less than that in maximum power. The temperature-induced changes in these two parameters appear to be independent of the type of radiation, solar-cell base resistivity, and doping element.

Temperature coefficients of the average short-circuit current, maximum power, and open-circuit voltage before and after irradiation are given in tables V and VI.

TABLE V

TEMPERATURE COEFFICIENTS FOR THE TEMPERATURE RANGE 32° C TO 71° C, BEFORE AND AFTER IRRADIATION WITH 22 MeV PROTONS

Solar-cell type	$C_{I_{sc}}$		$C_{P_{max}}$		$C_{V_{oc}}$	
	%/°C	μA/°C	%/°C	mW/°C	%/°C	mV/°C
Before irradiation						
1 ohm-cm boron	0.061	41.0	-0.512	-0.143	-0.408	-2.30
1 ohm-cm aluminum	.041	28.21	-.511	-.143	-.399	-2.26
10 ohm-cm boron	.012	7.7	-.642	-.171	-.400	-2.15
10 ohm-cm aluminum	.040	28.2	-.552	-.143	-.419	-2.28
After irradiation						
1 ohm-cm boron	0.156	74.35	-0.491	-0.084	-0.436	-2.18
1 ohm-cm aluminum	.144	71.8	-.523	-.094	-.479	-2.38
10 ohm-cm boron	.113	58.97	-.588	-.102	-.50	-2.38
10 ohm-cm aluminum	.148	76.92	-.600	-.102	-.517	-2.46

TABLE VI

TEMPERATURE COEFFICIENTS FOR THE TEMPERATURE RANGE 32° C TO 71° C, BEFORE AND AFTER IRRADIATION WITH 2.4 MeV ELECTRONS

Solar-cell type	$C_{I_{sc}}$		$C_{P_{max}}$		$C_{V_{oc}}$	
	%/°C	μA/°C	%/°C	mW/°C	%/°C	mV/°C
Before irradiation						
1 ohm-cm boron	0.037	25.6	-0.50	-0.138	-0.37	-2.12
1 ohm-cm aluminum	.024	16.7	-.51	-.131	-.38	-2.14
10 ohm-cm boron	.037	25.6	-.52	-.133	-.40	-2.19
10 ohm-cm aluminum	.016	11.5	-.55	-.143	-.40	-2.19
After irradiation						
1 ohm-cm boron	0.305	110	-0.55	-0.064	-0.56	-2.50
1 ohm-cm aluminum	.186	74	-.60	-.074	-.53	-2.38
10 ohm-cm boron	.194	85	-.63	-.083	-.60	-2.25
10 ohm-cm aluminum	.185	82	-.64	-.080	-.54	-2.35

The effect of temperature on load current before and after irradiation is presented in figures 35 to 42 for operating voltages from 0.25 volt to 0.4 volt. These data were taken from the solar-simulator I-V characteristic curves and are the average of two cells in each group. The differences observed in the temperature coefficients of boron-doped and aluminum-doped cells having the same base resistivity are small. The load-current temperature coefficients for the 10 ohm-cm cells are slightly higher before irradiation than those for the 1 ohm-cm cells, particularly at higher voltages. After irradiation, the decrease in effective output of the 10 ohm-cm cells is more apparent as the temperature is increased.

The temperature coefficients of silicon solar cells vary from cell to cell, and two cells of any given type are not enough to establish a reasonable average. Also, the observed changes, particularly in short-circuit current before irradiation, were small, and a determination of temperature coefficients was difficult because of the limited temperature range of these measurements. However, the purpose of these temperature tests was to compare boron-doped and aluminum-doped solar cells, and the results should not be considered complete data for space power-system design purposes. References 10 and 11 give temperature coefficients for similar boron-doped cells that were derived from measurements over a much wider temperature range. The temperature coefficients

of the present investigation are in reasonably good agreement with those shown in the references except that the values for short-circuit current are considerably lower in the present investigation.

Effects of Type of Light on Radiation Damage

The spectral response of solar cells changes when they are subjected to particulate radiation. Therefore, measurements of radiation-induced degradation of short-circuit current and maximum power are strongly influenced by the spectral irradiance of the light used for the measurements. Figure 43 shows the relative spectral response of one of the 10 ohm-cm aluminum-doped cells before and after irradiation with 2.4 MeV electrons. The relative response, which is the output short-circuit current per unit radiant power, is plotted as a function of wavelength, for constant input radiant power at each wavelength. The curve is typical of all cells tested. No significant difference was found in the spectral response of the aluminum- and boron-doped cells, whether 1 ohm-cm or 10 ohm-cm. Also, the observed effect of 22 MeV protons on the spectral response of the cells was very similar to that shown for 2.4 MeV electrons.

The measured spectral irradiance of each of the two light sources used in these tests and the spectral distribution of space sunlight (ref. 12) are given in figure 44. Although the tungsten light is obviously a poor simulator of space sunlight, it is widely used for solar-cell testing because of its convenience, stability, and reliability. The spectral irradiance of the solar simulator is considerably closer to that of space sunlight.

By multiplying the relative spectral response of the solar cell (fig. 43) by the appropriate spectral irradiance curve (fig. 44) at each wavelength of interest, it is possible to determine the spectral response of the cell when illuminated by each type of light. The results of such calculations, before and after irradiation, are shown in figures 45, 46, and 47. The total short-circuit current output of the cell is proportional to the area under each curve, and the preirradiation spectral-response curves were normalized so that their areas were equal. Note that for the tungsten light (fig. 45) the peak response is in the infrared portion of the spectrum where the solar cell degrades the fastest (fig. 43). For this reason, considerably more degradation is found when tungsten light is used than would be expected in space sunlight where the peak response is in the visible region (fig. 47).

From the spectral-response curves in each type of light, it is possible to compute factors which can be used to predict the output, or the damage as a function of radiation flux, for a cell in space sunlight from direct measurements made under the tungsten light or the solar simulator. These conversion factors are the ratios of the areas under the

appropriate spectral-response curves. For example, the factor for conversion from tungsten light to space sunlight is:

$$f_{su/W} = \frac{\text{Area under spectral response curve in space sunlight}}{\text{Area under spectral response curve in tungsten light}}$$

and for conversion from the solar simulator to space sunlight:

$$f_{su/sim} = \frac{\text{Area under spectral response curve in space sunlight}}{\text{Area under spectral response curve in solar simulator}}$$

As the radiation damage increases, these factors vary because of the gradual change in cell spectral response. Figure 48 shows curves of $f_{su/W}$ and $f_{su/sim}$, plotted as a function of percentage of initial short-circuit current, obtained by direct measurements under the light source of interest. The factors computed for all 16 cells included in the 2.4 MeV electron tests are plotted. Similar factors were obtained for the several cells irradiated with 22 MeV protons. Note that the maximum value of the factor for converting solar-simulator to space-sunlight data is only 1.10 at 50-percent degradation.

To check the accuracy of this method, factors were computed for conversion of tungsten-light data to solar-simulator data by taking the ratio of the data obtained with these two light sources. The calculated factors and the factors computed from experimental data agreed to within 4 percent.

The short-circuit current degradation shown in figures 9, 10, 23, and 24 as percentage of initial short-circuit current can be corrected to degradation in space sunlight by using the appropriate factor from figure 48. Limited testing has shown that the degradation of maximum power, figures 11, 12, 25, and 26, can be similarly corrected with small errors. The degradation of open-circuit voltage and the changes in temperature characteristics have been found to be reasonably insensitive to changes in cell spectral response, and hence the correction factors are not applicable to these data.

Effect of Room-Temperature Storage

Subsequent tests were made to determine the effect of room-temperature storage on the radiation-induced damage experienced by the cells used in these two experiments. After the final postirradiation measurements, the cells were stored in a cabinet at room temperature. Three months after each experiment, I-V characteristics under both light sources were measured on all cells in each group. As mentioned earlier, a calibrated, unirradiated solar cell was employed to insure the same intensity of the light sources and repeatability of the instruments. At all points along the I-V curve, data taken after 3 months were within ±1 percent of the data from the same cells taken shortly after the final exposure. This close agreement was observed in those cells subjected to 71° C

during the short-term elevated-temperature tests as well as those cells withheld from the tests. These limited tests show that during long-term storage at room temperature and short-term exposures to moderately elevated temperatures, the annealing rate of the aluminum-doped cells is low and comparable to that of the boron-doped cells.

CONCLUSIONS

The following conclusions regarding the effects of 22 MeV proton and 2.4 MeV electron irradiation on the electrical properties of boron- and aluminum-doped silicon solar cells are derived from this investigation:

1. An increase in base resistivity from approximately 1 ohm-cm to approximately 10 ohm-cm reduces the sensitivity to particulate radiation of both boron- and aluminum-doped cells.

2. Silicon solar cells having the same base resistivity differ little in sensitivity to 22 MeV proton irradiation, indicating that the effect of the doping element on the cell's sensitivity to protons at this energy is insignificant.

3. The critical fluxes for short-circuit current and maximum power of 1 ohm-cm aluminum-doped cells were from 1.2 to 1.5 times higher than the critical fluxes of 1 ohm-cm boron-doped cells after irradiation with 2.4 MeV electrons. However, for the 10 ohm-cm cells, the critical fluxes of the boron-doped cells were higher than those of the aluminum-doped cells by about the same factor.

4. When evaluated under the solar simulator, the percentage degradation of open-circuit voltage with irradiation is approximately 1/2 the percentage degradation of short-circuit current for both boron- and aluminum-doped cells.

5. In the temperature range from 32° C to 71° C, short-circuit current of both boron- and aluminum-doped cells increases linearly and maximum power and open-circuit voltage decrease linearly with increasing temperature before and after irradiation with 2.4 MeV electrons and 22 MeV protons.

6. The temperature coefficients of the various parameters under investigation changed with irradiation. However, there was no significant difference in temperature coefficients between the aluminum-doped and boron-doped cells having the same resistivity.

7. The effect of irradiation on the spectral response of aluminum-doped and boron-doped cells is nearly identical.

8. No recovery of the electrical properties was observed after 3 months' storage at room temperature following these radiation tests.

9. In most respects, the commercially produced aluminum-doped solar cells tested in this investigation and the boron-doped counterparts were found to be equally resistant to high-energy particulate radiation.

Langley Research Center,
National Aeronautics and Space Administration,
Langley Station, Hampton, Va., May 22, 1967,
120-33-01-01-23.

REFERENCES

1. Mandelkorn, Joseph; Kesperis, James; et al.: Comparison of p-n and n-p Silicon Solar Cells. Proceedings 14th Annual Power Sources Conference, U.S. Army Signal Res. Develop. Lab., May 1960, pp. 42-45.

2. Mandelkorn, J.; McAfee, C.; et al.: A New Radiation-Resistant High-Efficiency Solar Cell. Tech. Rept. 2162, U.S. Army Signal Res. Develop. Lab., Oct. 1960.

3. Rosenzweig, W.; Gummel, H. K.; and Smits, F. M.: Solar Cell Degradation Under 1 MeV Electron Bombardment. Nuclear Electronic Effects Program, Tenth Triannual Technical Note, ASD-TDR-62-808, U.S. Air Force, July 15, 1962, pp. 85-97.

4. Mandelkorn, Joseph; Schwartz, Lawrence; et al.: Effects of Impurities on Radiation Damage of Silicon Solar Cells. NASA TN D-2711, 1965.

5. Mandelkorn, Joseph; Schwartz, Lawrence; et al.: Effects of Impurities on Radiation Damage of Silicon Solar Cells. J. Appl. Phys. (Commun.), vol. 35, no. 7, July 1964, pp. 2258-2260.

6. Statler, R. L.: Electron-Bombardment Damage in Silicon Solar Cells. NRL Rept. 6091, U.S. Naval Res. Lab., Oct. 7, 1964.

7. Brandhorst, Henry W., Jr.: Airplane Testing of Solar Cells. Proceedings of the Fourth Photovoltaic Specialists Conference. Volume II – Thin Film Solar Cells and Solar Cell Testing, PIC-SOL 209/5.1, Interagency Advanced Power Group, Aug. 1964, pp. C-2-1 – C-2-17.

8. Hulten, W. C.; Honaker, W. C.; and Patterson, John L.: Irradiation Effects of 22 and 240 MeV Protons on Several Transistors and Solar Cells. NASA TN D-718, 1961.

9. Haynes, Gilbert A.; and Miller, William E.: Effects of 1.2 and 0.30 MeV Electrons on the Optical Transmission Properties of Several Transparent Materials. NASA TN D-2620, 1965.

10. Cunningham, Brian T.; Sharp, Robert L.; and Slifer, Luther W.: The Electrical Characteristics of Irradiated Silicon Solar Cells as a Function of Temperature. Proceedings of the Fourth Photovoltaic Specialists Conference. Volume I - Radiation Effects on Solar Cells and Photovoltaic Devices, PIC-SOL 209/5, Interagency Advanced Power Group, Aug. 1964, pp. A-7-1 – A-7-43.

11. Martin, J. H.; Teener, J. W.; and Ralph, E. L.: Some Effects of Electron Irradiation and Temperature on Solar Cell Performance. Proceedings 17th Annual Power Sources Conference, U.S. Army Electron. Res. Develop. Lab., May 1963, pp. 15-19.

12. Johnson, F. S.: The Solar Constant. J. Meteorol., vol. 11, no. 6, Dec. 1954, pp. 431-439.

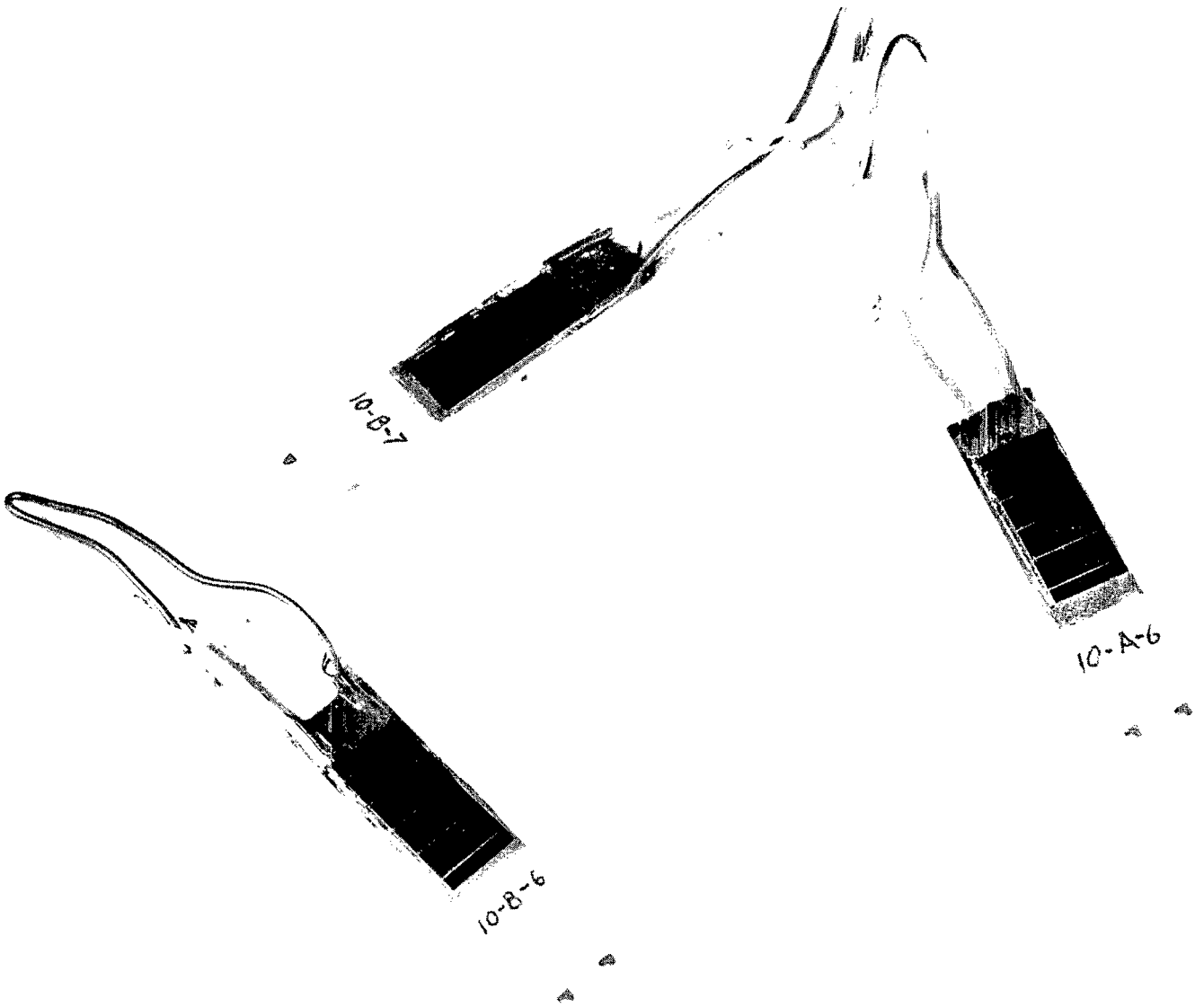

Figure 1.- Test solar cells mounted on anodized aluminum strips.

L-66-2973

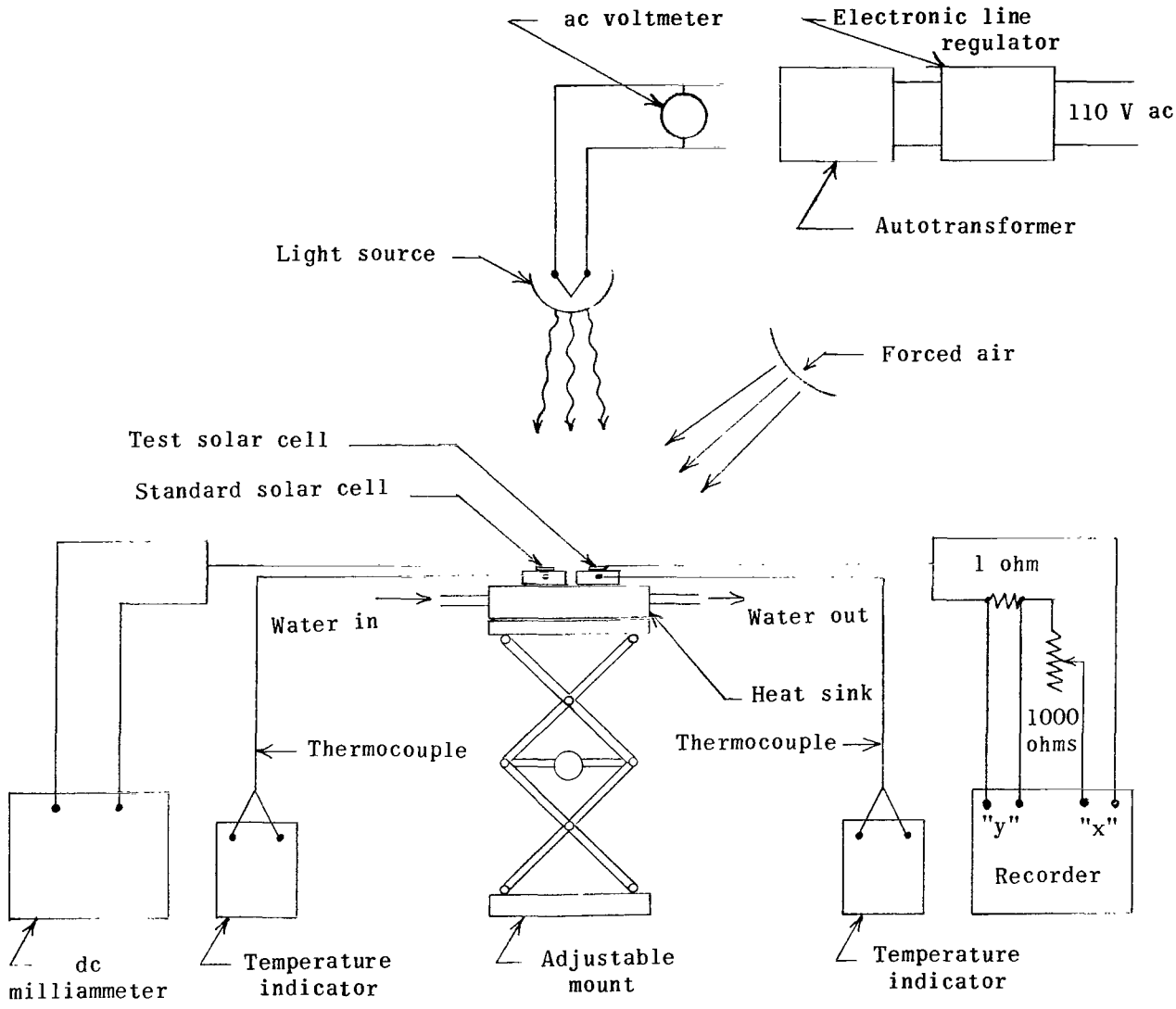

Figure 2.- Test setup for measurement of I-V characteristics of solar cells.

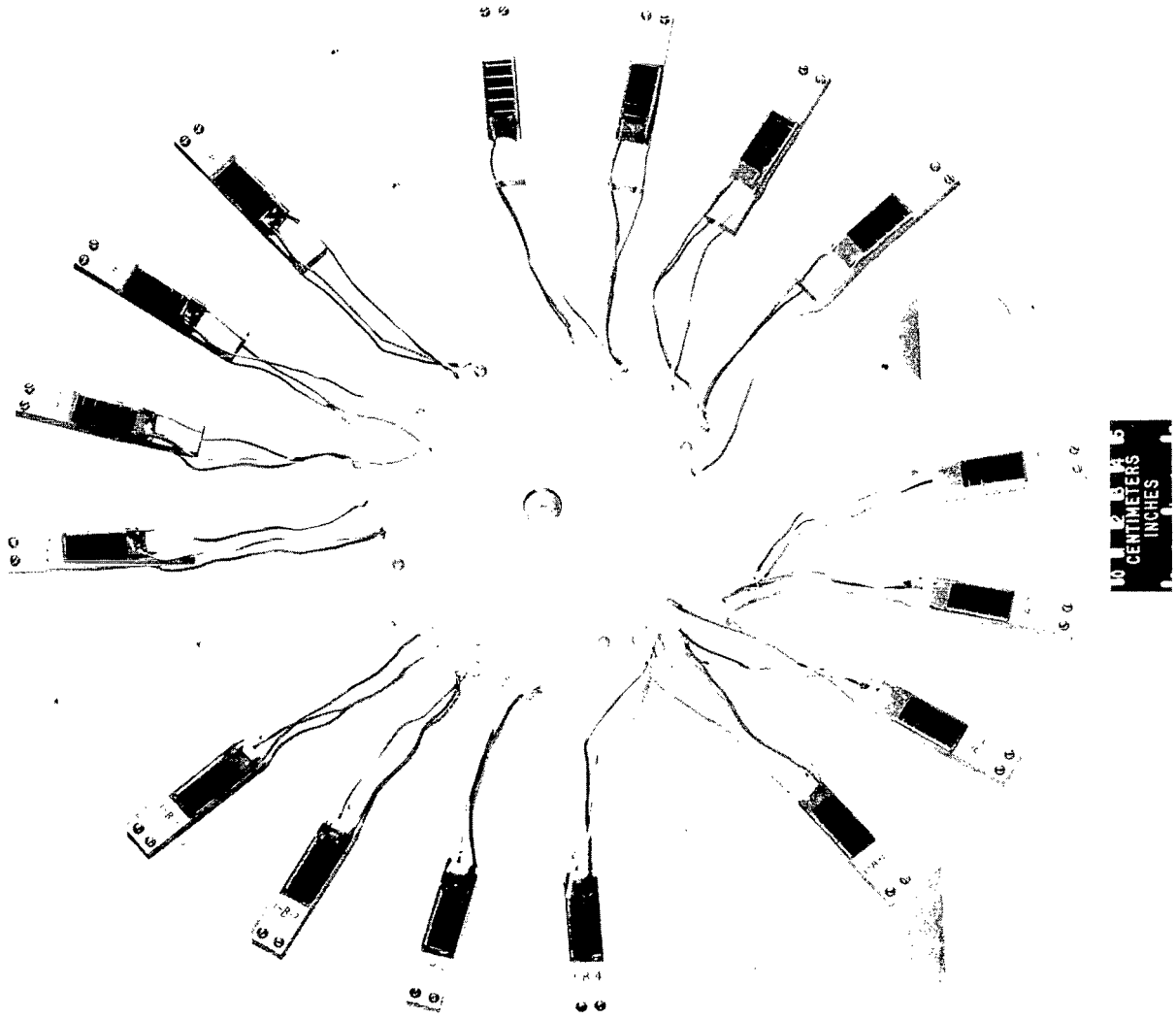

Figure 3.- Cells mounted on wheel for irradiation in the Oak Ridge cyclotron.

L-66-2971

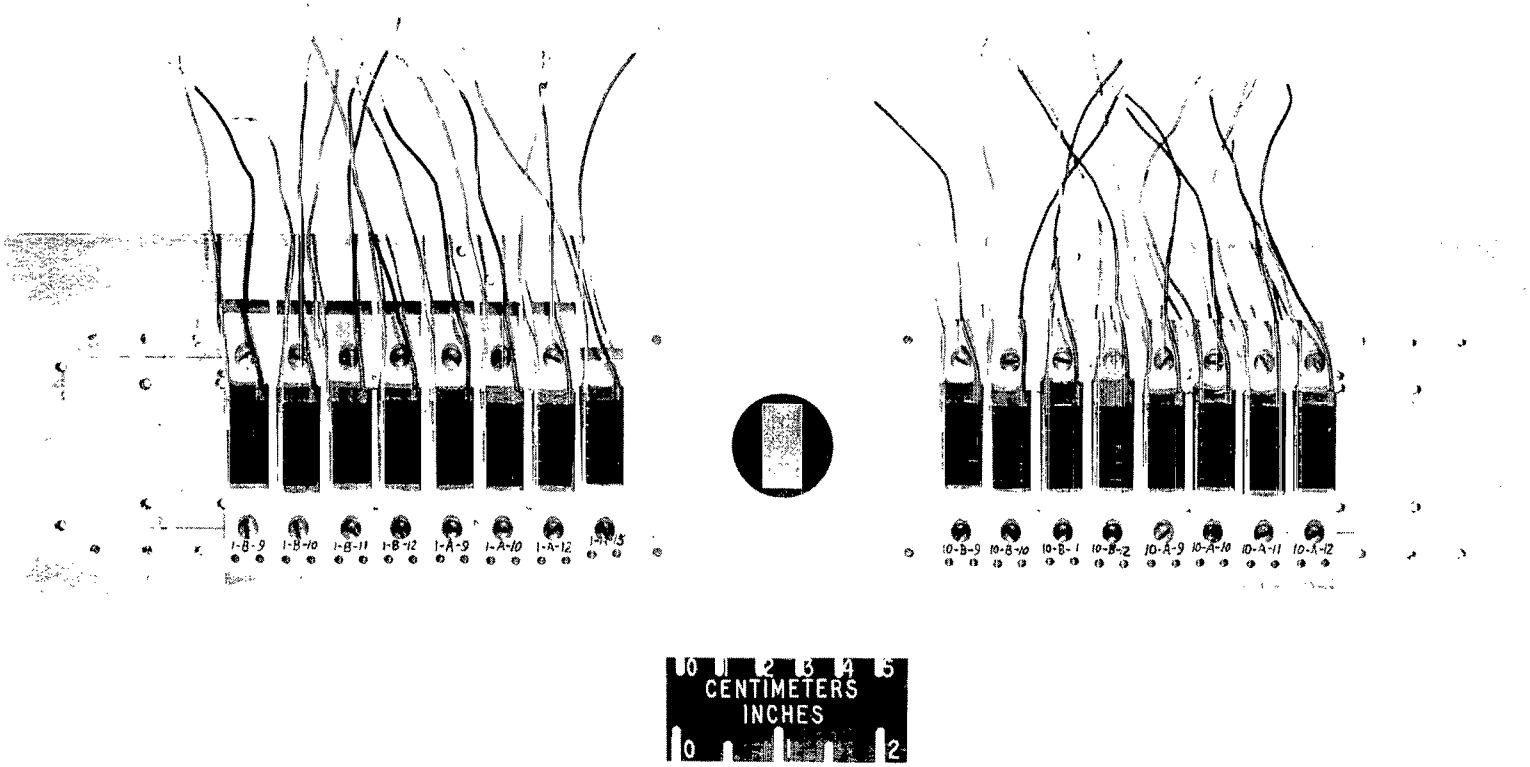

Figure 4.- Cells mounted on plate for irradiation in the electron accelerator at Langley Research Center. L-66-2972

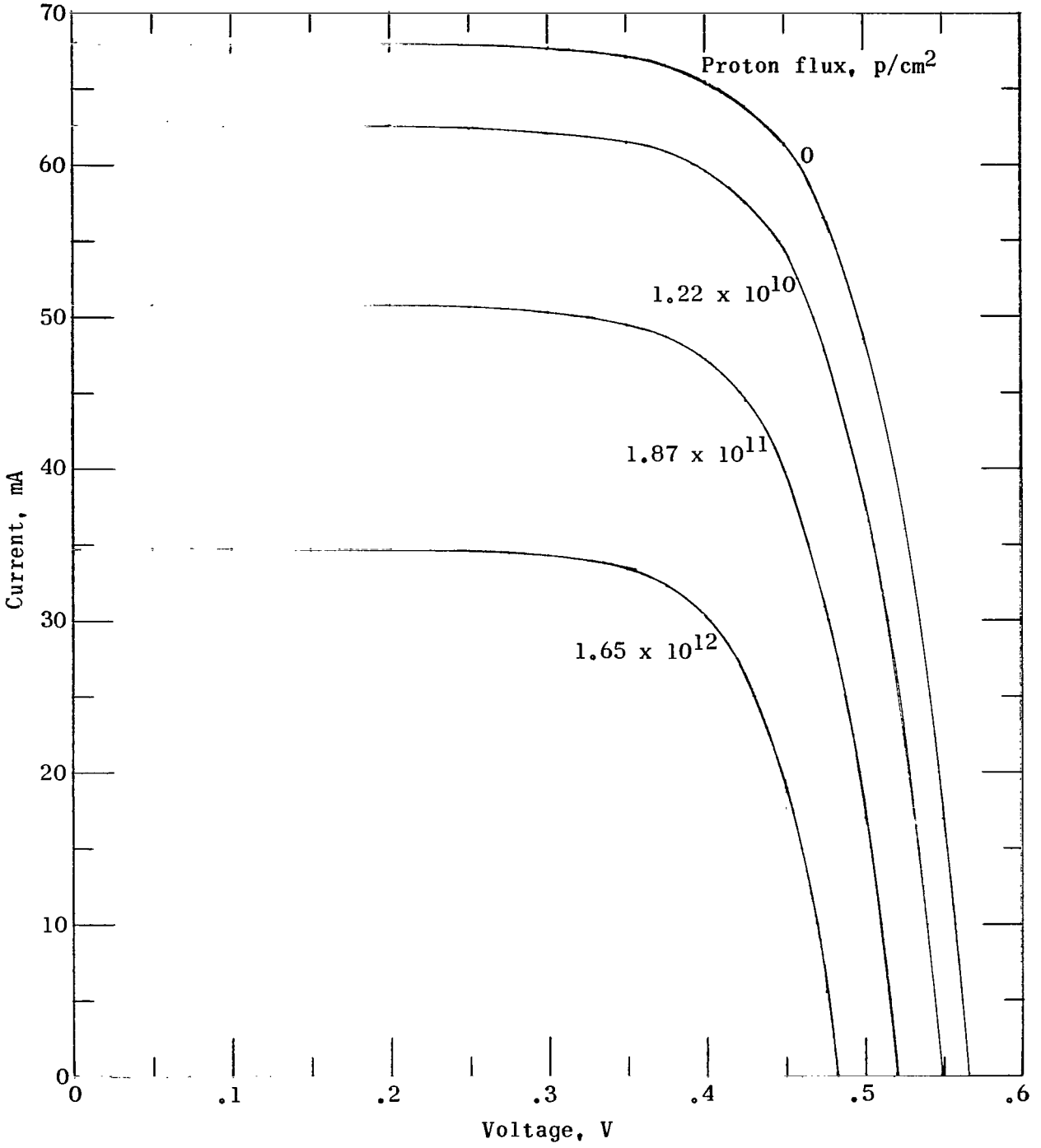

Figure 5.- Typical I-V characteristics of 1 ohm-cm boron-doped silicon solar cells before and after irradiation with 22 MeV protons.

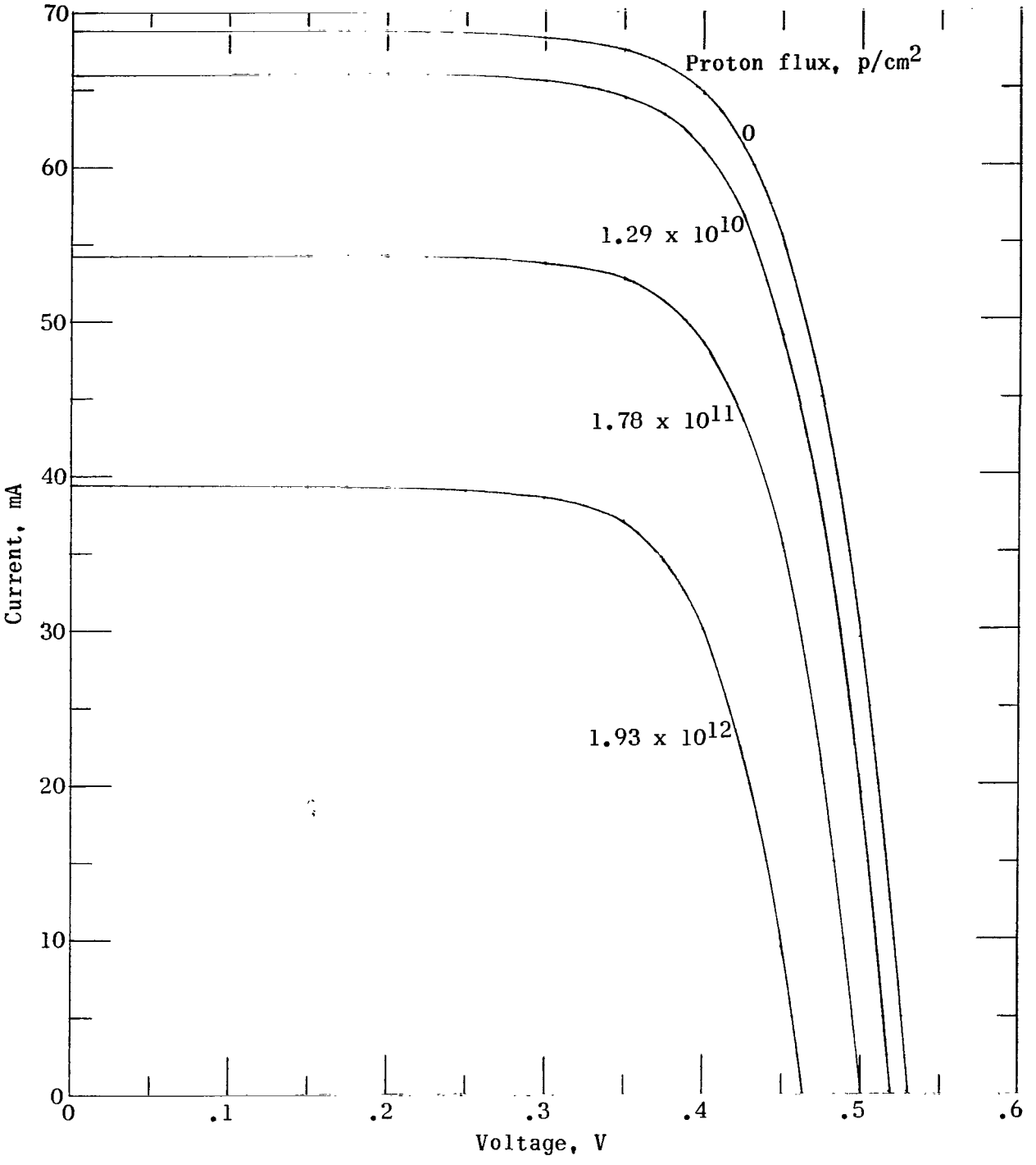

Figure 6.- Typical I-V characteristics of 10 ohm-cm boron-doped silicon solar cells before and after irradiation with 22 MeV protons.

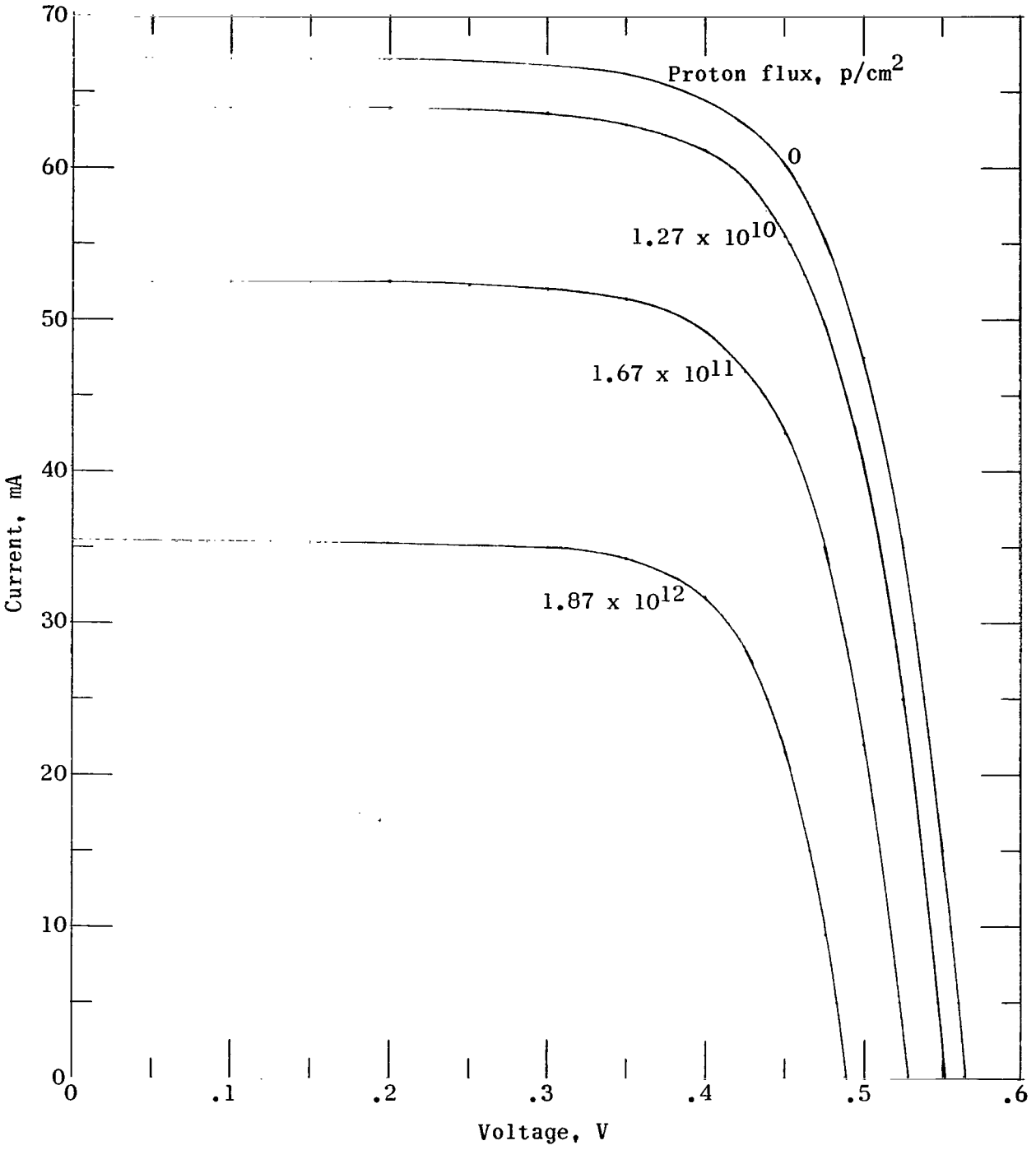

Figure 7.- Typical I-V characteristics of 1 ohm-cm aluminum-doped silicon solar cells before and after irradiation with 22 MeV protons.

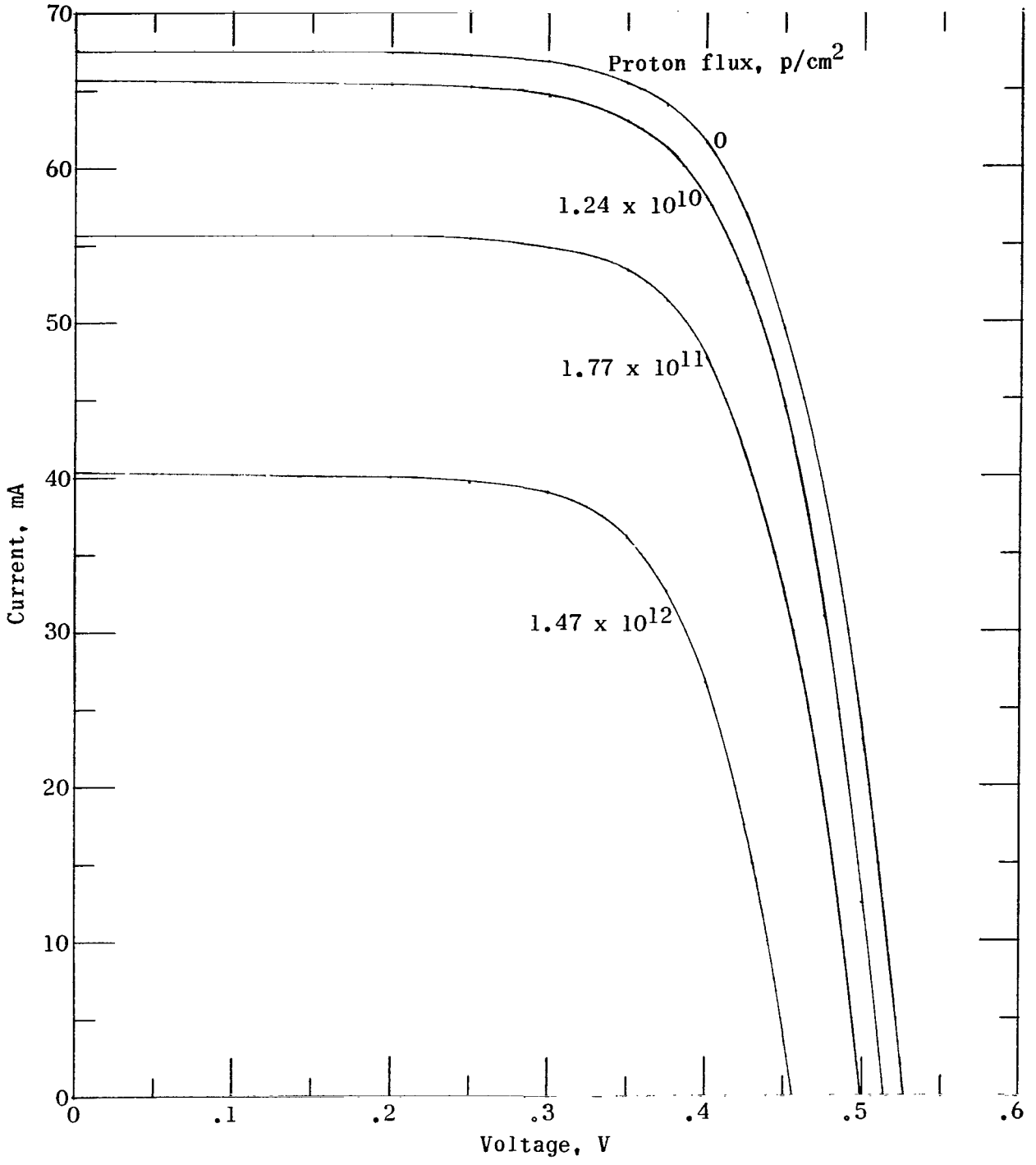

Figure 8.- Typical I-V characteristics of 10 ohm-cm aluminum-doped silicon solar cells before and after irradiation with 22 MeV protons.

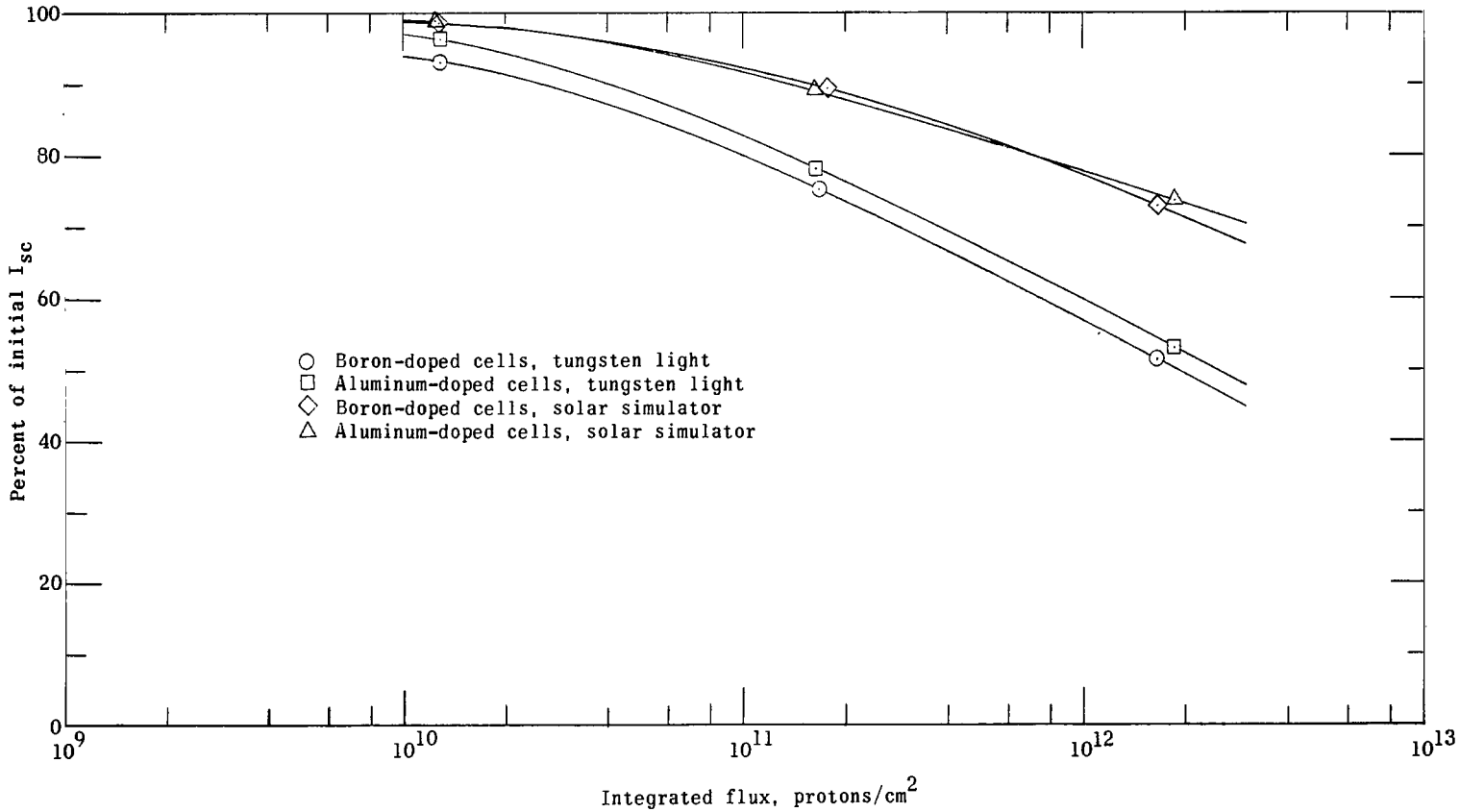

Figure 9.- Short-circuit current degradation of 1 ohm-cm silicon solar cells due to 22 MeV proton irradiation.

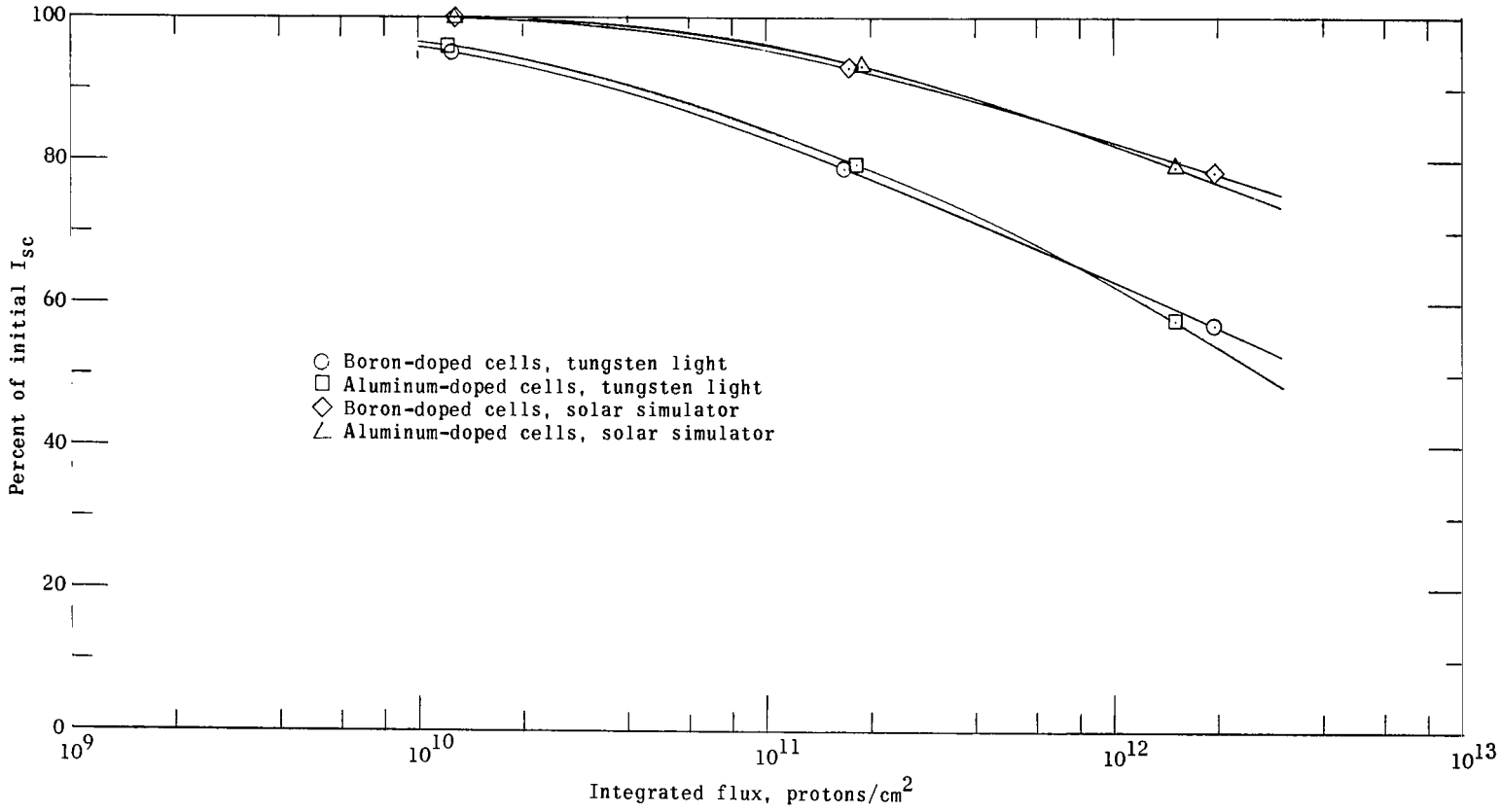

Figure 10.- Short-circuit current degradation of 10 ohm-cm silicon solar cells due to 22 MeV proton irradiation.

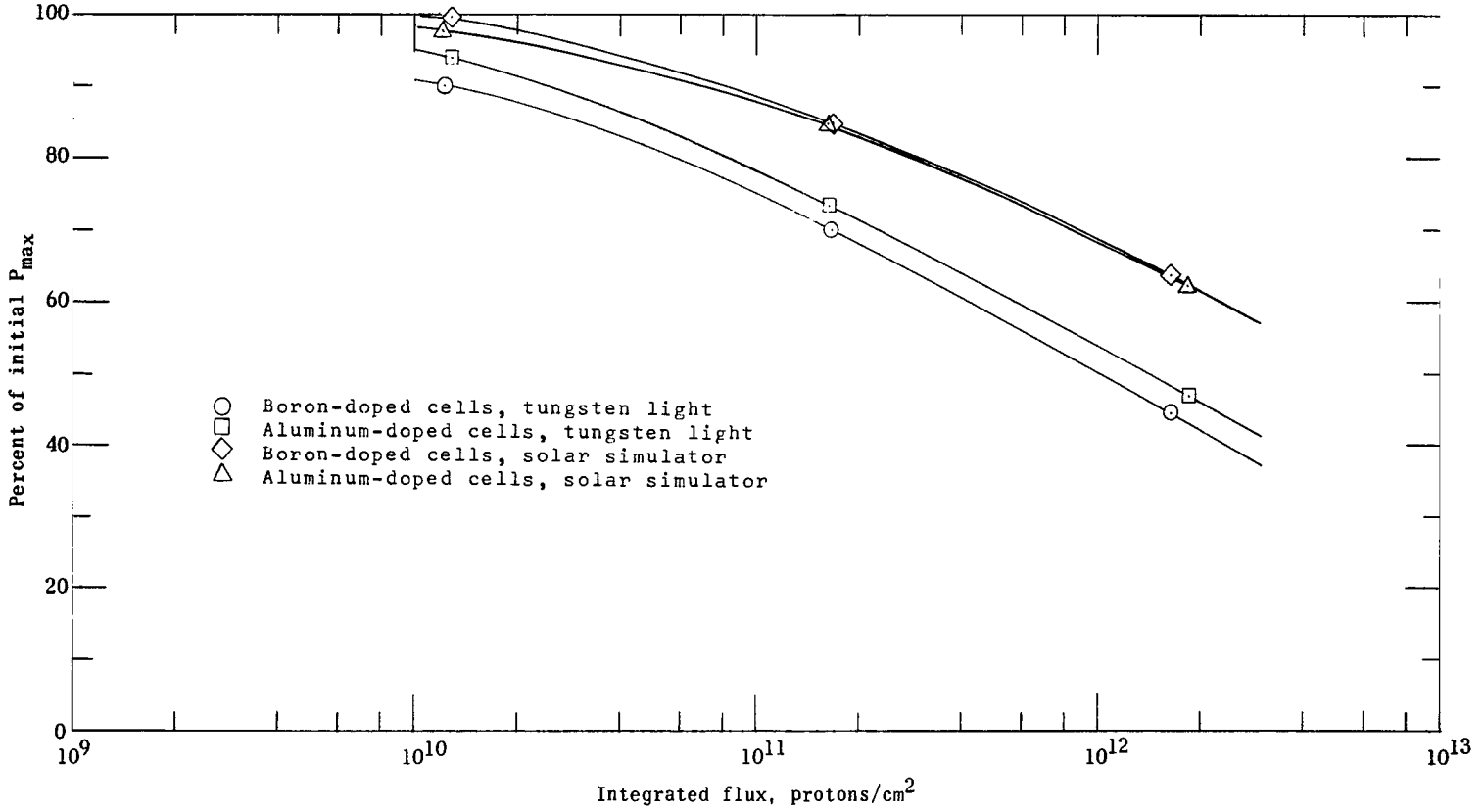

Figure 11.- Maximum-power degradation of 1 ohm-cm silicon solar cells due to 22 MeV proton irradiation.

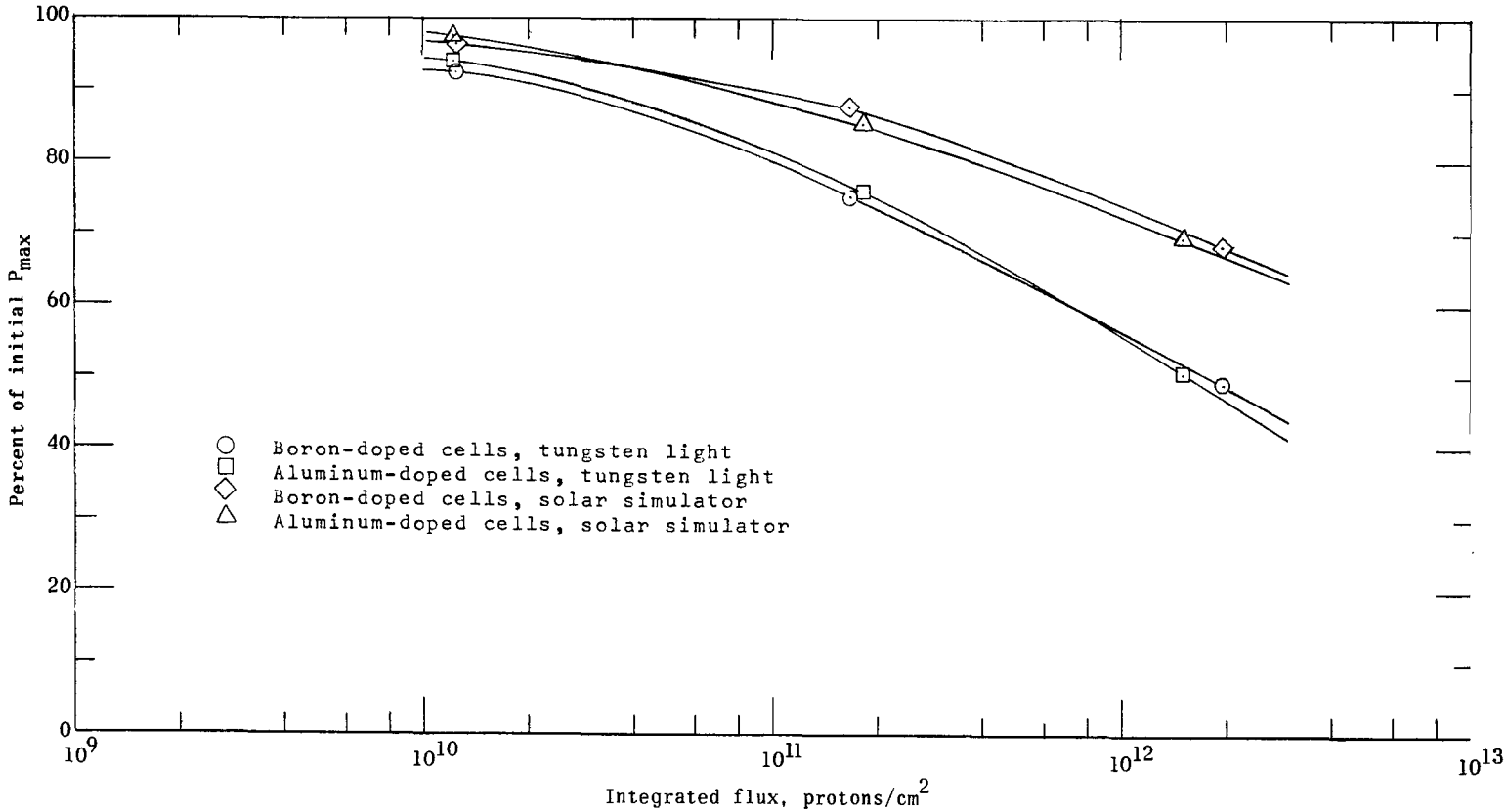

Figure 12.- Maximum-power degradation of 10 ohm-cm silicon solar cells due to 22 MeV proton irradiation.

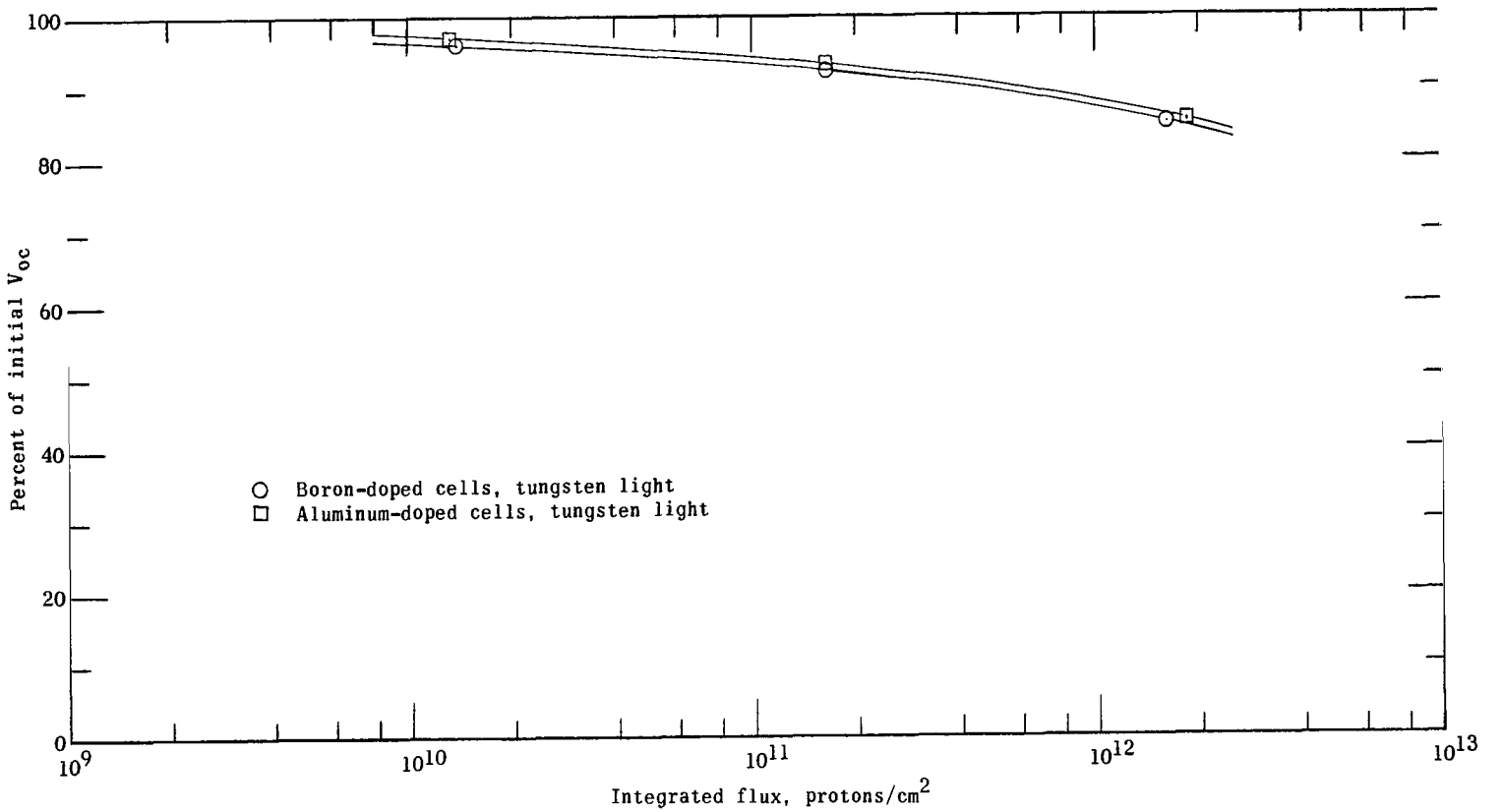

Figure 13. Open-circuit voltage degradation of 1 ohm-cm silicon solar cells due to 22 MeV proton irradiation.

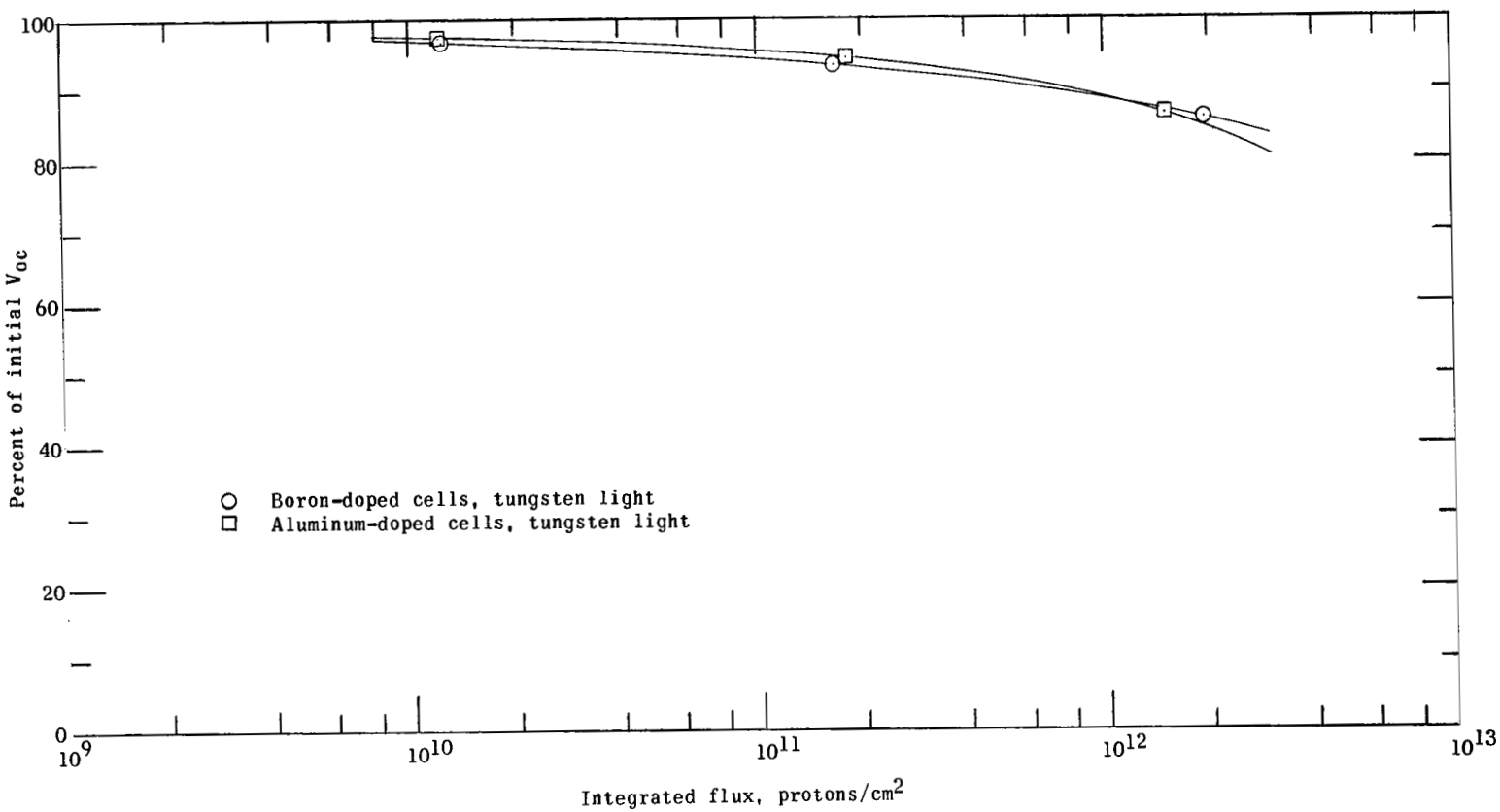

Figure 14.- Open-circuit voltage degradation of 10 ohm-cm silicon solar cells due to 22 MeV proton irradiation.

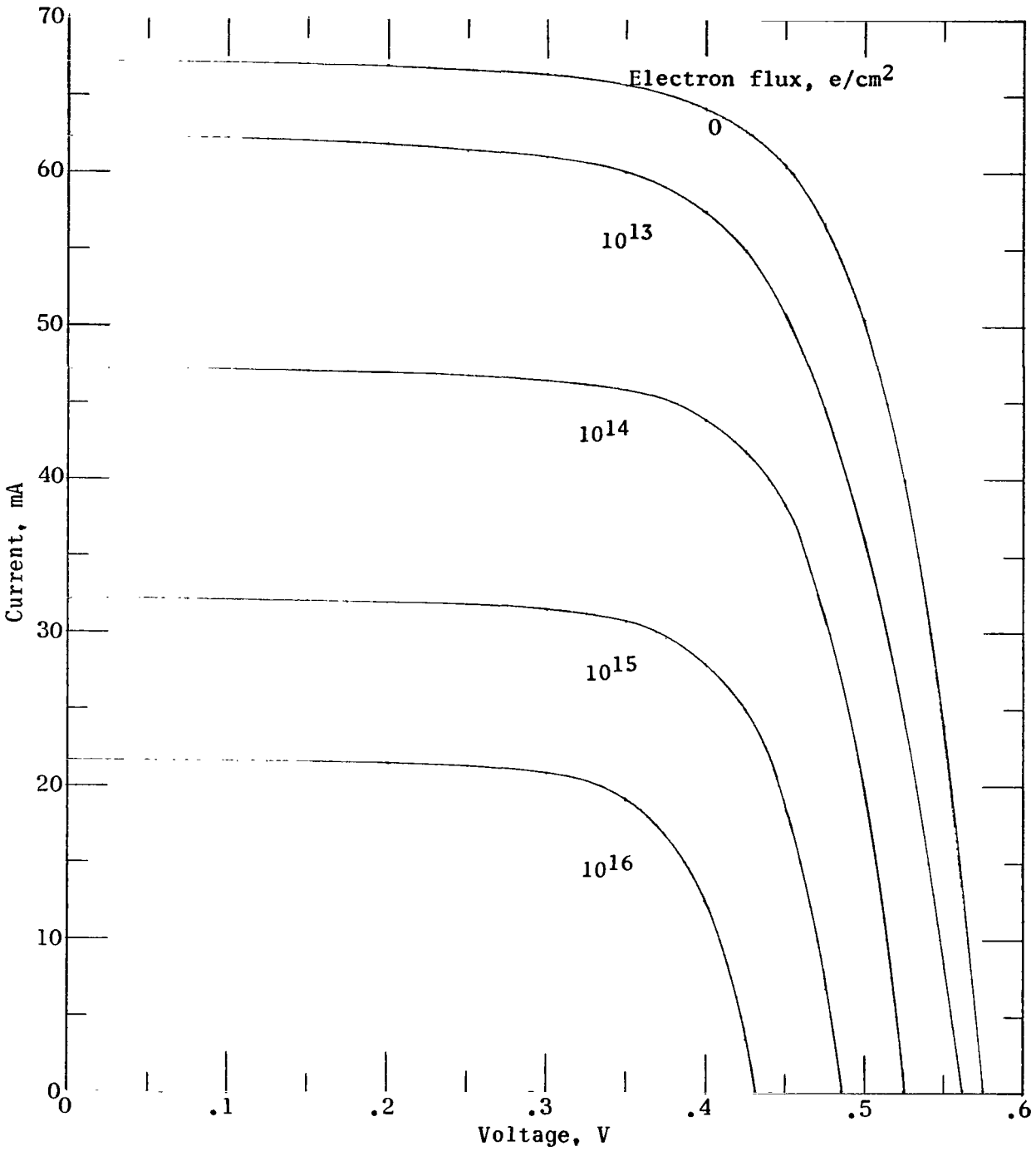

Figure 15.- Typical I-V characteristics of 1 ohm-cm boron-doped silicon solar cells before and after irradiation with 2.4 MeV electrons.

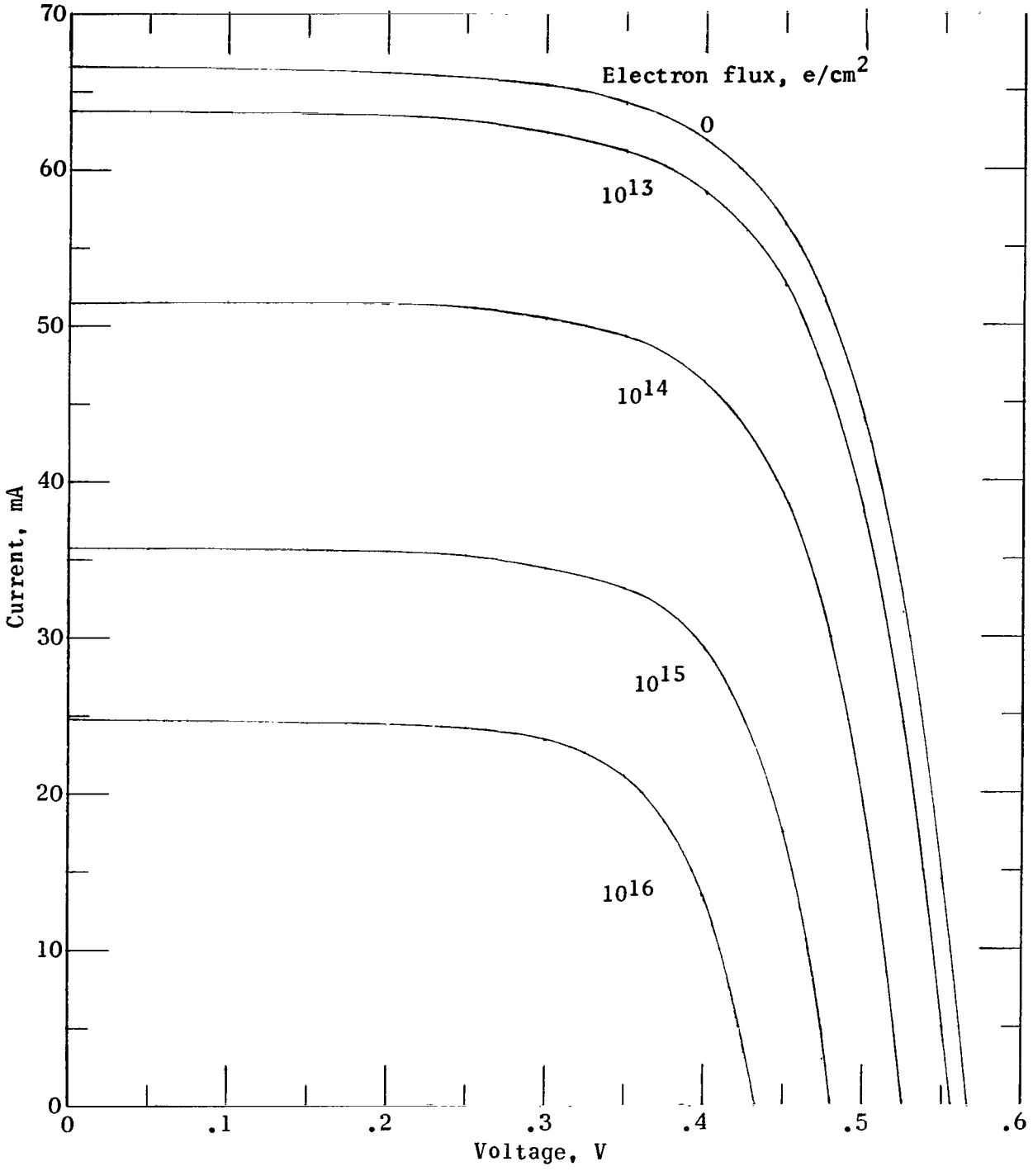

Figure 16.- Typical I-V characteristics of 1 ohm-cm aluminum-doped silicon solar cells before and after irradiation with 2.4 MeV electrons.

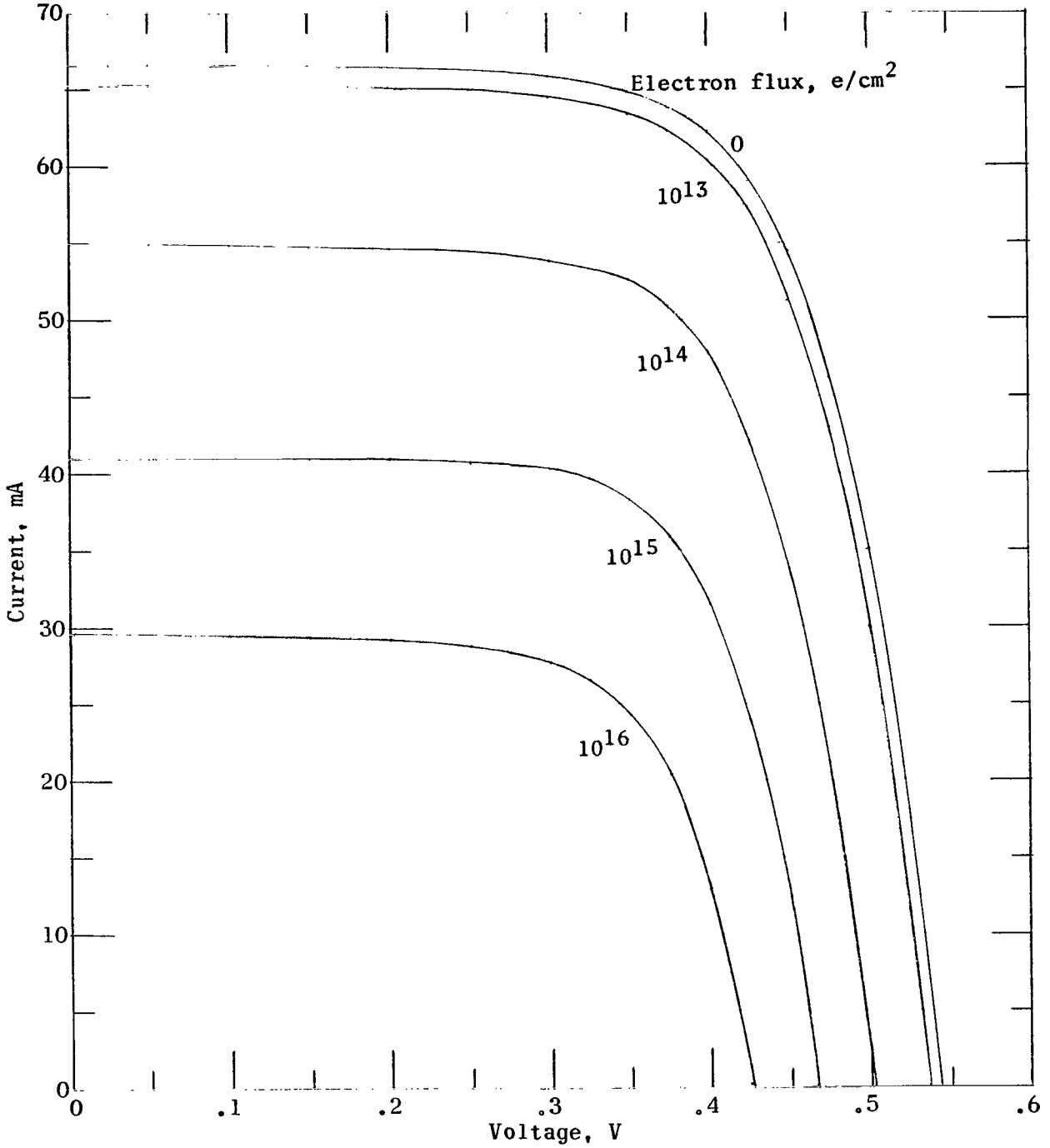

Figure 17.- Typical I-V characteristics of 10 ohm-cm boron-doped silicon solar cells before and after irradiation with 2.4 MeV electrons.

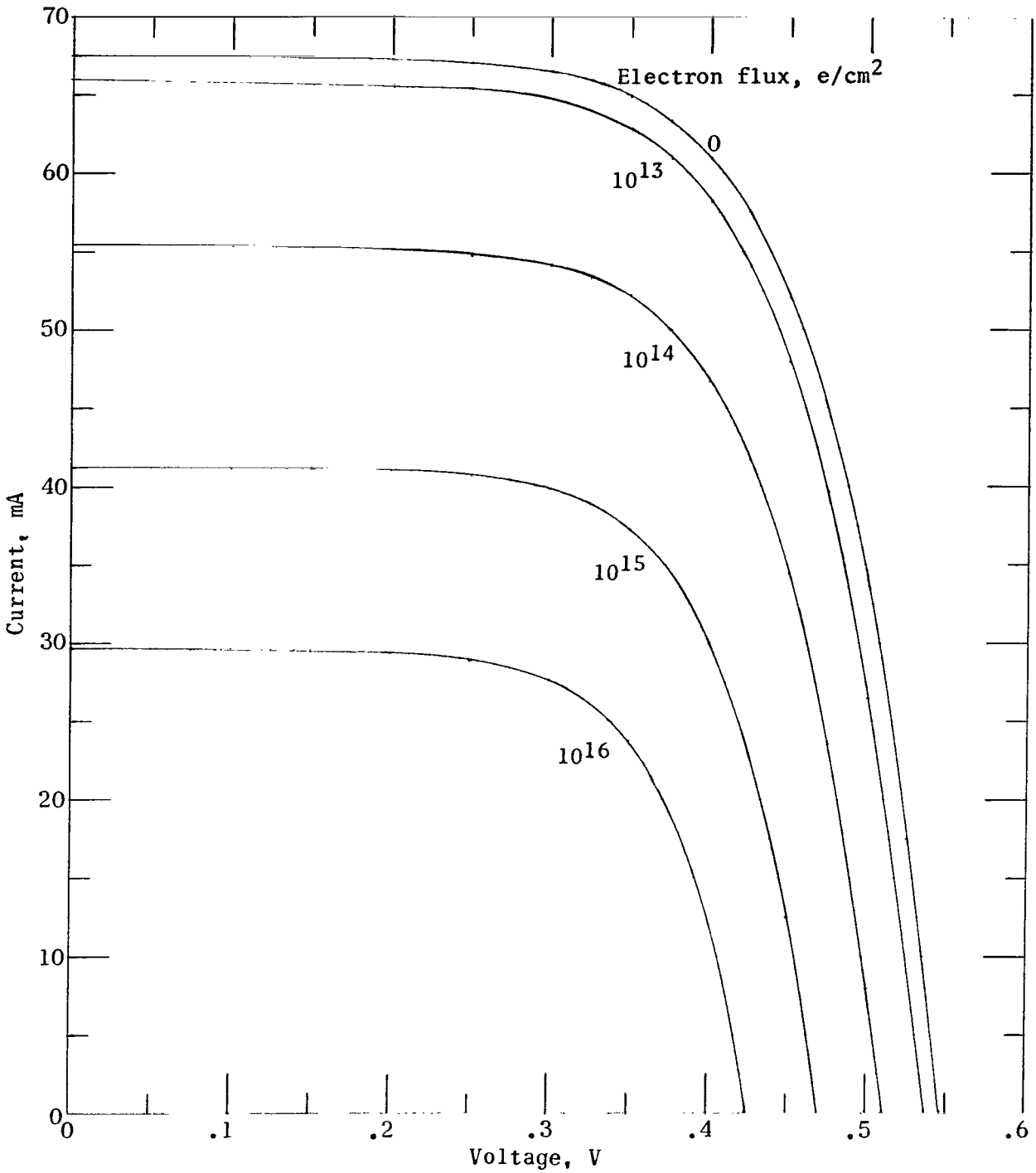

Figure 18.- Typical I-V characteristics of 10 ohm-cm aluminum-doped silicon solar cells before and after irradiation with 2.4 MeV electrons.

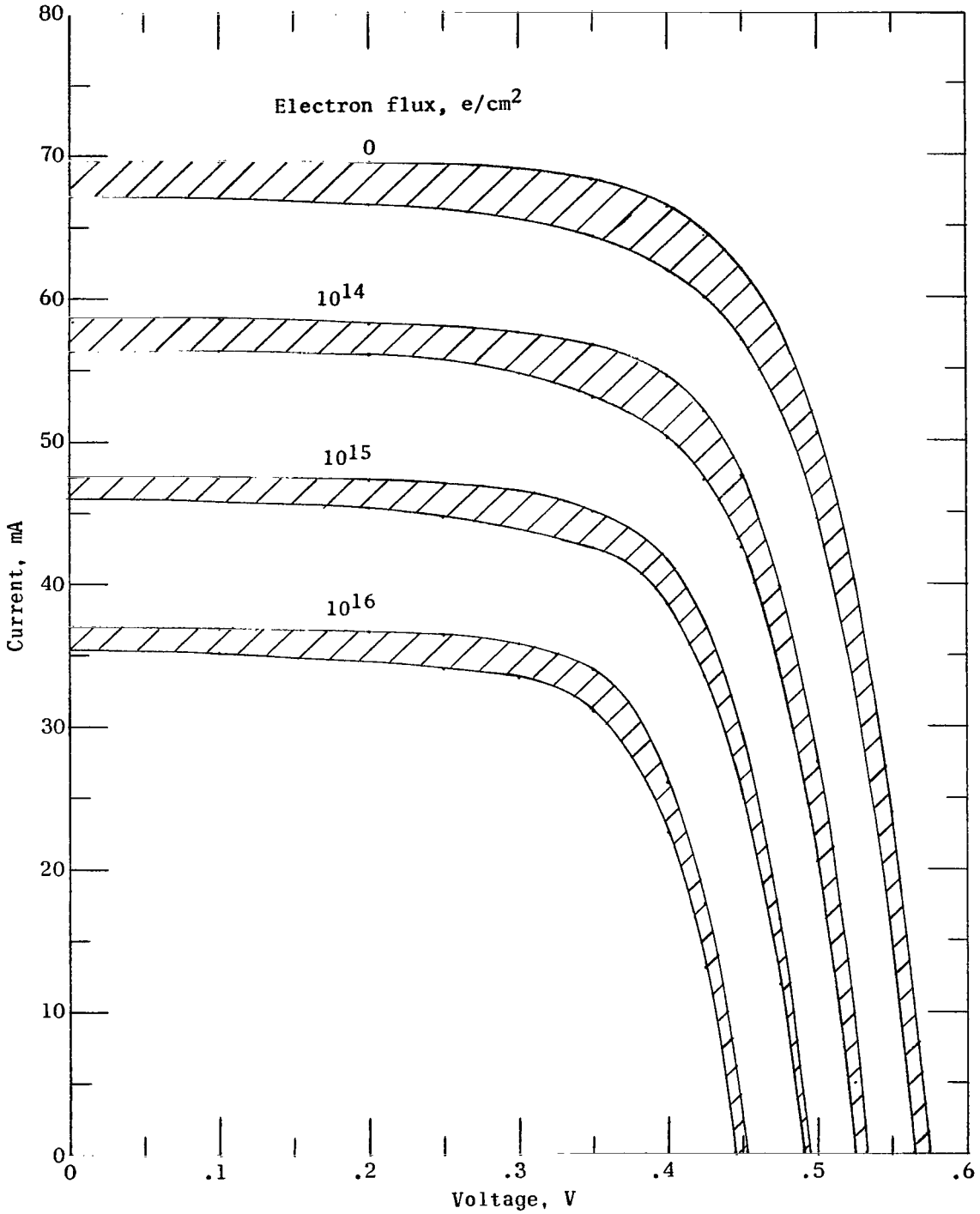

Figure 19.- I-V characteristics of 1 ohm-cm boron-doped silicon solar cells before and after irradiation with 2.4 MeV electrons.

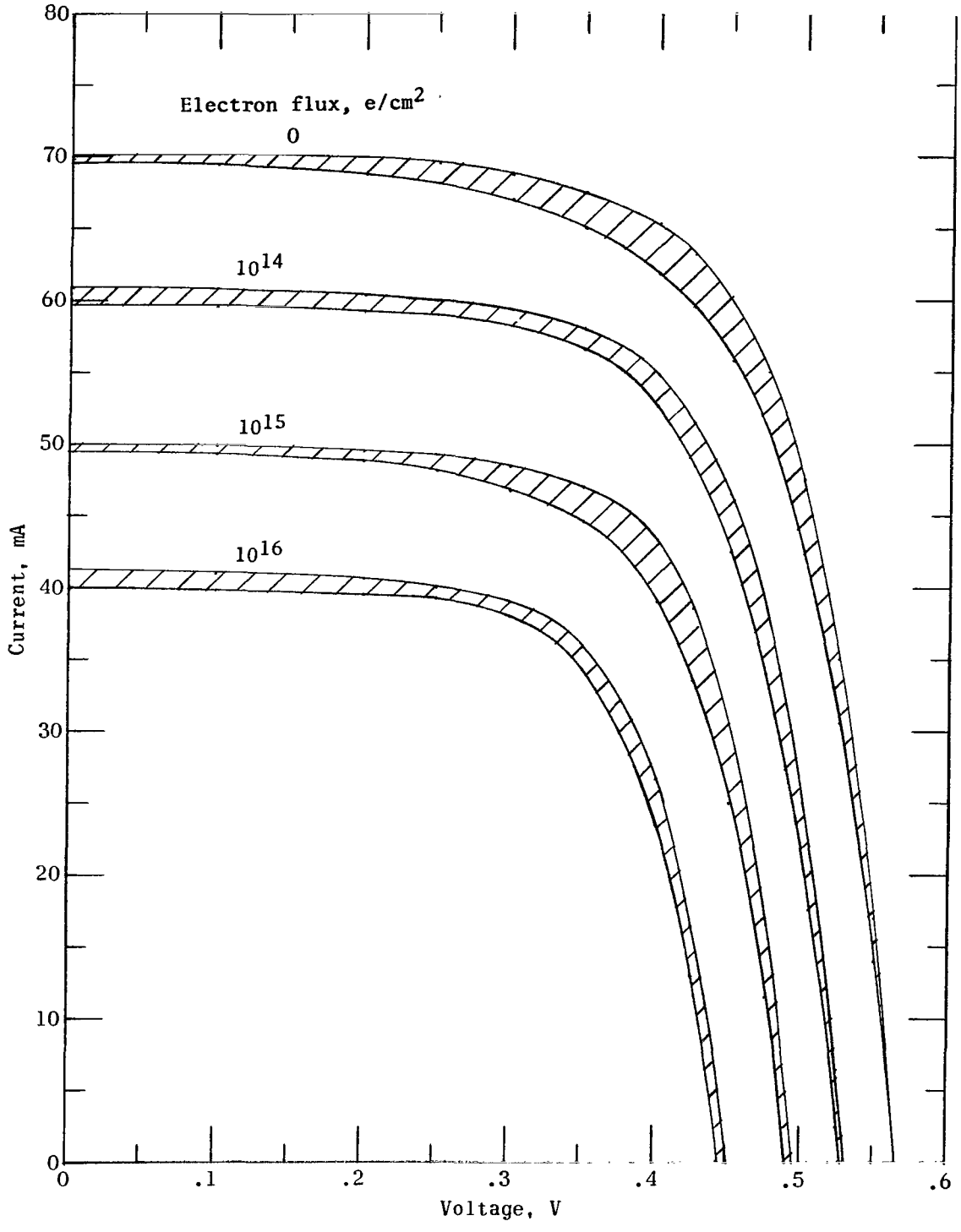

Figure 20.- I-V characteristics of 1 ohm-cm aluminum-doped silicon solar cells before and after irradiation with 2.4 MeV electrons.

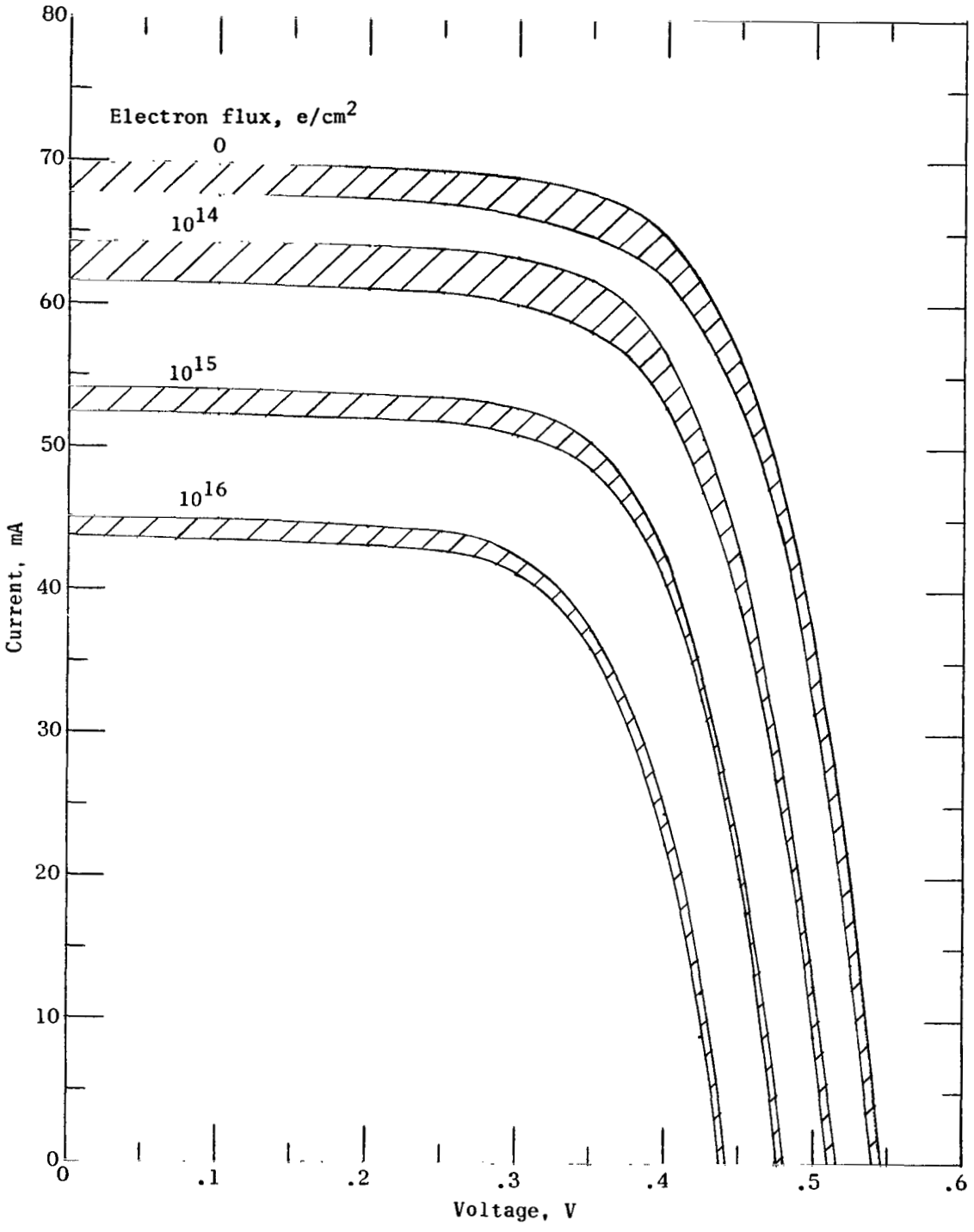

Figure 21.- I-V characteristics of 10-ohm-cm boron-doped silicon solar cells before and after irradiation with 2.4 MeV electrons.

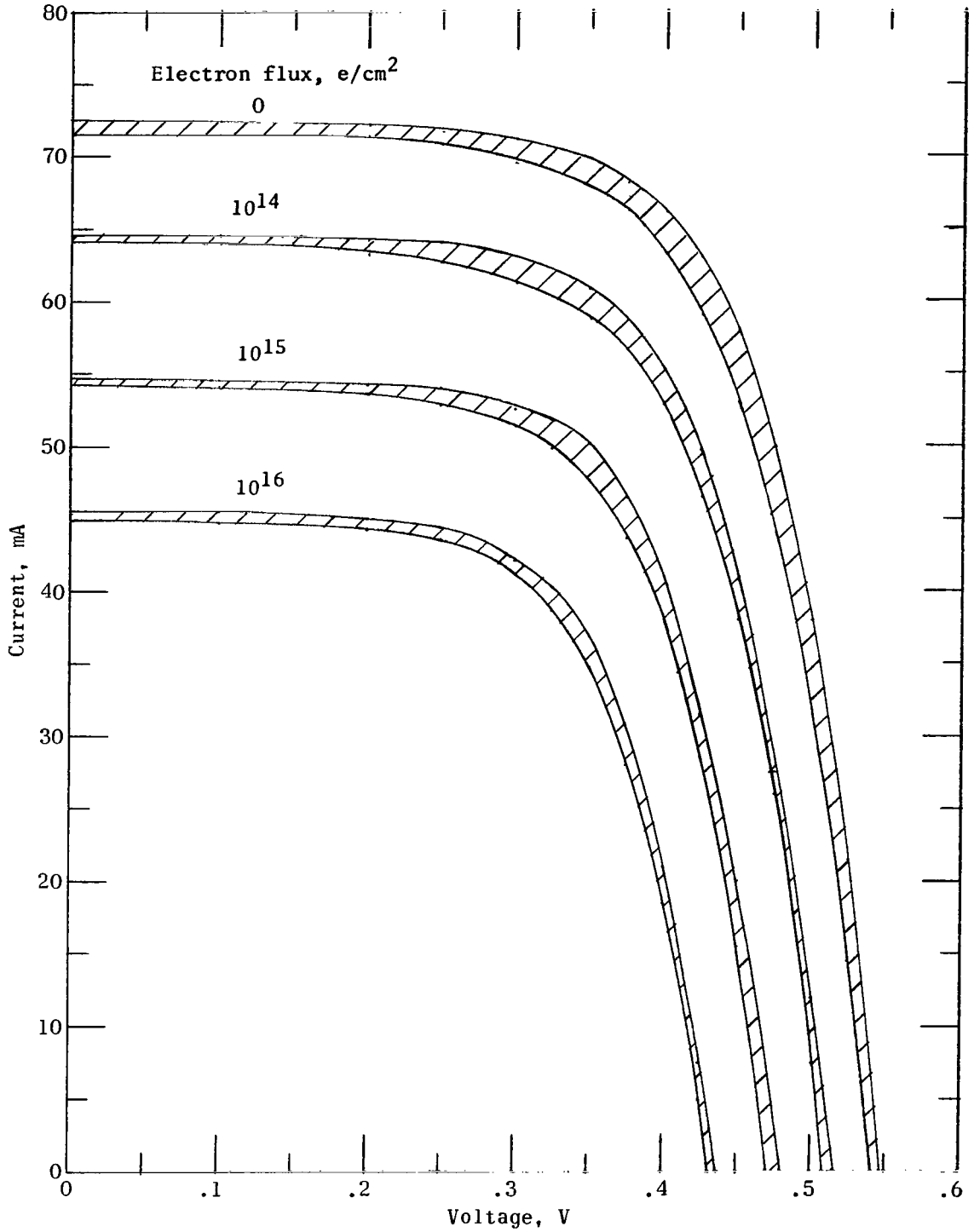

Figure 22.- I-V characteristics of 10 ohm-cm aluminum-doped silicon solar cells before and after irradiation with 2.4 MeV electrons.

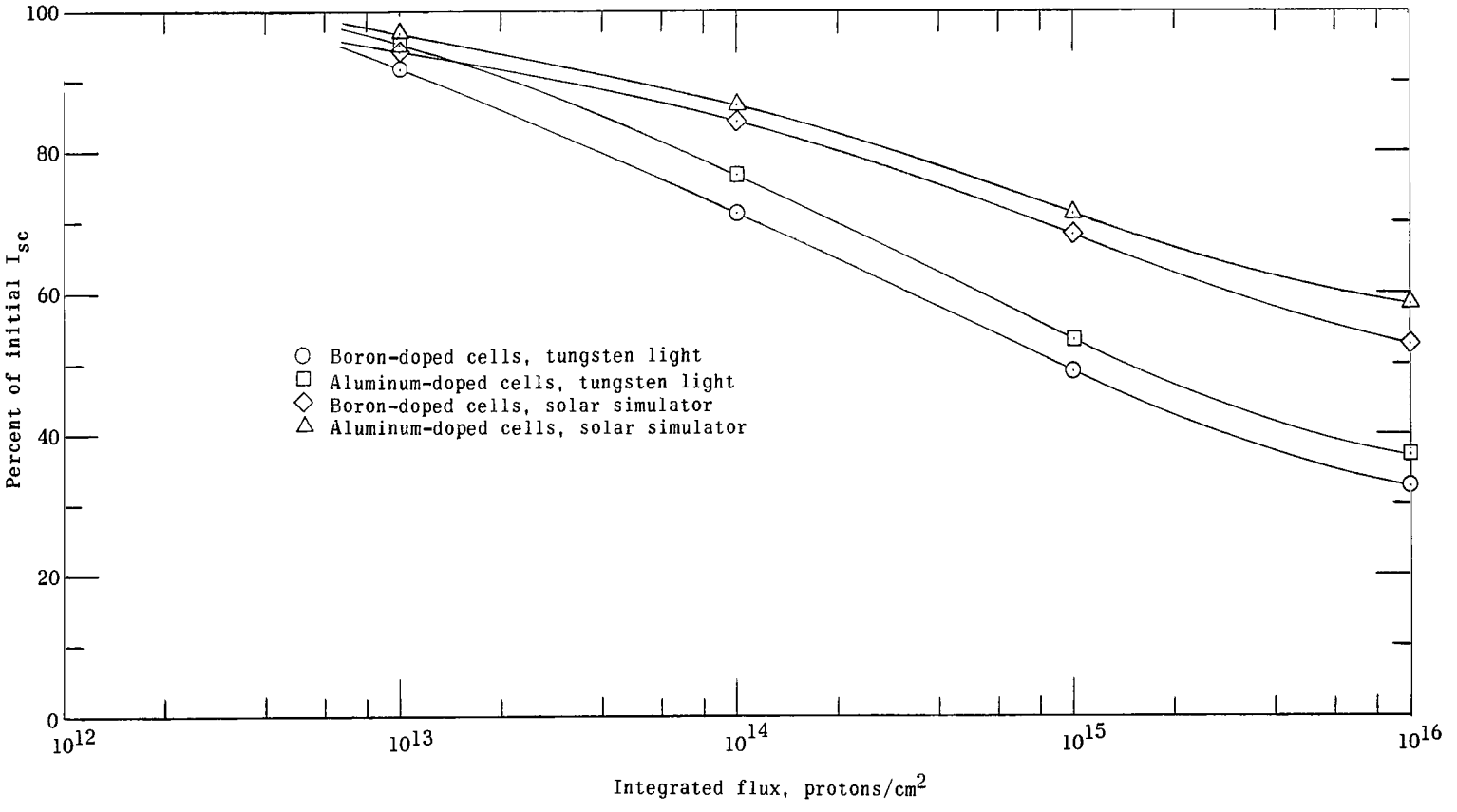

Figure 23.- Short-circuit current degradation of 1 ohm-cm silicon solar cells due to 2.4 MeV electron irradiation.

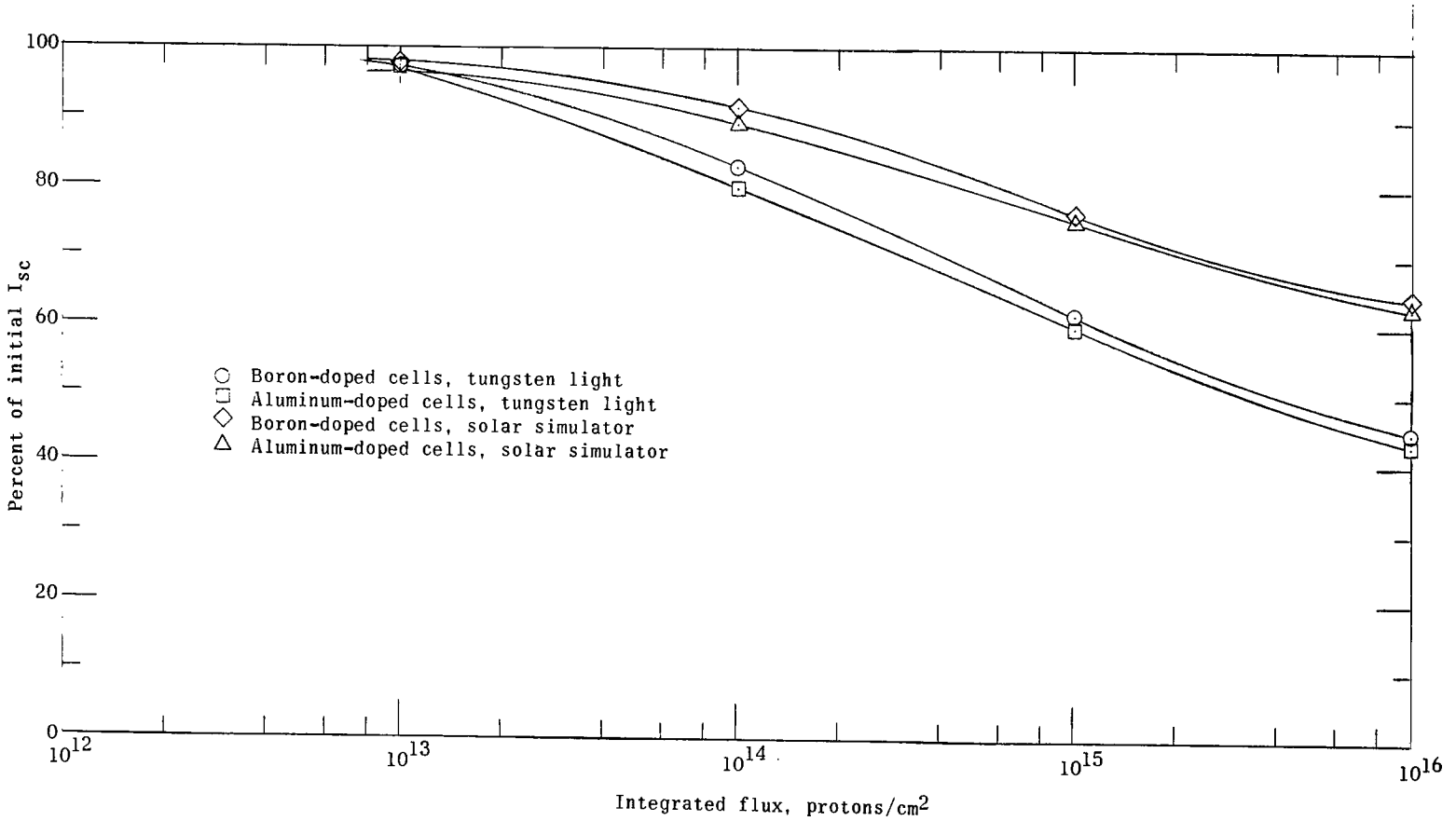

Figure 24.- Short-circuit current degradation of 10 ohm-cm silicon solar cells due to 2.4 MeV electron irradiation.

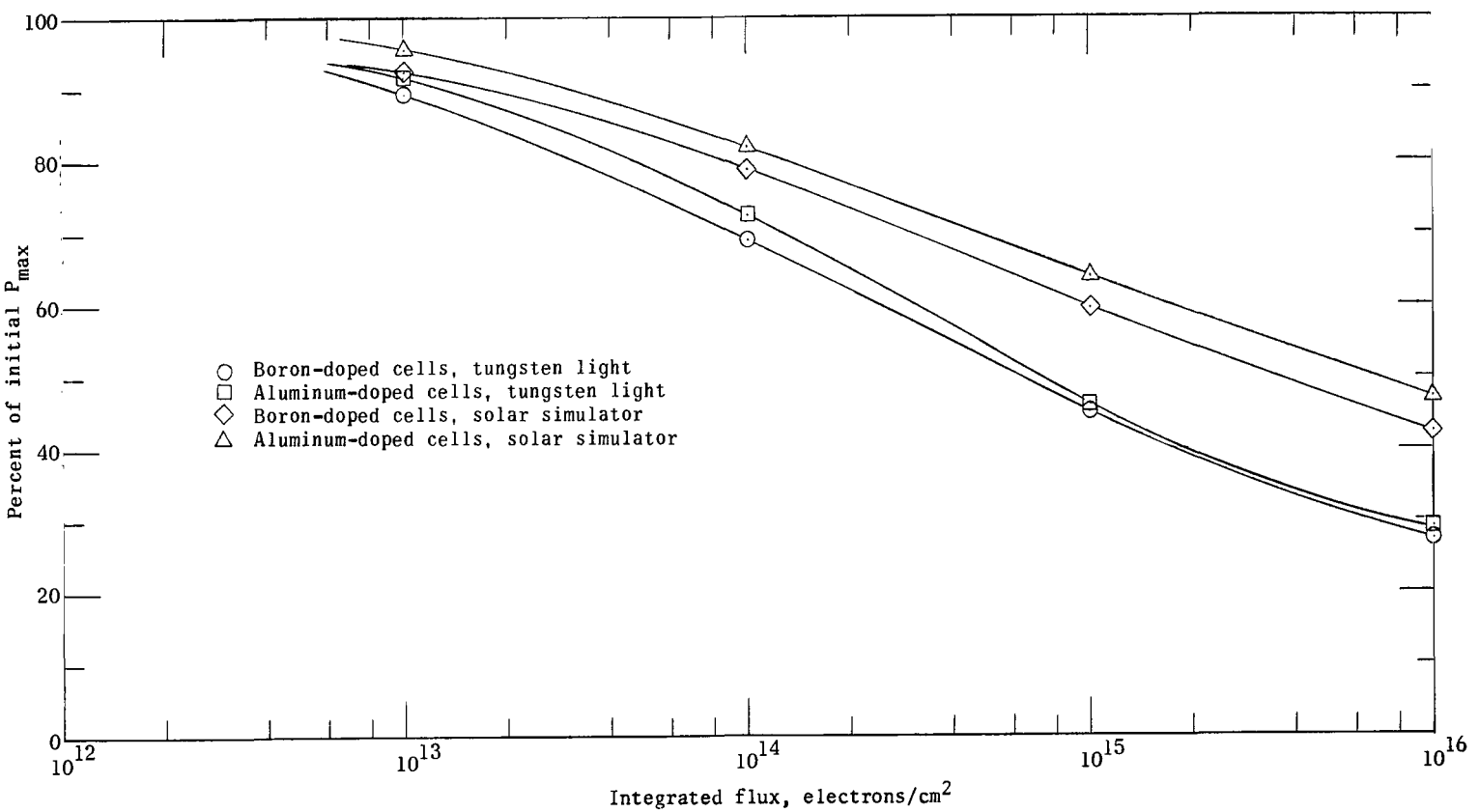

Figure 25.- Maximum-power degradation of 1 ohm-cm silicon solar cells due to 2.4 MeV electron irradiation.

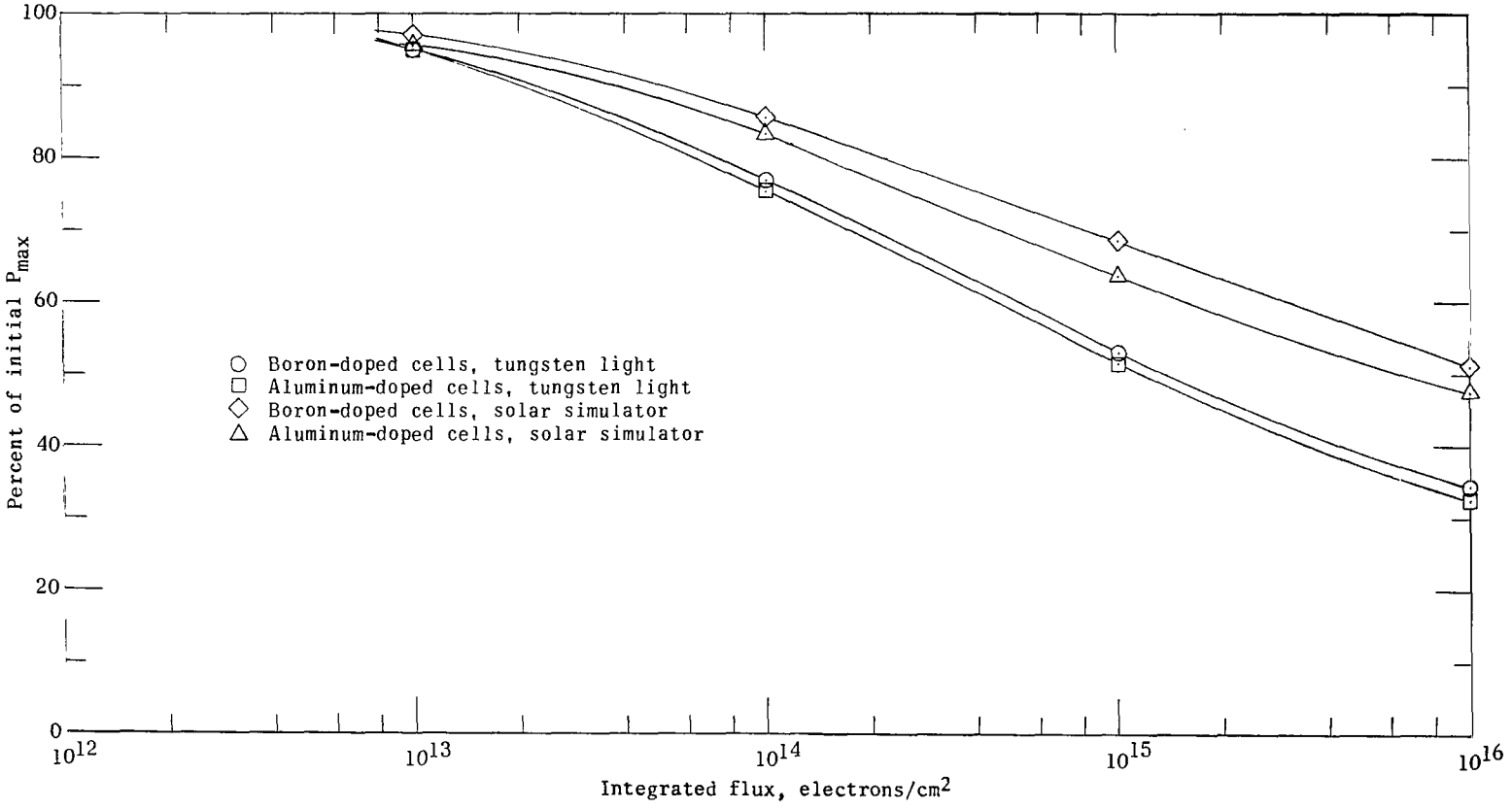

Figure 26.- Maximum-power degradation of 10 ohm-cm silicon solar cells due to 2.4 MeV electron irradiation.

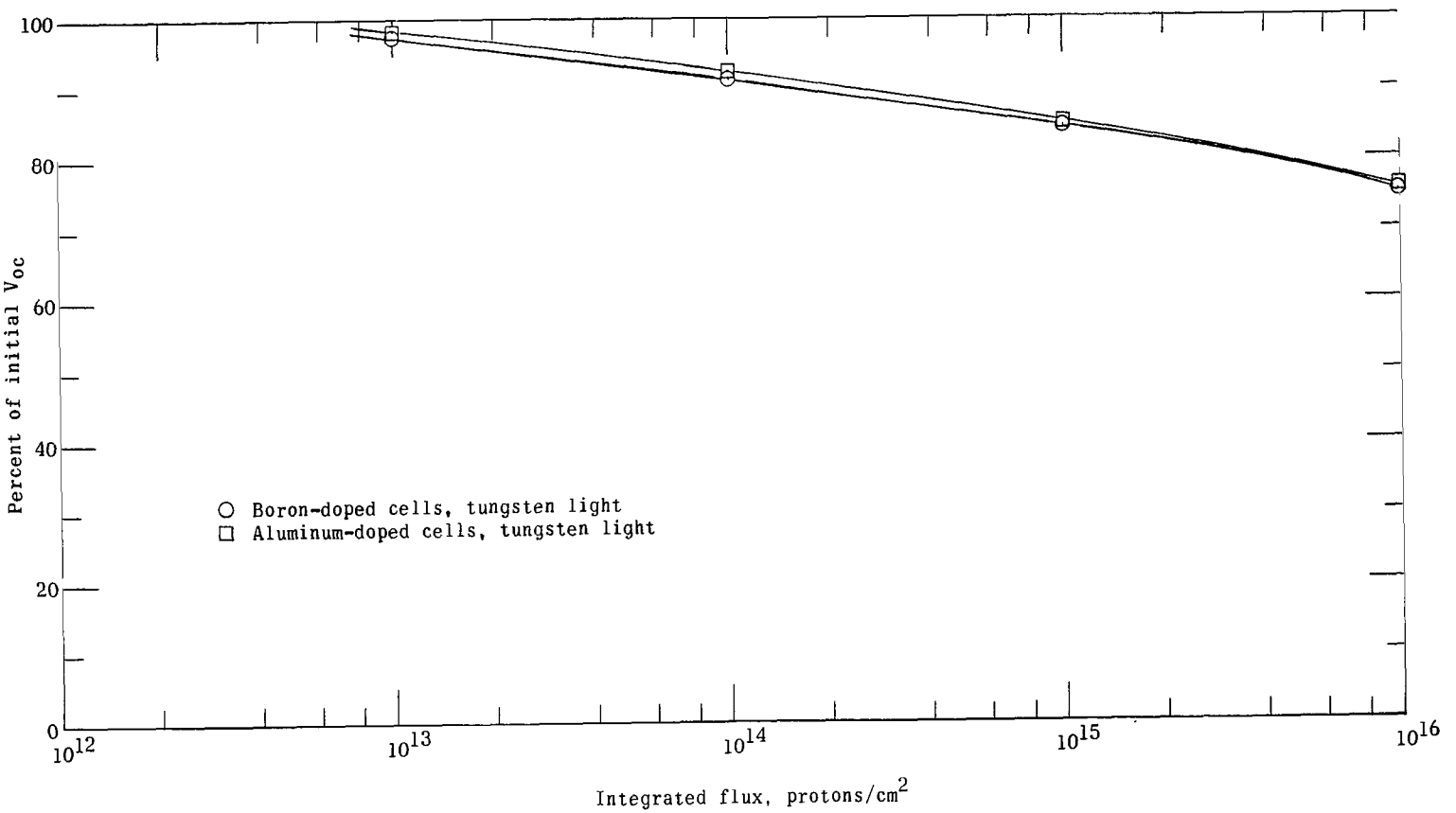

Figure 27.- Open-circuit voltage degradation of 1 ohm-cm silicon solar cells due to 2.4 MeV electron irradiation.

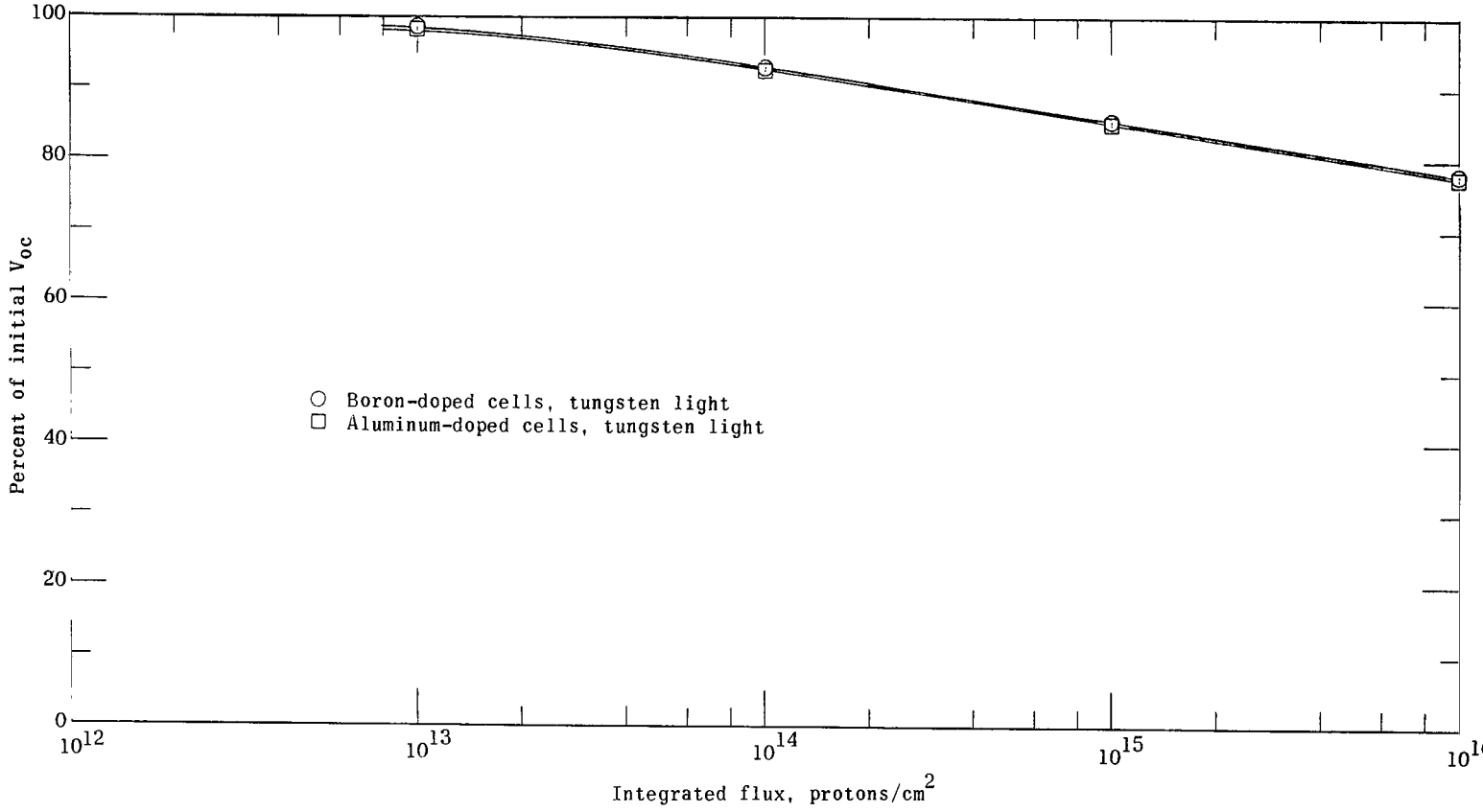

Figure 28.- Open-circuit voltage degradation of 10 ohm-cm silicon solar cells due to 2.4 MeV electron irradiation.

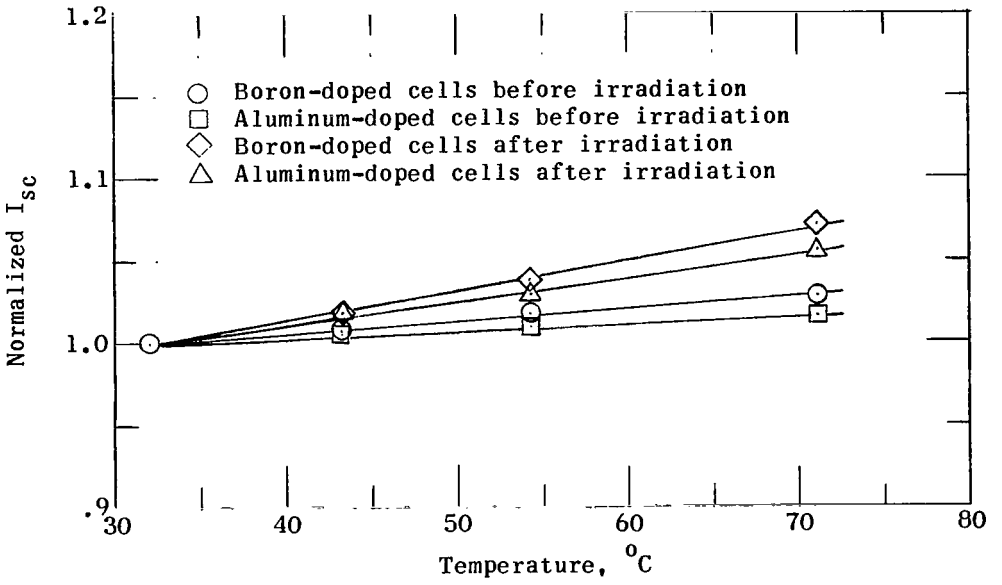

(a) Short-circuit current, normalized to 32° C.

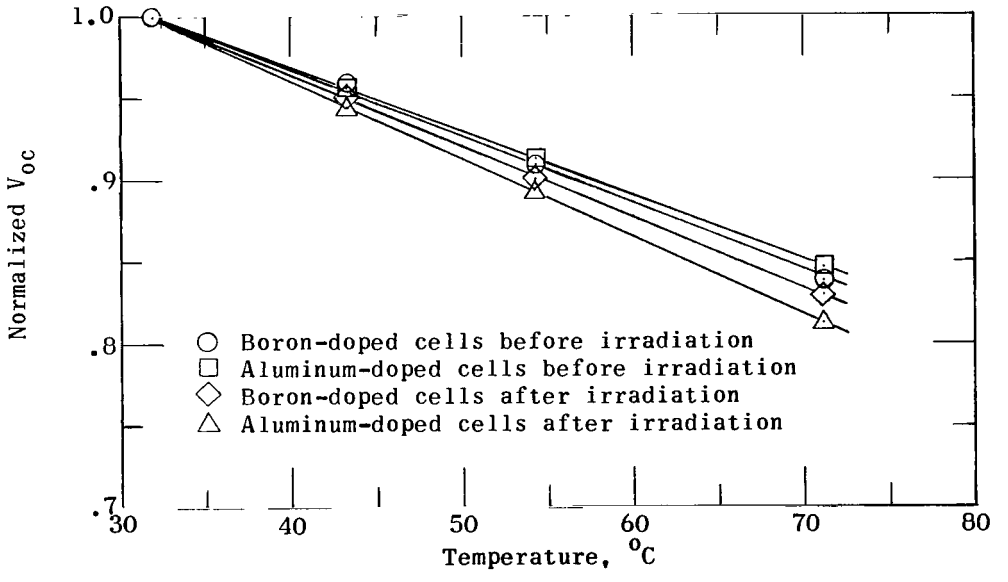

(b) Open-circuit voltage, normalized to 32° C.

Figure 29.- Effect of temperature on short-circuit current and open-circuit voltage of 1 ohm-cm boron- and aluminum-doped silicon solar cells before and after irradiation with 22 MeV protons.

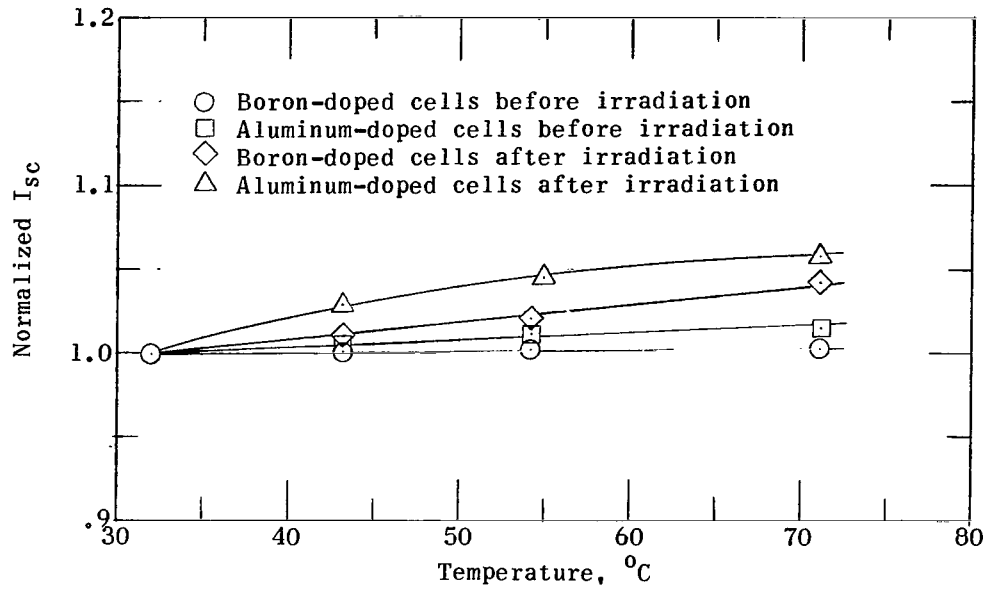

(a) Short-circuit current, normalized to 32° C.

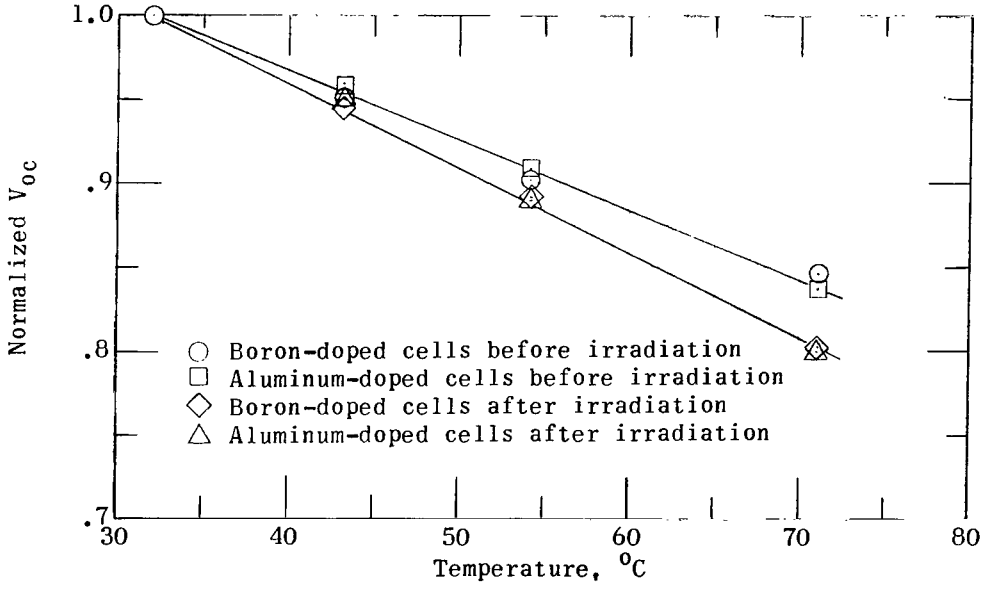

(b) Open-circuit voltage, normalized to 32° C.

Figure 30.- Effect of temperature on short-circuit current and open-circuit voltage of 10 ohm-cm boron- and aluminum-doped silicon solar cells before and after irradiation with 22 MeV protons.

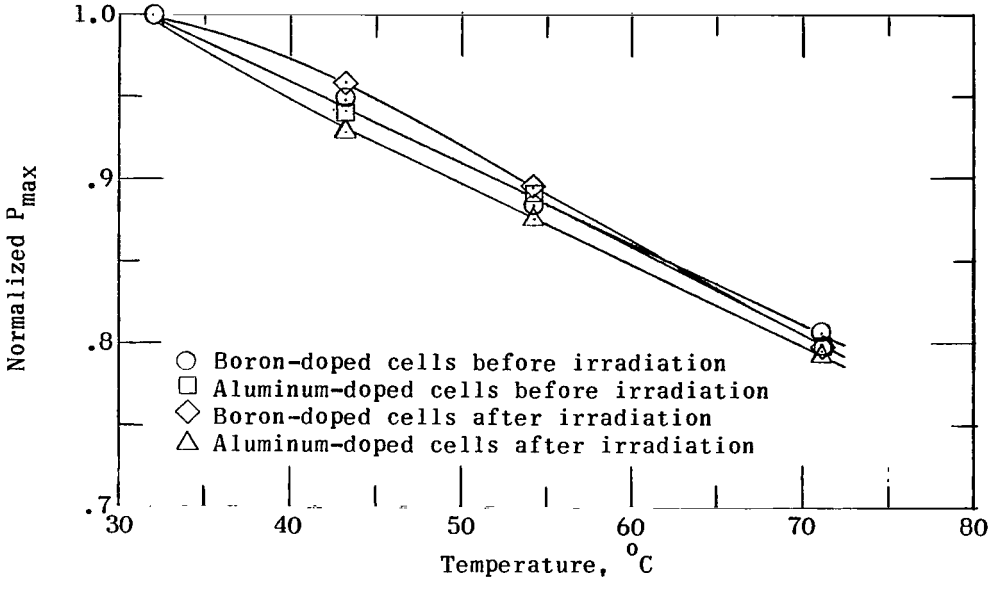

(a) 1 ohm-cm solar cells.

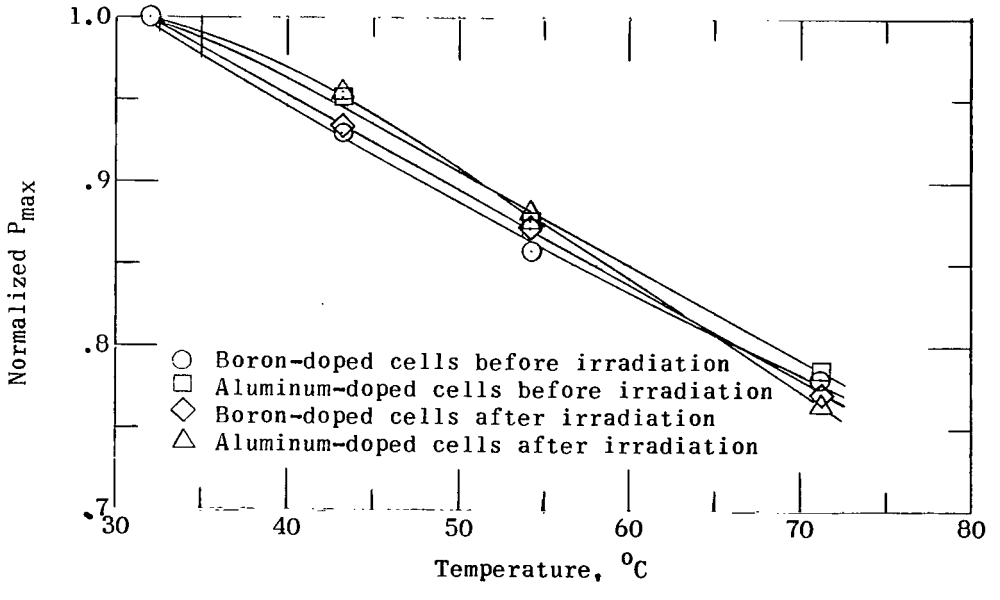

(b) 10 ohm-cm solar cells.

Figure 31.- Effect of temperature on maximum power of boron- and aluminum-doped silicon solar cells before and after irradiation with 22 MeV protons.

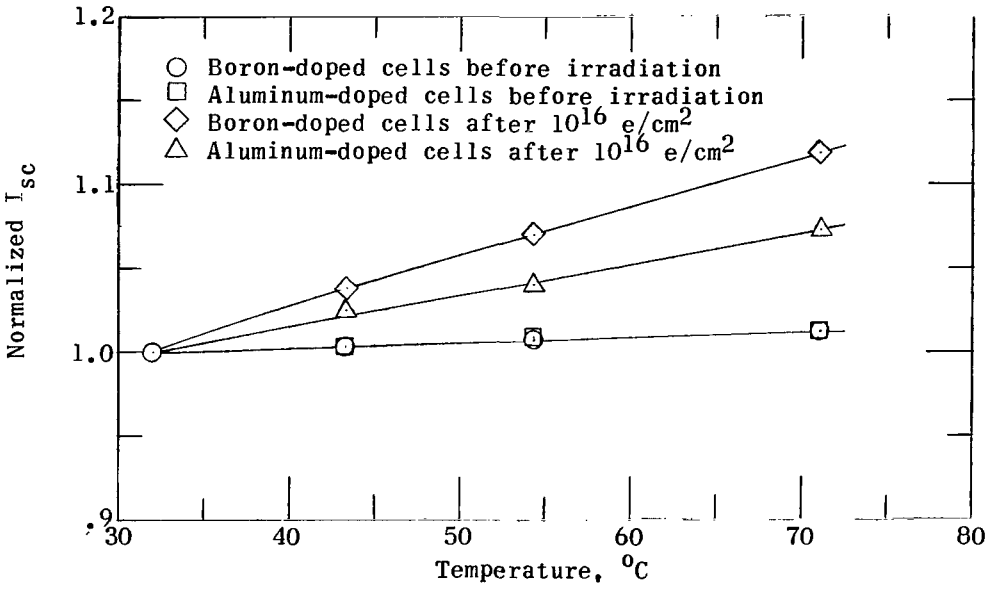

(a) Short-circuit current, normalized to 32° C.

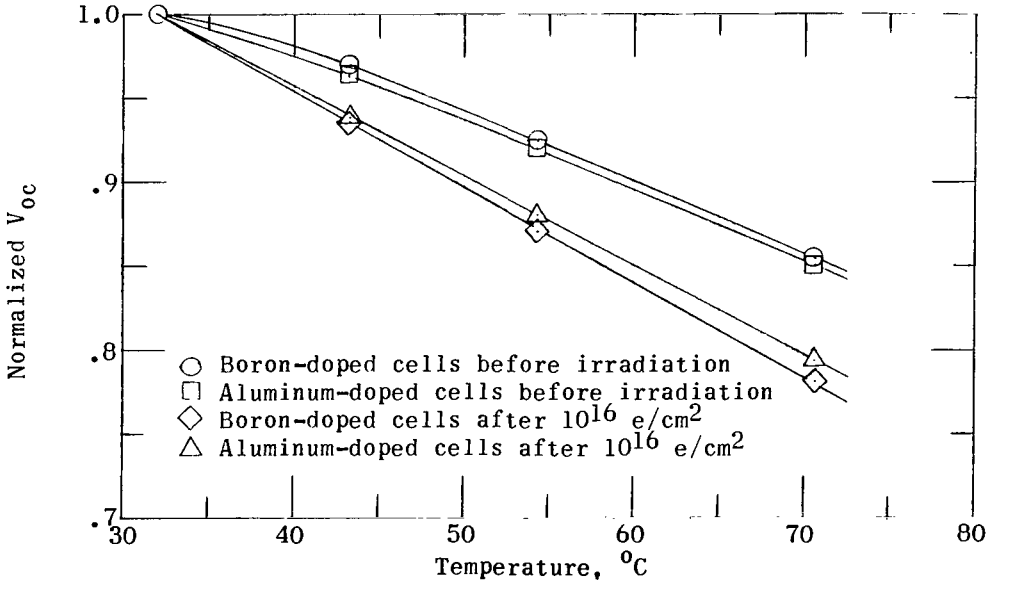

(b) Open-circuit voltage, normalized to 32° C.

Figure 32.- Effect of temperature on short-circuit current and open-circuit voltage of 1 ohm-cm boron- and aluminum-doped silicon solar cells before and after irradiation with 2.4 MeV electrons.

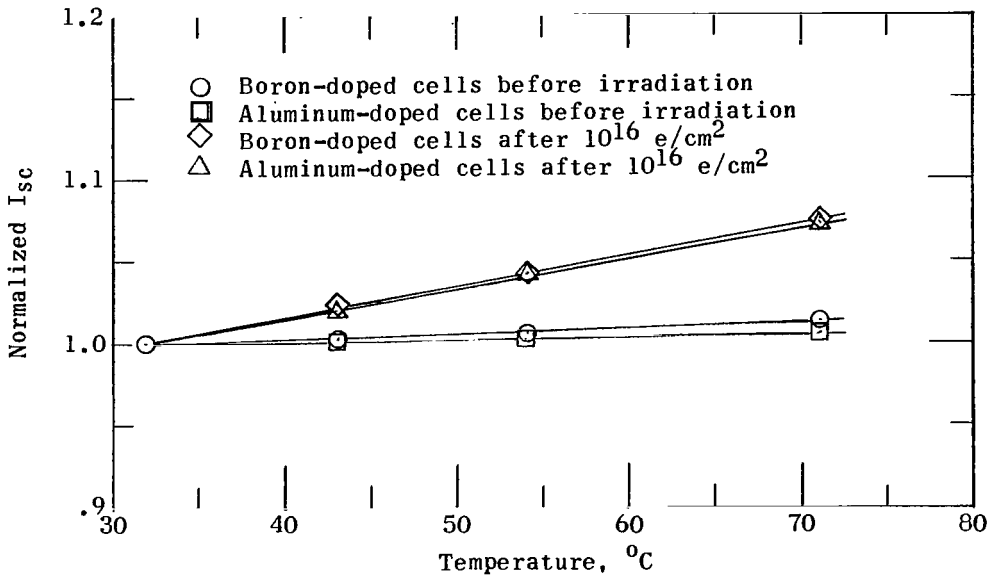

(a) Short-circuit current, normalized to 32° C.

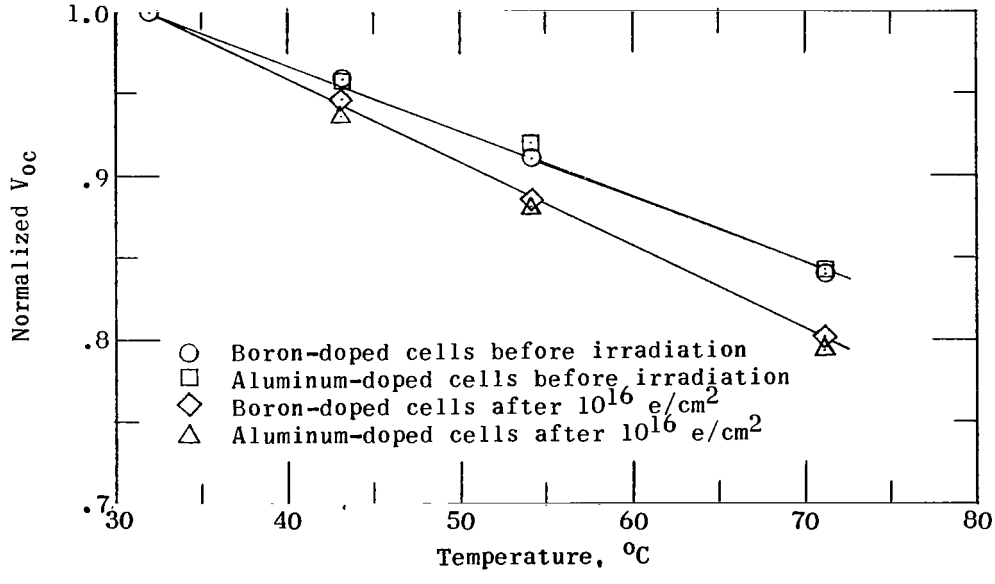

(b) Open-circuit voltage, normalized to 32° C.

Figure 33.- Effect of temperature on short-circuit current and open-circuit voltage of 10 ohm-cm boron- and aluminum-doped silicon solar cells before and after irradiation with 2.4 MeV electrons.

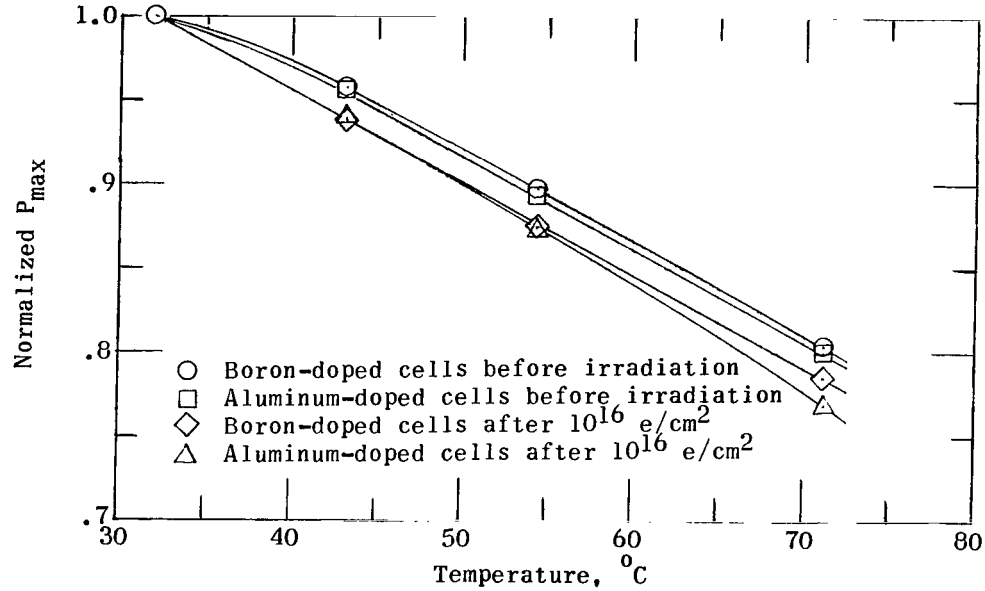

(a) 1 ohm-cm solar cells.

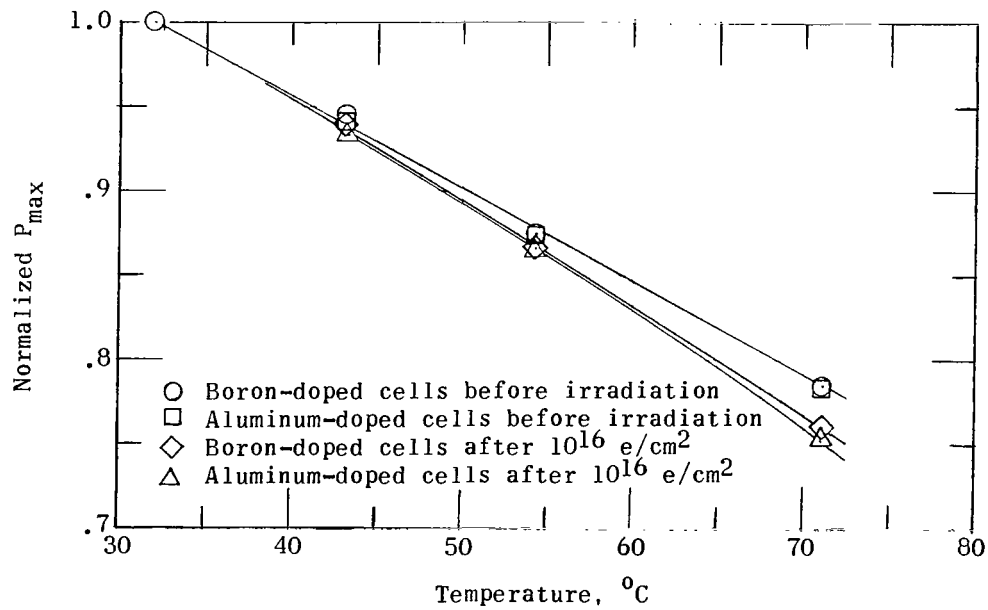

(b) 10 ohm-cm solar cells.

Figure 34.- Effect of temperature on maximum power of boron- and aluminum-doped silicon solar cells before and after irradiation with 2.4 MeV electrons.

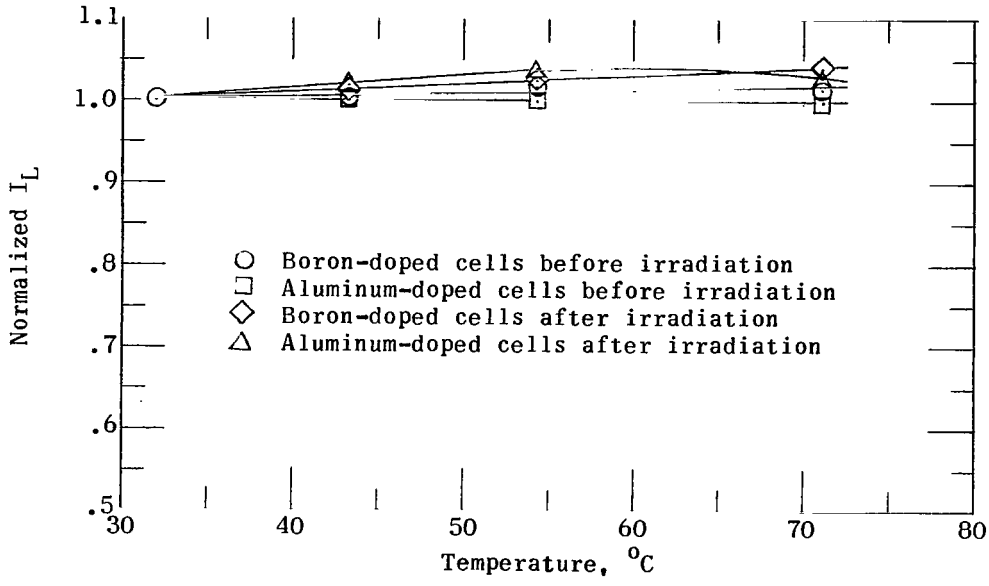

(a) 1 ohm-cm solar cells.

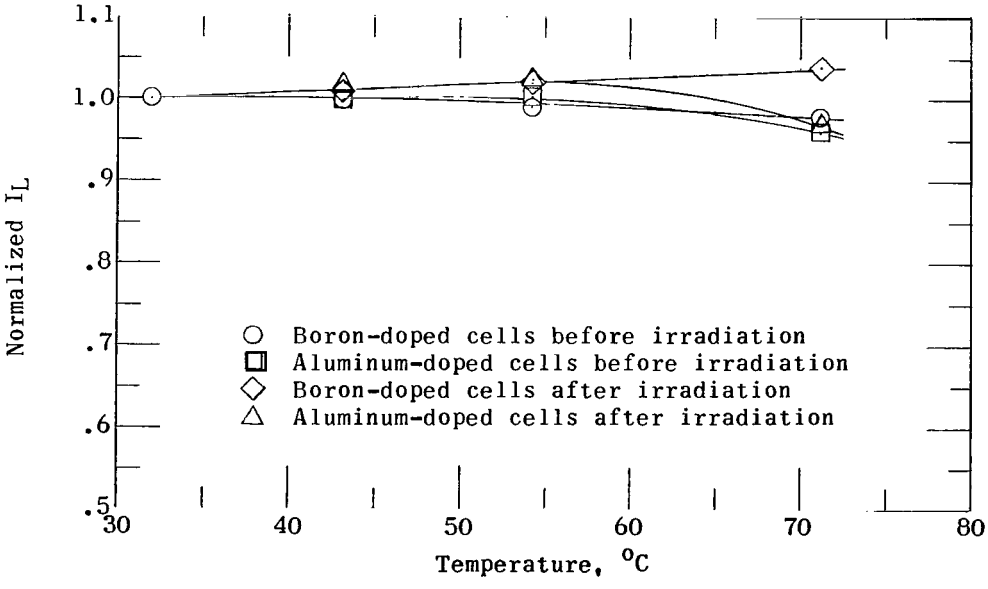

(b) 10 ohm-cm solar cells.

Figure 35.- Effect of temperature on load current at 0.25 volt before and after irradiation with 22 MeV protons.

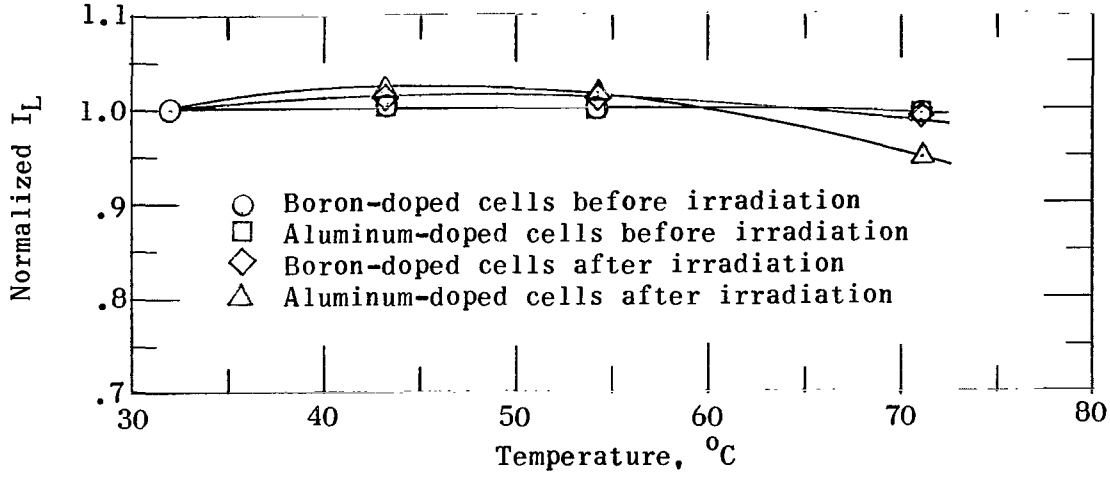

(a) 1 ohm-cm solar cells.

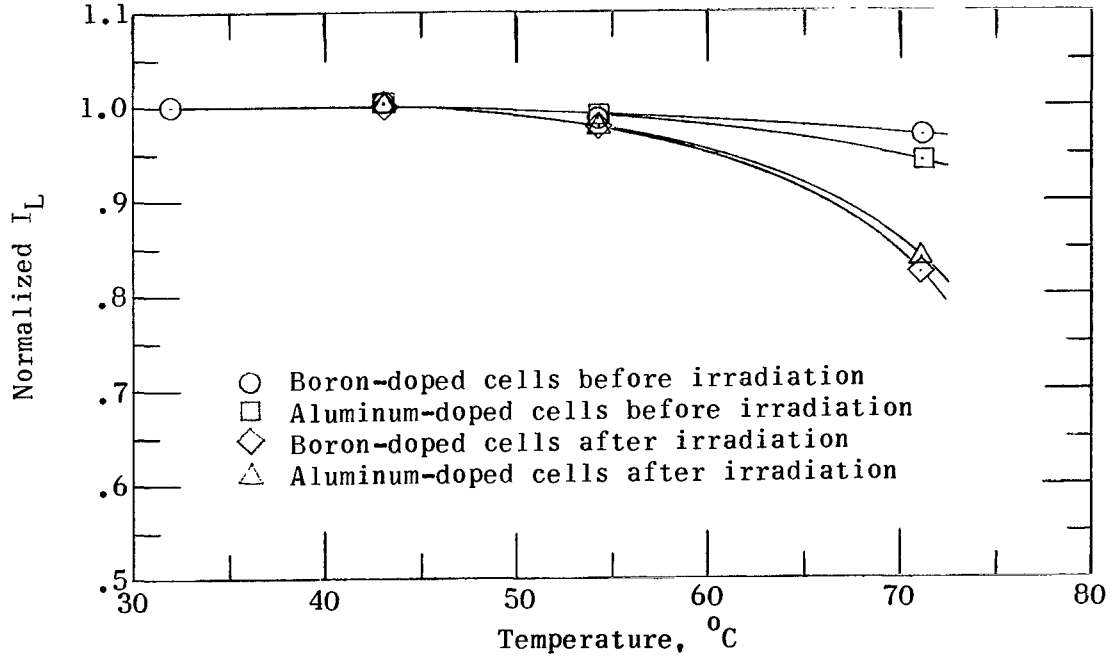

(b) 10 ohm-cm solar cells.

Figure 36.- Effect of temperature on load current at 0.3 volt before and after irradiation with 22 MeV protons.

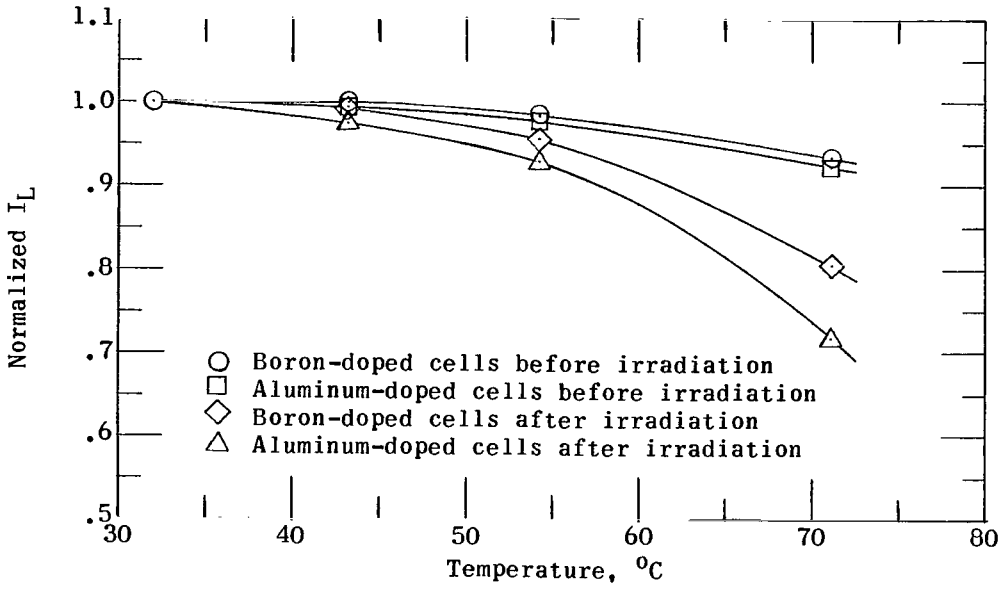

(a) 1 ohm-cm solar cells.

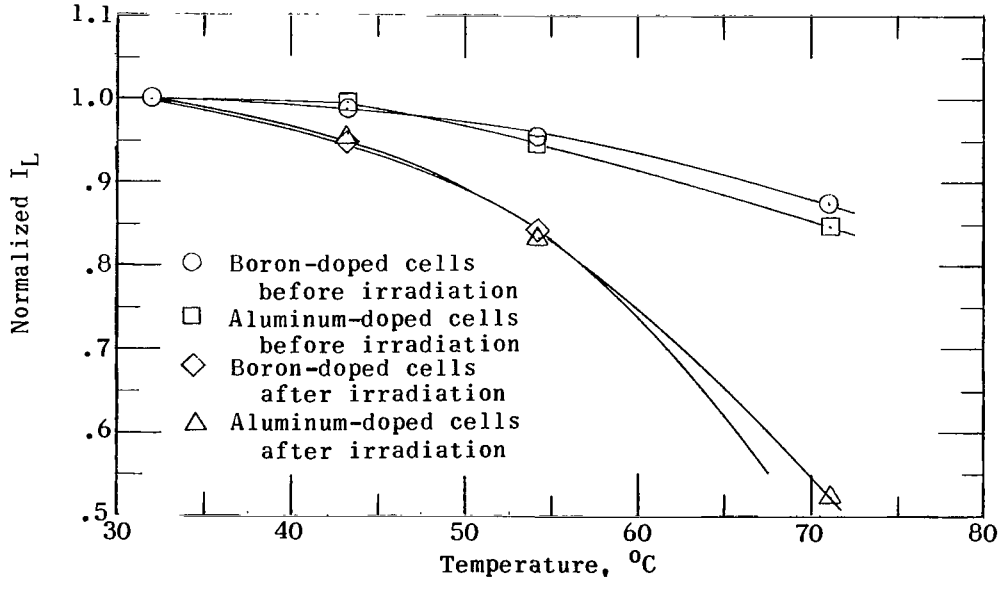

(b) 10 ohm-cm solar cells.

Figure 37.- Effect of temperature on load current at 0.35 volt before and after irradiation with 22 MeV protons.

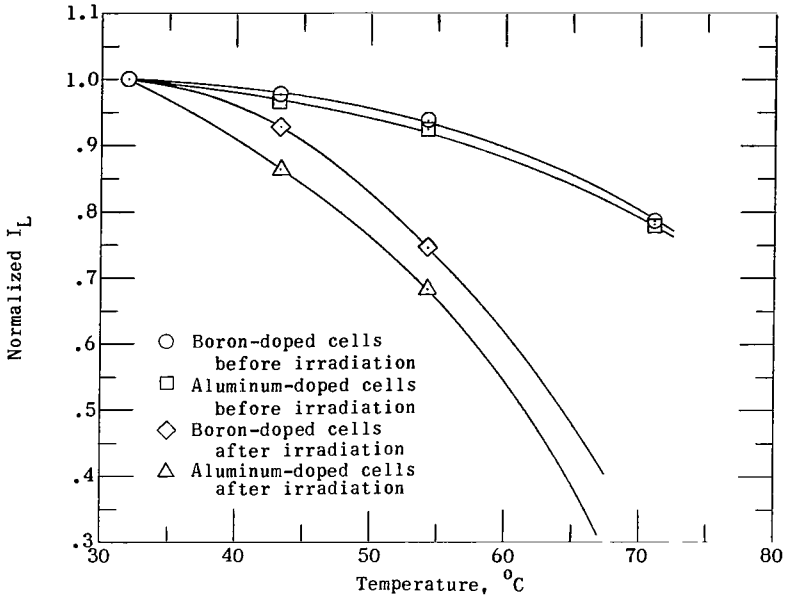

(a) 1 ohm-cm solar cells.

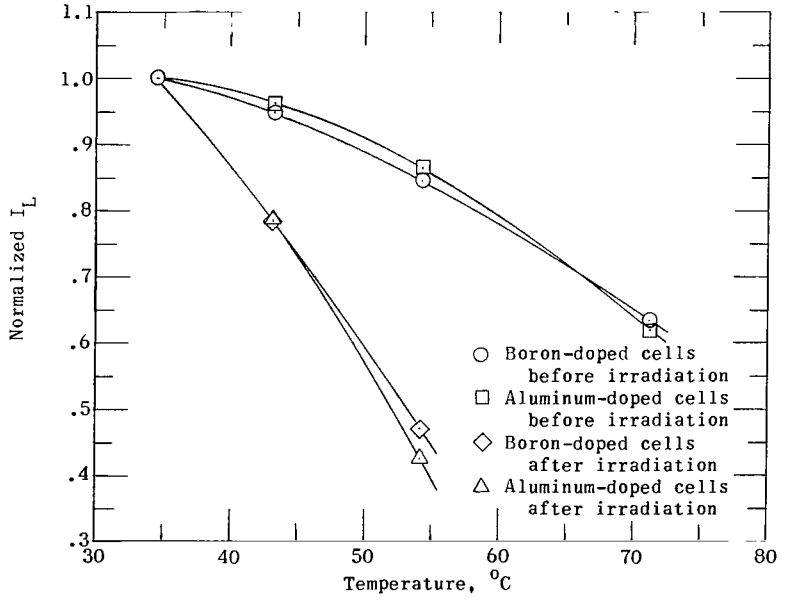

(b) 10 ohm-cm solar cells.

Figure 38.- Effect of temperature on load current at 0.4 volt before and after irradiation with 22 MeV protons.

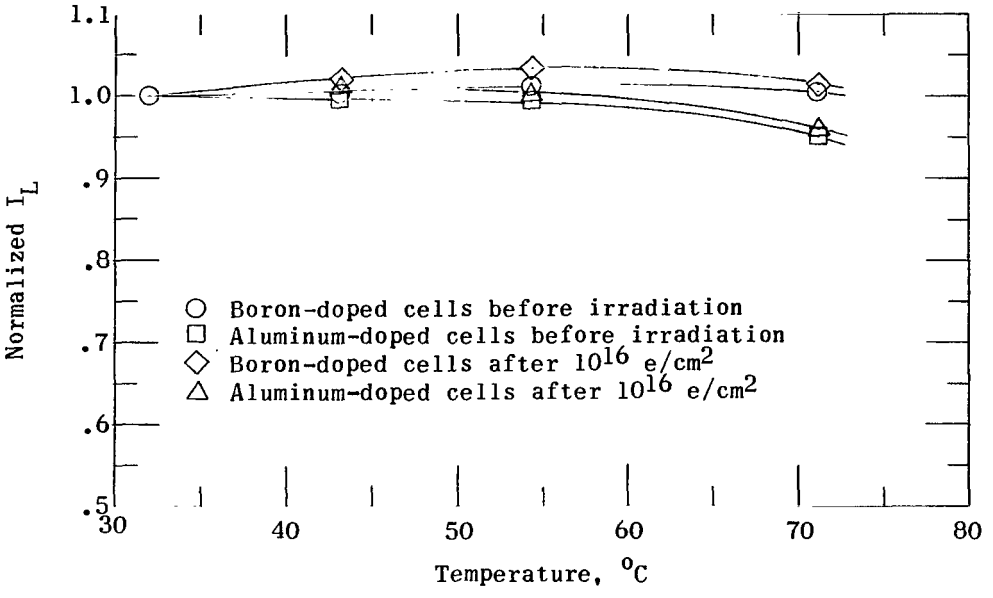

(a) 1 ohm-cm solar cells.

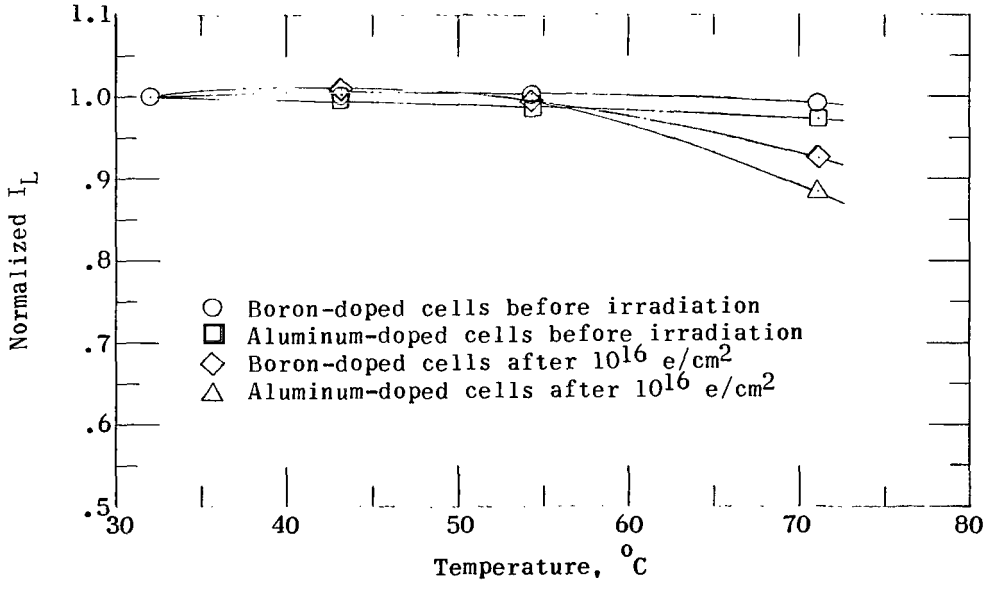

(b) 10 ohm-cm solar cells.

Figure 39.- Effect of temperature on load current at 0.25 volt before and after irradiation with 2.4 MeV electrons.

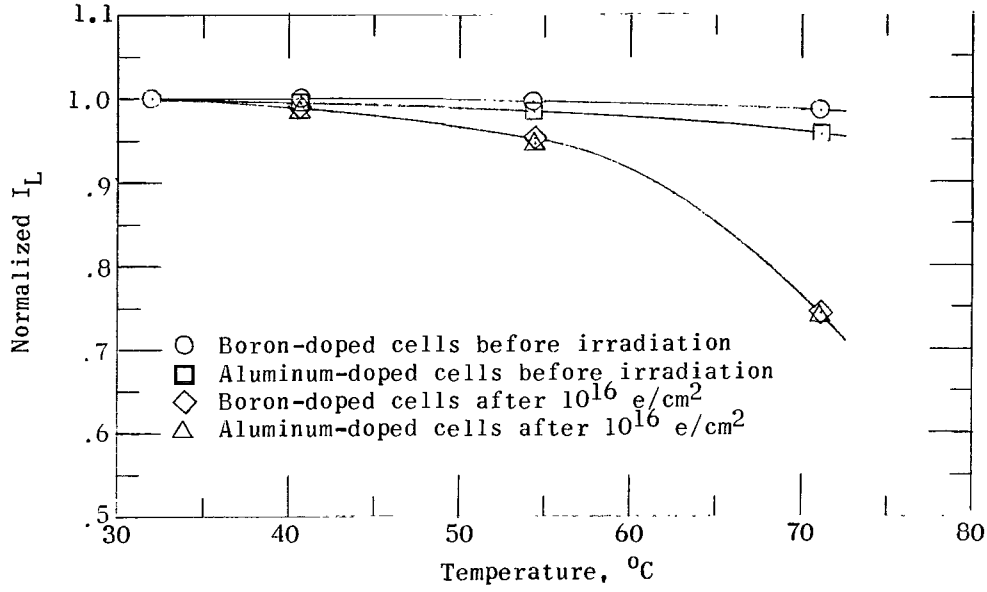

(a) 1 ohm-cm solar cells.

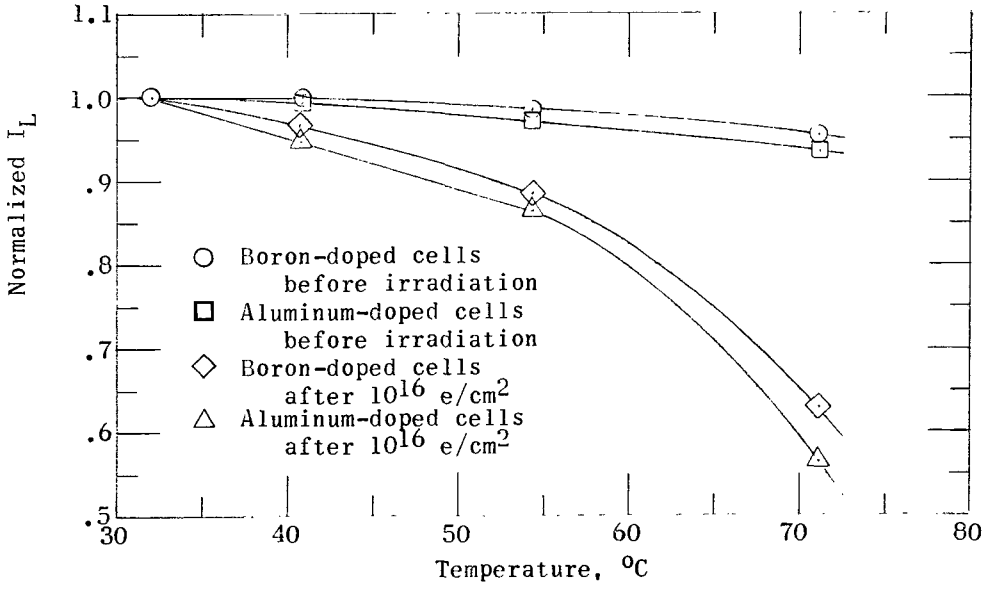

(b) 10 ohm-cm solar cells.

Figure 40.- Effect of temperature on load current at 0.3 volt before and after irradiation with 2.4 MeV electrons.

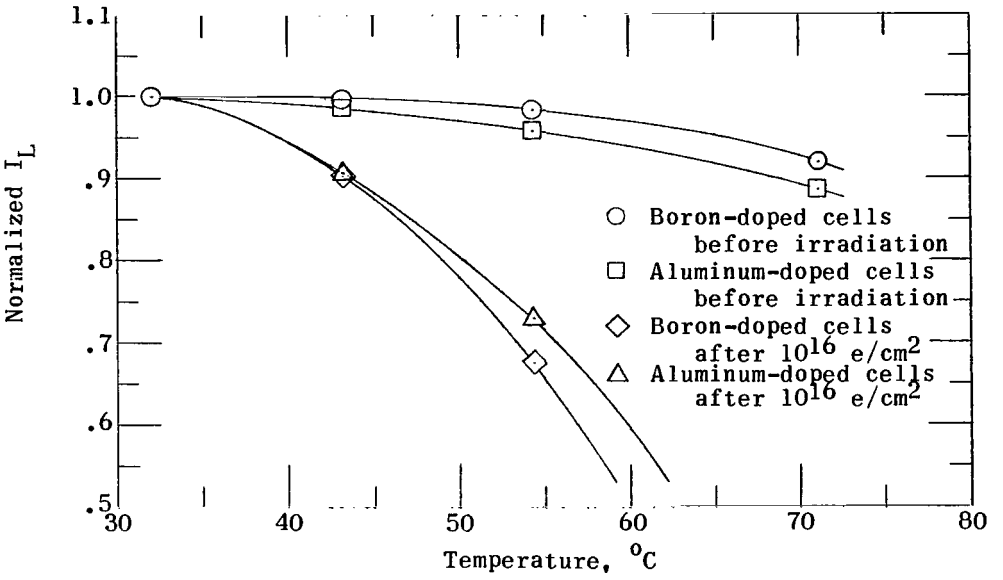

(a) 1 ohm-cm solar cells.

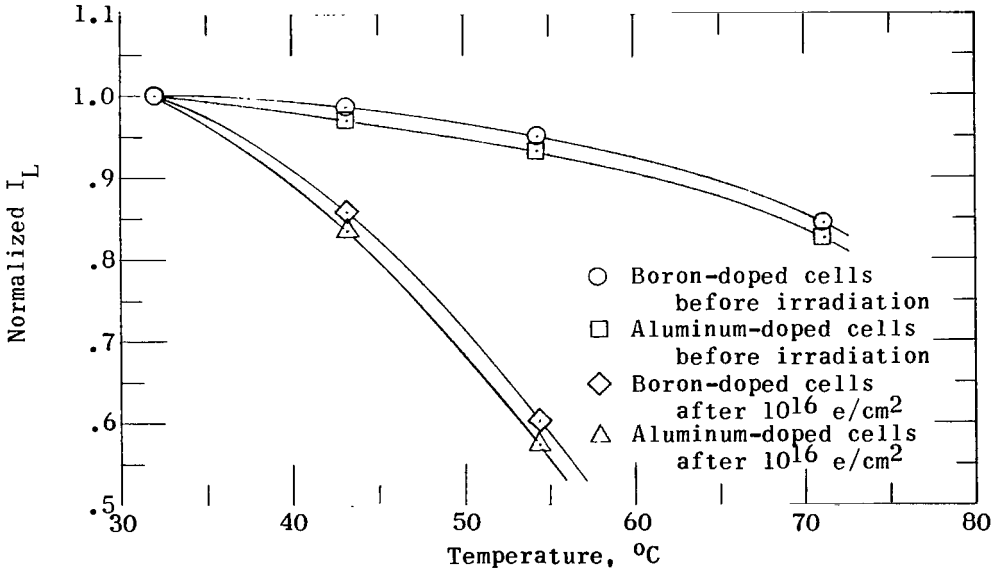

(b) 10 ohm-cm solar cells.

Figure 41.- Effect of temperature on load current at 0.35 volt before and after irradiation with 2.4 MeV electrons.

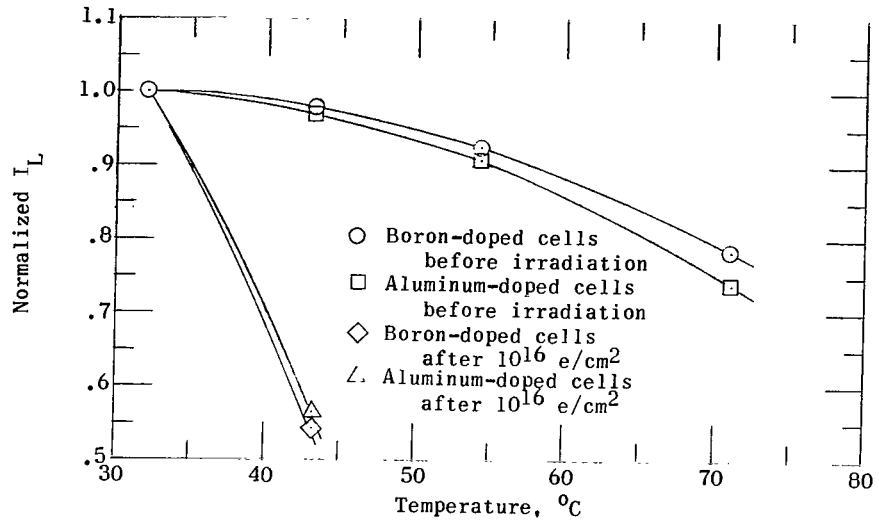

(a) 1 ohm-cm solar cells.

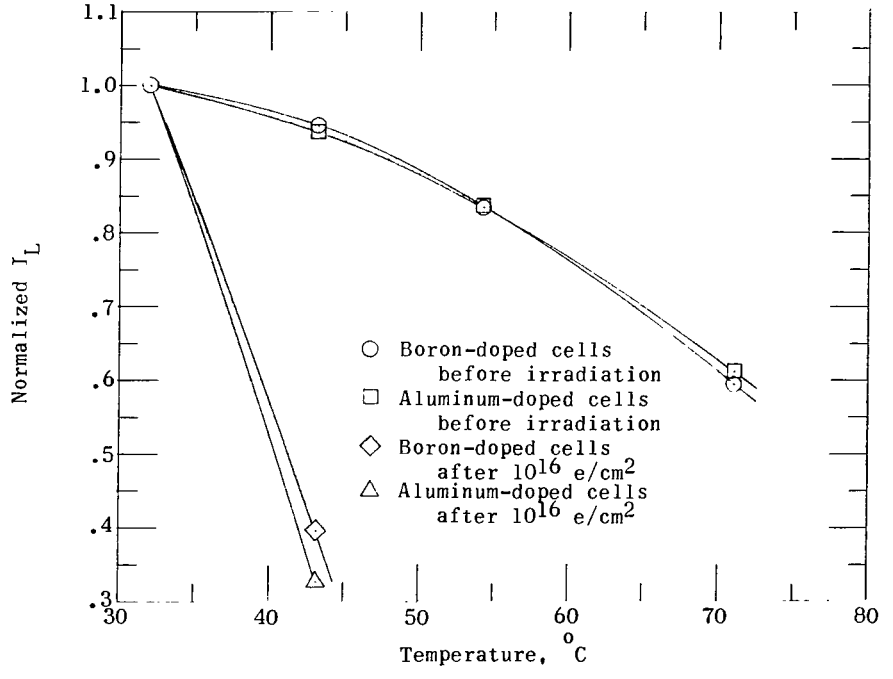

(b) 10 ohm-cm solar cells.

Figure 42.- Effect of temperature on load current at 0.4 volt before and after irradiation with 2.4 MeV electrons.

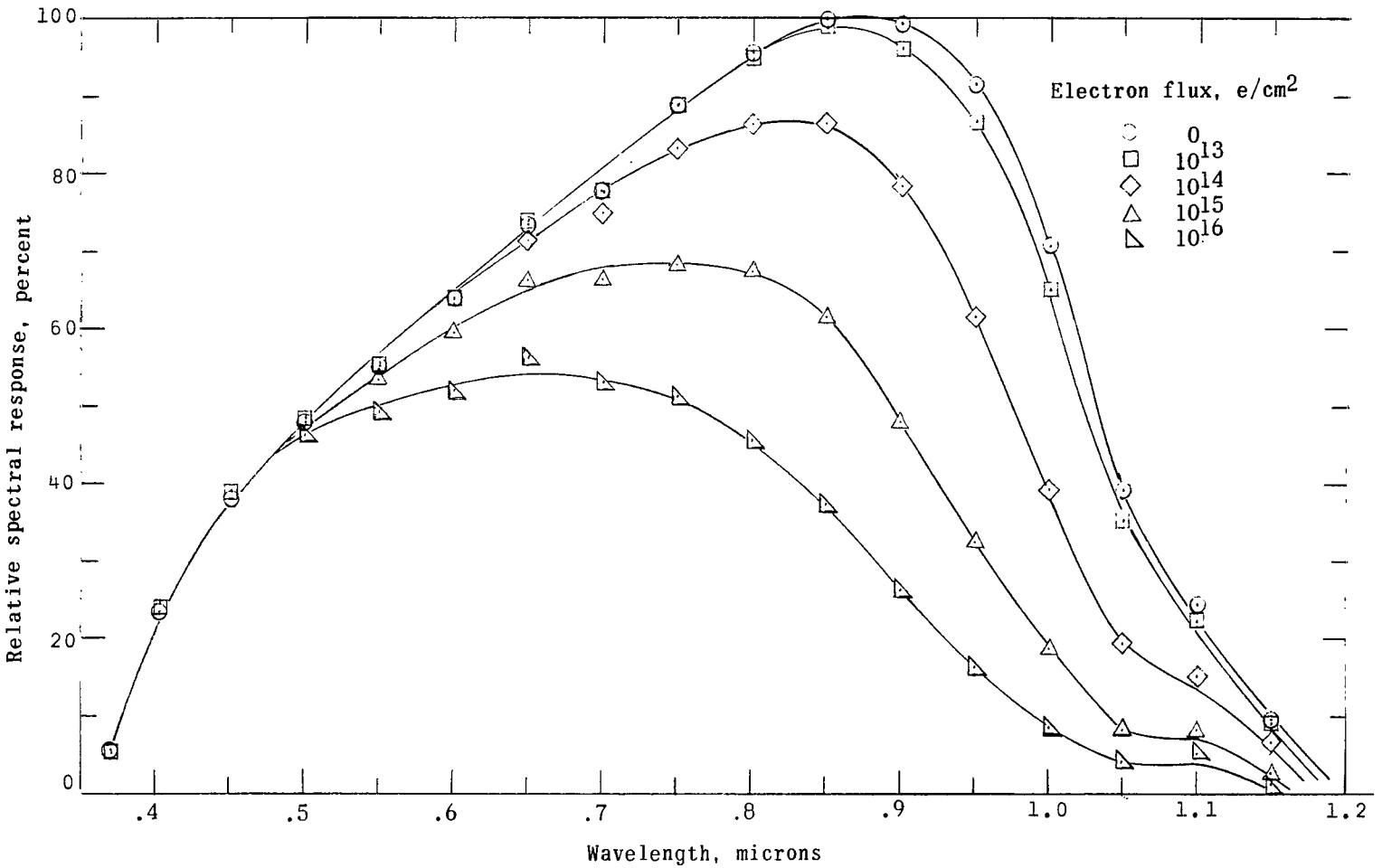

Figure 43.- Relative spectral response (for constant spectral energy input) of a 10 ohm-cm aluminum-doped silicon solar cell before and after irradiation.

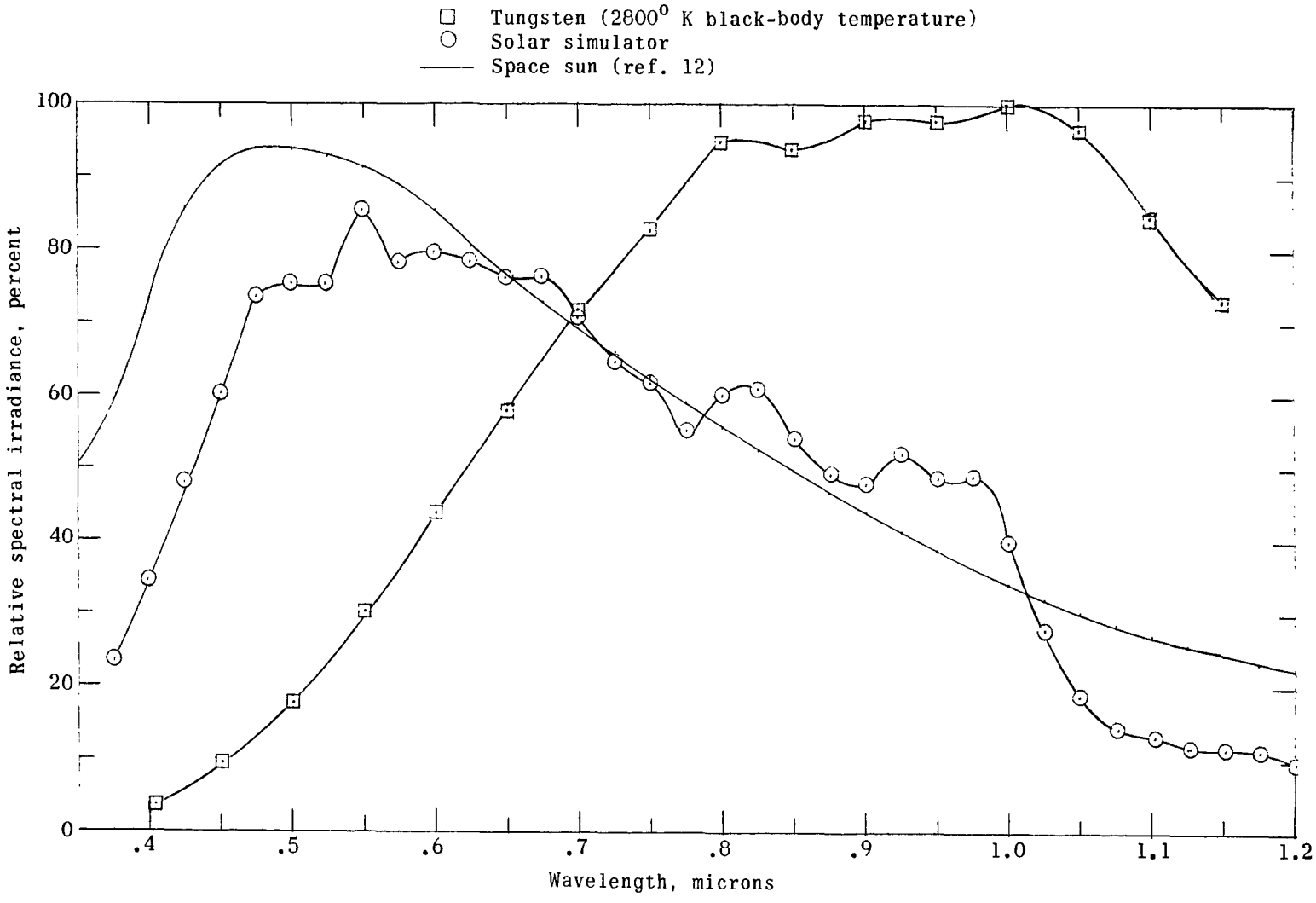

Figure 44.- Relative spectral radiant power of several light sources.

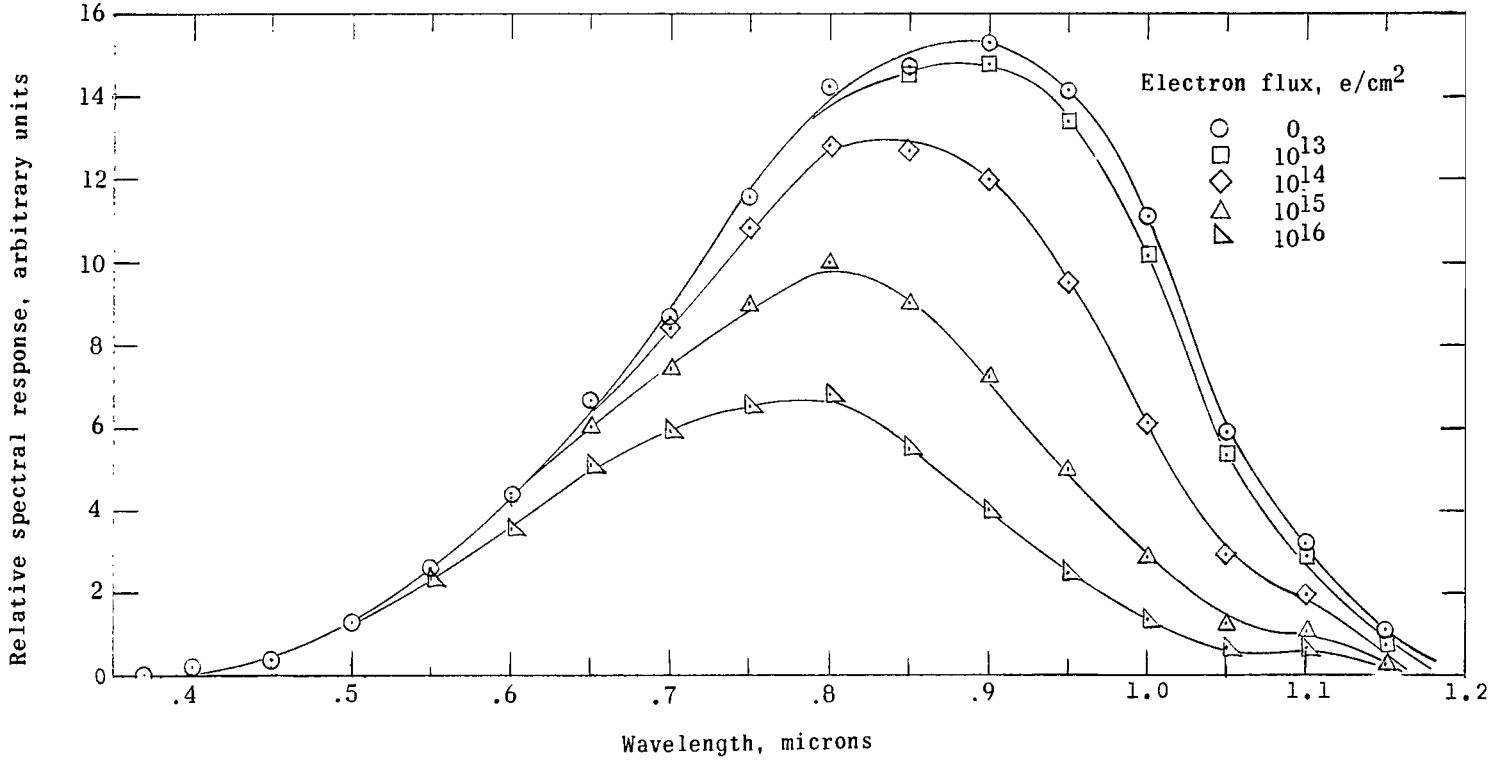

Figure 45.- Spectral response of a 10 ohm-cm aluminum-doped silicon solar cell (under tungsten illumination) before and after irradiation with 2.4 MeV electrons.

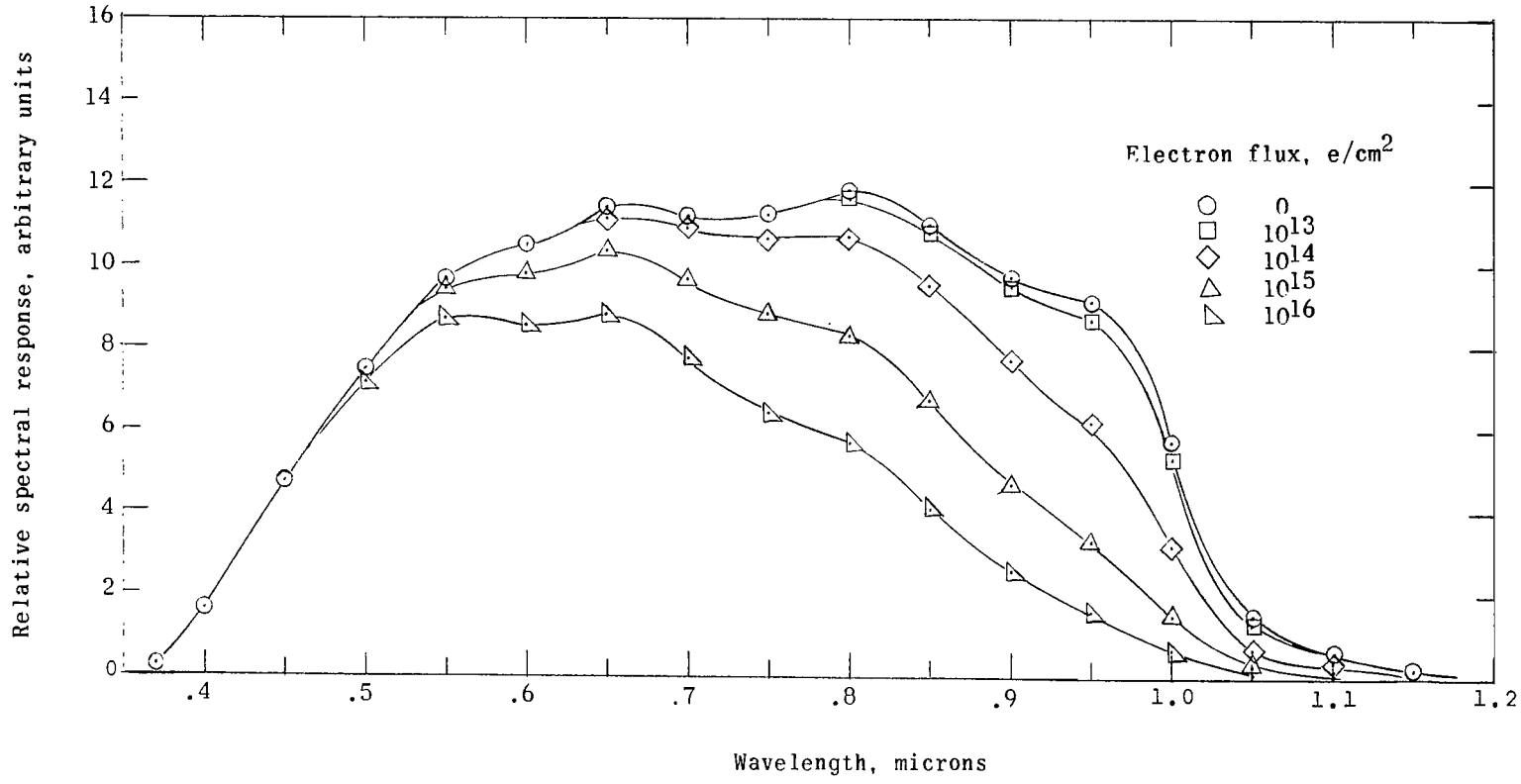

Figure 46.- Spectral response of a 10 ohm-cm aluminum-doped silicon solar cell (under solar-simulator illumination) before and after irradiation with 2.4 MeV electrons.

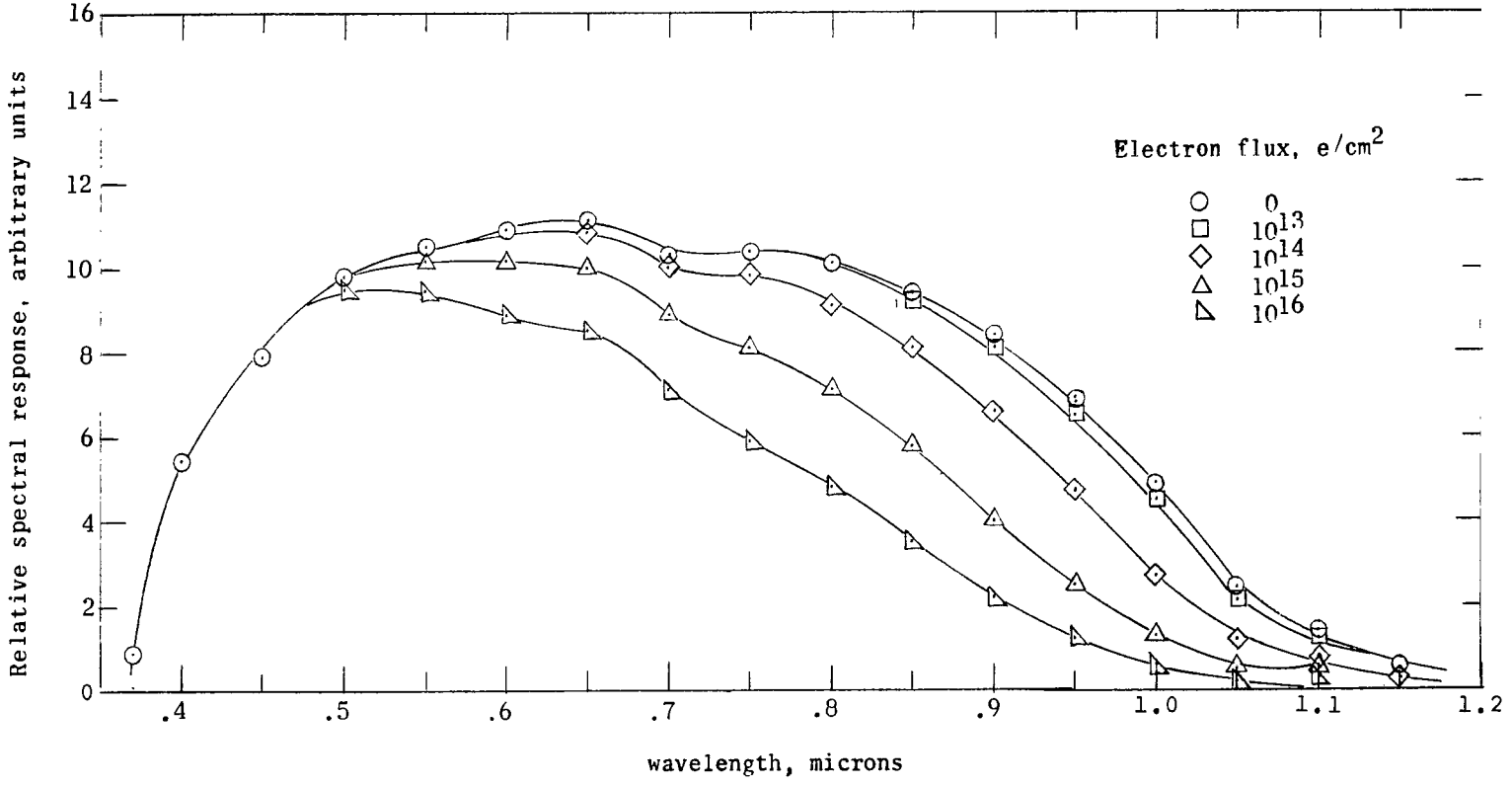

Figure 47.- Spectral response of a 10 ohm-cm aluminum-doped silicon solar cell (calculated for zero-air-mass sun illumination) before and after irradiation with 2.4 MeV electrons.

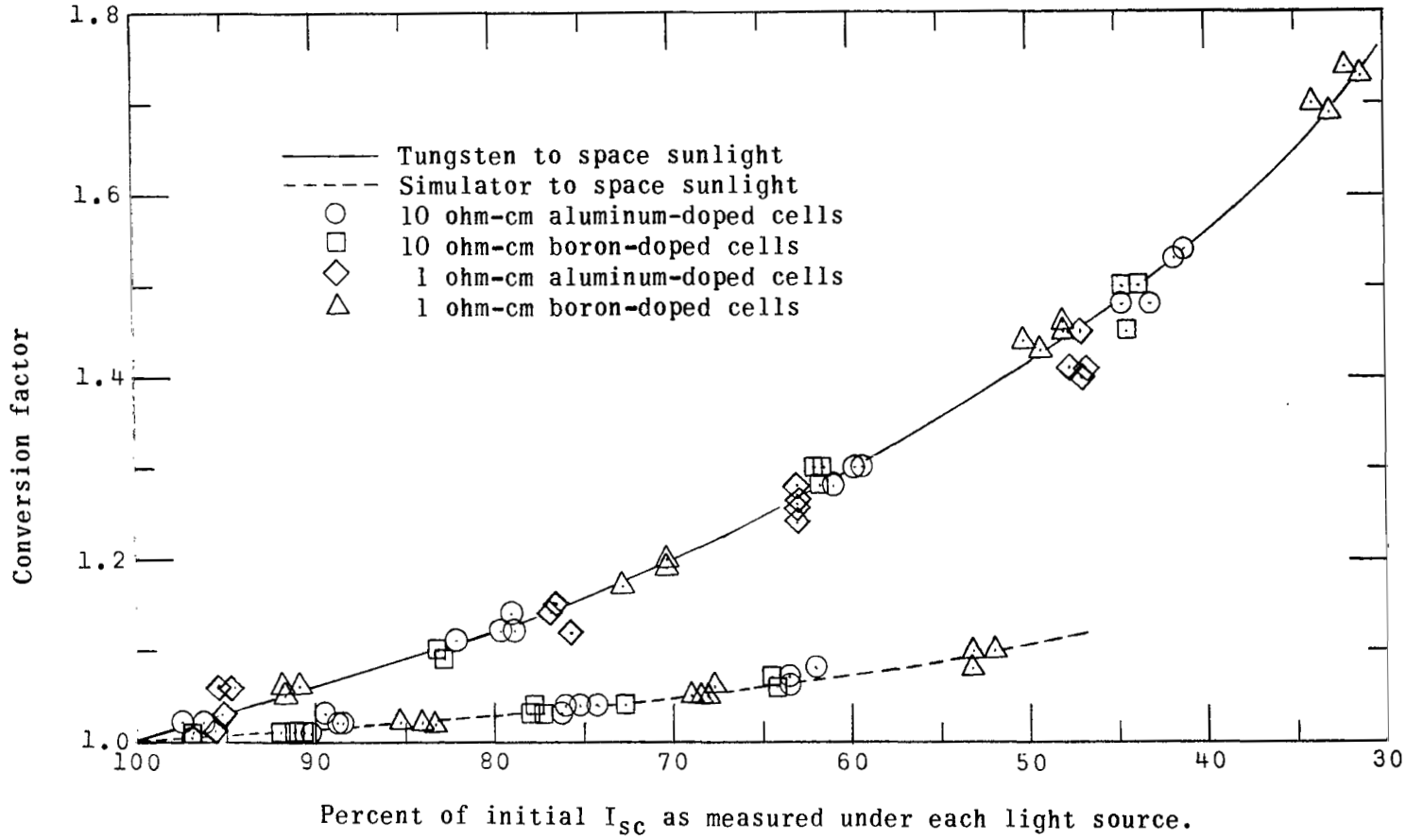

Figure 48.- Conversion of short-circuit current output of silicon solar cells from space-sunlight-equivalent tungsten illumination and space-sunlight-equivalent simulator illumination to space sunlight illumination.

"The aeronautical and space activities of the United States shall be conducted so as to contribute . . . to the expansion of human knowledge of phenomena in the atmosphere and space. The Administration shall provide for the widest practicable and appropriate dissemination of information concerning its activities and the results thereof."

—NATIONAL AERONAUTICS AND SPACE ACT OF 1958

NASA SCIENTIFIC AND TECHNICAL PUBLICATIONS

TECHNICAL REPORTS: Scientific and technical information considered important, complete, and a lasting contribution to existing knowledge.

TECHNICAL NOTES: Information less broad in scope but nevertheless of importance as a contribution to existing knowledge.

TECHNICAL MEMORANDUMS: Information receiving limited distribution because of preliminary data, security classification, or other reasons.

CONTRACTOR REPORTS: Scientific and technical information generated under a NASA contract or grant and considered an important contribution to existing knowledge.

TECHNICAL TRANSLATIONS: Information published in a foreign language considered to merit NASA distribution in English.

SPECIAL PUBLICATIONS: Information derived from or of value to NASA activities. Publications include conference proceedings, monographs, data compilations, handbooks, sourcebooks, and special bibliographies.

TECHNOLOGY UTILIZATION PUBLICATIONS: Information on technology used by NASA that may be of particular interest in commercial and other non-aerospace applications. Publications include Tech Briefs, Technology Utilization Reports and Notes, and Technology Surveys.

Details on the availability of these publications may be obtained from:

SCIENTIFIC AND TECHNICAL INFORMATION DIVISION

NATIONAL AERONAUTICS AND SPACE ADMINISTRATION

Washington, D.C. 20546